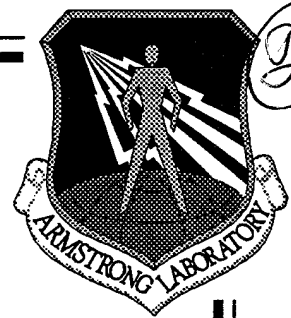


AL/CF-TR-1995-0037



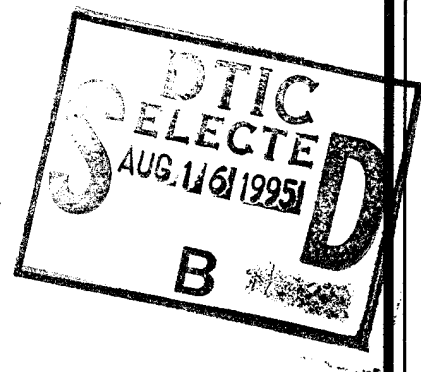
ARMSTRONG

LABORATORY

**STATISTICAL BUBBLE DYNAMICS ALGORITHMS FOR  
ASSESSMENT OF ALTITUDE DECOMPRESSION  
SICKNESS INCIDENCE**

**Wayne A. Gerth  
Richard D. Vann**

**F.G. Hall Environmental Laboratory  
Hyper-Hypobaric Center  
Duke University Medical Center  
Durham, North Carolina 27710**



**CREW SYSTEMS DIRECTORATE  
Crew Technology Division  
2504 Gillingham Drive, Suite 1  
Brooks Air Force Base, TX 78235-5104**

JULY 1995

19950814 066

**Final Technical Report for Period June 1992 - October 1994**

Approved for public release; distribution is unlimited.

**AIR FORCE MATERIEL COMMAND  
BROOKS AIR FORCE BASE, TEXAS**

DTIC QUALITY INSPECTED 1

0615

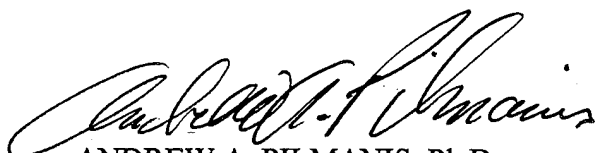
## NOTICES

This final report was submitted by the F.G. Hall Environmental Laboratory, Duke University Medical Center, Durham, North Carolina, under contract F33615-90-D0606, delivery order 0026, with the Armstrong Laboratory, Human Systems Center, AFMC, Brooks Air Force Base, Texas.

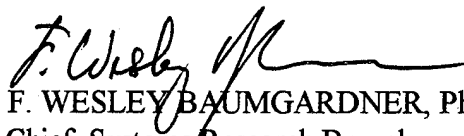
When Government drawings, specifications, or other data are used for any purpose other than in connection with a definitely Government-related procurement, the United States Government incurs no responsibility or any obligation whatsoever. The fact that the Government may have formulated or in any way supplied the said drawings, specifications, or other data, is not to be regarded by implication, or otherwise in any manner construed, as licensing the holder of any other person or corporation; or as conveying any rights or permission to manufacture, use, or sell any patented invention that may in any way be related thereto.

The Office of Public Affairs has reviewed this report, and it is releasable to the National Technical Information Service, where it will be available to the general public, including foreign nationals.

This report has been reviewed and is approved for publication.



ANDREW A. PILMANIS, Ph.D.  
Chief, High Altitude Protection



F. WESLEY BAUMGARDNER, Ph.D.  
Chief, Systems Research Branch



JAMES P. DIXON, Colonel, USAF, BSC  
Chief, Crew Technology Division

Accession For	
NTIS GRA&I	<input checked="checked" type="checkbox"/>
DTIC TAB	<input type="checkbox"/>
Unannounced	<input type="checkbox"/>
Justification	
By _____	
Distribution/ _____	
Availability Codes	
Dist	Avail and/or Special
A-1	

REPORT DOCUMENTATION PAGE			Form Approved OMB No. 0704-0188	
Public reporting burden for this collection of information is estimated to average 1 hour per response, including the time for reviewing instructions, searching existing data sources, gathering and maintaining the data needed, and completing and reviewing the collection of information. Send comments regarding this burden estimate or any other aspect of this collection of information, including suggestions for reducing this burden, to Washington Headquarters Services, Directorate for Information Operations and Reports, 1215 Jefferson Davis Highway, Suite 1204, Arlington, VA 22202-4302, and to the Office of Management and Budget, Paperwork Reduction Project (0704-0188), Washington, DC 20503.				
1. AGENCY USE ONLY (Leave blank)		2. REPORT DATE July 1995	3. REPORT TYPE AND DATES COVERED Final June 92 - October 94	
4. TITLE AND SUBTITLE Statistical Bubble Dynamics Algorithms for Assessment of Altitude Decompression Sickness Incidence			5. FUNDING NUMBERS C - F33615-90-D-0606 PE - 63231F PR - 2830 TA - 01 WU - 15	
6. AUTHOR(S) Wayne A. Gerth, Ph.D. Richard D. Vann, Ph.D.				
7. PERFORMING ORGANIZATION NAME(S) AND ADDRESS(ES) F.G. Hall Environmental Laboratory Hyper-Hypobaric Center Duke University Medical Center Durham, N.C. 27710			8. PERFORMING ORGANIZATION REPORT NUMBER	
9. SPONSORING / MONITORING AGENCY NAME(S) AND ADDRESS(ES) Armstrong Laboratory (AFMC) Crew Systems Directorate Crew Technology Division 2504 Gillingham Drive Ste 25 Brooks Air Force Base, TX 78235-5104			10. SPONSORING / MONITORING AGENCY REPORT NUMBER  AL/CF-TR-1995-0037	
11. SUPPLEMENTARY NOTES  Armstrong Laboratory Technical Monitor: Captain Robert B. O'Connor, (210)536-3545				
12a. DISTRIBUTION / AVAILABILITY STATEMENT  Approved for public release; distribution is unlimited			12b. DISTRIBUTION CODE	
13. ABSTRACT (Maximum 200 words)  Air Force personnel are routinely exposed to atmospheric decompressions that often incur significant risk of decompression sickness (DCS). Management of these risks requires analytic methods able to: a) define risk/hazard envelopes for all routine and emergency decompressions, b) assess the DCS risks included or introduced in the contemplation or design of new operational procedures and equipment, and; c) support real-time monitoring of DCS risk incurred by personnel during various chamber and aircraft operations. Present work contributed to meeting these requirements through development and application of methods by which DCS risks during decompression profiles are determined from statistical/biophysical models of in vivo gas exchange and bubble growth and resolution. Using maximum likelihood, both logistic and survival models were fit to DCS incidence data from the USAF Armstrong Laboratory (USAFAL) for a wide variety of decompression profiles. The models were incorporated into software that operates on personal computers. System software, including a data transcription routine to serve as a software interface between the USAFAL Hypobaric Decompression Sickness Database and the present modeling system, was delivered for use and evaluation of USAFAL personnel.				
14. SUBJECT TERMS Decompression sickness Model development Maximum likelihood			15. NUMBER OF PAGES 106 16. PRICE CODE	
17. SECURITY CLASSIFICATION OF REPORT UNCLASSIFIED		18. SECURITY CLASSIFICATION OF THIS PAGE UNCLASSIFIED	19. SECURITY CLASSIFICATION OF ABSTRACT UNCLASSIFIED	
20. LIMITATION OF ABSTRACT UL				

## TABLE OF CONTENTS

Section	Page
<b>List of Figures</b> .....	v
<b>List of Tables</b> .....	vi
<b>Acknowledgements</b> .....	vii
<b>Project Summary</b> .....	viii
<b>1. Introduction</b> .....	1
1.1. Background and Significance .....	1
1.2. Program Objectives .....	2
<b>2. Model Theory and Implementation</b> .....	3
2.1. Model Structure .....	3
2.1.1. Probability Distribution Functions .....	3
2.1.1.1. Logistic .....	5
2.1.1.2. Survival .....	6
2.1.2. Bubble Dynamics .....	12
2.1.3. Incorporation .....	12
2.2. Model Parameterization .....	15
2.3. Software Implementation .....	17
<b>3. Model Optimization</b> .....	17
3.1. Training Data .....	22
3.2. Results and Evaluation .....	36
<b>4. Application</b> .....	36
4.1. Specific Examples .....	36
4.1.1. Type I Altitude Training Flight .....	40
4.1.2. Type II Altitude Training Flight .....	41
4.1.3. USAF HALO Training Flight .....	42
4.1.4. Reconnaissance Flight .....	42
4.1.5. T-37B Cross-Country Flight .....	42

**TABLE OF CONTENTS (*CONTINUED*)**

<b>Section</b>	<b>Page</b>
4.1. Specific Examples ( <i>continued</i> ) .....	
4.1.6. Inflight Denitrogenation Study .....	43
4.2. Prescriptive Applications .....	45
4.2.1. Acceptable Risk .....	45
4.2.2. Prebreathe Minimization .....	46
<b>5. Future Work</b> .....	48
5.1. Time of DCS Onset .....	48
5.2. Model Enhancements .....	48
5.2.1. Severity of DCS .....	49
5.2.2. Effects of Exercise .....	49
5.2.3. Variable Bubble Number Density .....	49
5.2.4. Bubble Damage/Repair .....	51
5.2.5. Alternative Bubble Dynamics Models .....	51
Multiple Gas Dynamics	
Diffusion Shell	
5.3. Training Dataset Expansion .....	52
<b>6. Conclusions</b> .....	52
<b>7. References</b> .....	54
<b>8. Appendices</b>	
Appendix A. Node Descriptions of Profiles in Text. ....	57
Appendix B. <b>README.DOC</b> file included with USAF release Version 2.1 of the Duke University DCS Incidence Modeling System ....	61
Appendix C. System Software Parameterization Files. ....	77
Appendix D. Supplemental Update to Model Development .....	79

## LIST OF FIGURES

Figure		Page
1.	Frequency Distribution of DCS Incidence vs. Decompression Stress .....	4
2.	Cumulative Dose-Response Distribution Function; P(DCS) vs DOSE .....	5
3.	Schematic of Bubble Dose/Risk Model .....	7
4.	System Software Modules and Organization .....	16
5.	Altitude Frequency Distribution of Stages of 5 minutes Duration or More in the USAFAL Dataset .....	19
6.	Distribution of Observed vs. Estimated DCS Incidences; Logistic Model I on its USAFAL Training Dataset .....	32
7.	Distribution of Observed vs. Estimated DCS Incidences; Logistic Model I-C on its Combined USAFAL + USN/NMRI Training Dataset .....	33
8.	Distribution of Observed vs. Estimated DCS Incidences; Logistic Model I-C on the USAFAL Subset of its USAFAL + USN/NMRI Training Dataset .....	34
9.	Distribution of Observed vs. Estimated DCS Incidences; Survival Model S-IIb on its USAFAL Training Dataset .....	35
10.	Distribution of Observed vs. Estimated DCS Incidences; Survival Model IIa-C on the USAFAL Subset of its USAFAL + USN/NMRI Training Dataset .....	36
11.	Analysis of USAF Type I Altitude Training Flight Using Logistic Model I-C. ....	37
12.	Calculated Dissolved N <sub>2</sub> Tension Profiles for the Three Tissue Compartments in Logistic Model I-C During a USAF Type I Altitude Training Flight .....	38
13.	Cumulative P(DCS) During a USAF Type I Altitude Training Flight Calculated Using Survival Model S-IIa .....	39
14.	Cumulative P(DCS) During a USAF Type I Altitude Training Flight Calculated Using Survival Model S-IIa-C .....	40
15.	Cumulative P(DCS) During a USAF Type II Altitude Training Flight .....	41
16.	Cumulative P(DCS) During a USAF HALO Training Flight .....	41
17.	Cumulative P(DCS) During a USAF Reconnaissance Flight .....	42
18.	Cumulative P(DCS) During a USAF T37-B Cross-Country Flight .....	43
19.	Cumulative P(DCS) During Control Profile of USAFAL Inflight Denitrogenation Study .....	44
20.	Cumulative P(DCS) During Experimental Profile with 12,000 ft Denitrogenation Stage in USAFAL Inflight Denitrogenation Study .....	44
21.	Cumulative P(DCS) During Experimental Profile with 16,000 ft Denitrogenation Stage in USAFAL Inflight Denitrogenation Study .....	45
22.	Pre-Breathe/Surface Interval Minimization; Process Illustration .....	47

## LIST OF TABLES

Table	Page
1. Training Datasets: Descriptions .....	18
2. Sample transcription of original USAFAL data for a breathing gas switch to specify completion within 1 min. ....	20
3. Pressure Conversion Functions .....	21
4. Log Likelihoods of USAFAL Training Dataset and Fitted Model Variants ....	24
5. Log Likelihoods of Combined USAFAL + USN/NMRI Training Dataset and Fitted Model Variants .....	26
6. Parameters for Logistic Models Fit to USAFAL Dataset .....	27
7. Parameters for Survival Models Fit to USAFAL Dataset .....	29
8. Parameters for Logistic Model I-C Fit to Combined USAFAL + USN/NMRI Dataset .....	30
9. Parameters for Survival Model S-IIa-C Fit to Combined USAFAL + USN/NMRI Dataset .....	31

## **ACKNOWLEDGEMENTS**

The authors are grateful to Dr. Andrew A. Pilmanis, Capt. John T. Demboski and other scientific staff of the USAF Armstrong Laboratory's High Altitude Protection Function for providing data from the USAF Armstrong Laboratory Hypobaric Decompression Sickness Database and for descriptions of flight profiles representative of those encountered by USAF personnel in various training and flight operations. The authors also gratefully acknowledge the provision of access to high-performance computers at the Central Computing Facility and Advanced Computing Laboratory of the University of California Los Alamos National Laboratory, Los Alamos, New Mexico, by Dr. Bruce R. Weinke, Director of the Advanced Computing Laboratory Computational Testbed for Industry. Such access facilitated completion of the highly compute-intensive parameter optimizations for the survival models that were undertaken in the latter parts of the program.



## PROJECT SUMMARY

Air Force personnel are routinely exposed to atmospheric decompressions that often present significant risk of decompression sickness (DCS). Management of these risks requires analytic methods able to: a) define risk/hazard envelopes for all routine and emergency decompressions encountered by USAF personnel; b) assess the DCS risks included or introduced in the contemplation or design of new operational procedures and equipment, and; c) support real-time monitoring of DCS risk incurred by personnel during various chamber and aircraft operations. Present work contributed to meeting these requirements through continued development and application of methods by which DCS risks during decompression profiles of arbitrary complexity are determined from statistical/biophysical models of *in vivo* gas exchange and bubble growth and resolution. Earlier *in vivo* gas exchange and bubble dynamics models were enhanced to accommodate continuous, time-linear changes in atmospheric pressure and respired gas. Survival analysis risk functions were added as alternatives to the logistic functions used in earlier work to transform computed bubble volumes into DCS probabilities. The resultant survival models enable prediction of the time courses of DCS risk accumulation and the most likely times of DCS onset, features that are theoretically inaccessible using the logistic approach. Using maximum likelihood, both logistic and survival models were fit to DCS incidence data from the USAF Armstrong Laboratory (USAFAL) and the USN Naval Medical Research Institute for a wide variety of decompression profiles, including both altitude and diving exposures. Selected models were used to evaluate DCS risk in decompression profiles representative of those encountered in USAF training and flight operations. Logistic models provided incidence-only correlations of the data superior to those provided by the survival models tested, although the latter provided more tenable estimates of DCS risk for representative USAF profiles of known low DCS risk. Survival models, which as a class show the greatest promise for operational applications, will better represent experience when fit to training datasets that include time of DCS occurrence, information that was lacking for hypobaric exposures in present training data. The models were incorporated into software that operates on personal computers, with a user-interface that allows profiles for processing to be read from pre-configured datafiles or interactively entered by the user from the keyboard, and that allows these profiles to be edited and saved for future processing. Model output is provided in a variety of graphical and tabular formats. System software, including a data transcription routine to serve as a software interface between the USAFAL Hypobaric Decompression Sickness Database and the present modeling system, was delivered for use and evaluation by USAFAL personnel.

## **1. INTRODUCTION**

### **1.1. Background and Significance**

Air Force personnel are routinely exposed to atmospheric decompressions that often present significant risk of decompression sickness (DCS). These exposures include chamber flights for physiologic training, flights in aircraft with hypobaric cabin pressures and decompressions in spaceflight for extravehicular activity (EVA). DCS risks incurred in such exposures have historically been assessed and managed on the basis of animal and human subjects' testing of prospective decompression profiles. Because results of such tests have had limited applicability to profiles other than those tested, new time-consuming and costly test series have been required as new profiles have been planned or encountered. In order to reduce or obviate the need for such tests, methods for evaluating DCS risk in hypobaric decompression profiles are required that enable reliable interpolations and extrapolations to be made from the large and diverse body of relevant laboratory and field experience that is already available. For reasonable expectations of success, such methods must rigorously integrate existing empirical information with an ever-evolving understanding of DCS etiology; be sufficiently flexible to accommodate revision and new factors as evolution of this understanding proceeds, and; include explicit consideration of biophysical factors that are known to be important in hypobaric decompression. Such factors include the influence of oxygen breathing on tissue-inert gas tensions, the influence of asymptomatic bubble formation on gas exchange during inflight denitrogenation, and the more predominant influences of Boyle's law effects on bubble dynamics during hypobaric decompression than during hyperbaric decompressions. The importance of these factors disqualifies calculations based on classical Haldanian models where gas is assumed always to remain in solution and DCS risk can only decrease monotonically with time after each decompression.

Present work entailed continued refinement and application of methods for such computations that meet the above criteria and incorporate quantitative consideration of the above biophysical factors. The methods use mathematical models of gas exchange and bubble dynamics in tissue to compute a hypothetical decompression stress throughout any given profile, from which DCS risk is estimated through a probability distribution function of either logistic or survival form. The models are parameterized from available DCS incidence data using maximum likelihood [34]. This statistical approach has several advantages. First, threshold decompressions below which DCS never occurs and above which DCS must always occur need not -- indeed, cannot -- be postulated. Instead, and consistent with a vast array of empirical information, DCS is recognized to occur with a given probability that is a function of the conditions that prevail before, during, and after decompression. Second, provided that the model function for the DCS probability is expressed in terms of independent variables common among different experimental and field decompression series, and that values for these variables are available for analysis from each series, the model can be fit to pooled DCS incidence data from all the series regardless of their diversity. The roles of given environmental and physiological variables can consequently be examined as common determinants of subject responses in widely different profiles. Finally, model parameterization through likelihood maximization forces model performance into best possible conformance with actual experience in the training dataset. This process obviates prejudice in model parameterization that otherwise can arise from preconceived ideas about parameter correspondence to biophysical properties of known value.

Once found through the fitting procedure, the optimized parameters are readily used in the model to compute DCS risk for arbitrary pressure/gas/time profiles, or conversely, to compute such profiles so that a given user-specified DCS risk is achieved but never exceeded. Algorithms have been developed to calculate: a) bottom time maxima in no-stop single or repetitive dive profiles; b) the staging required to bring a diver to surface when the no-stop limit has been exceeded, and; c) surface interval minima in repetitive dive profiles. In addition to computing minimum surface intervals for flying after diving in support of National Aeronautics and Space Administration's (NASA) Neutral Bouyancy Training Program [9,10] and evaluating existing guidelines for flying in commercial aircraft after typical recreational no-stop single and repetitive dives [11], earlier versions of the model were used to compute schedules for National Oceanic and Atmospheric Administration- (NOAA) and U.S. Navy-sponsored programs to study the use of nitrox and surface-interval oxygen breathing in repetitive dive profiles [3,4,7,8]. Profiles computed in the latter programs were successfully tested in both chamber [3,32] and open-water dives [4,33], with observed DCS incidences within specified limits.

## **1.2. Program Objectives**

Present program objectives were to refine bubble-based statistical models of DCS incidence, fit them to data extracted from the USAFAL Hypobaric Decompression Sickness Database, and evaluate resultant model performance on profiles representative of those encountered in USAF training and flight operations. Model refinements were to include modifications to enable more accurate treatment of pressure and respired gas profiles and to address the issue of DCS time of onset. Meeting these objectives required development of a software interface between the USAFAL Hypobaric Decompression Sickness Database and present system software. Delivery of software to support system operation and use by USAF personnel was a final objective that required enhancement of the system-user interface to simplify system use and increase system utility.

## **2. MODEL THEORY AND IMPLEMENTATION**

### **2.1. Model Structure**

#### **2.1.1. Probability Distribution Functions**

All models were based on the assumption that DCS is a probabilistic phenomenon. This requires that the probability of any given decompression outcome,  $P(\text{outcome})$ , which is defined as the sum of the probabilities of all possible outcomes, be unity:

$$P(\text{outcome}) = \sum_{i=0}^{(m-1)} P(i) = 1, \quad (1)$$

where  $P(i)$  is the probability of the  $i^{\text{th}}$  possible outcome. In order to simplify the analyses, only two possible outcomes were considered: Either DCS occurs or does not occur in any given decompression profile. Equation (1) then becomes:

$$P(\text{outcome}) = P(0) + P(1) = 1, \quad (2)$$

where  $P(1)$  = probability of DCS  $\equiv P(\text{DCS})$ , and;  
 $P(0)$  = probability of no DCS  $= 1 - P(1) = 1 - P(\text{DCS})$ .

The probability of DCS after any given decompression was then assumed to be some function,  $f$ , of various environmental and physiological effectors;  $x_1, x_2, x_3, \dots, x_j$ ; that are characteristic of the decompression:

$$P(\text{DCS}) = P(1) = f(x_1, x_2, x_3, \dots, x_j). \quad (3)$$

Depth, time at depth and respired gas composition were used in the present analyses, but are only a few of the possible effectors that could be considered.

Exact forms of the function  $f$  were developed using two different approaches.

##### **2.1.1.1. Logistic**

In the simplest approach, the probability of DCS in a given exposure profile  $P(\text{DCS})$  was assumed to be given by a logistic equation of the following general form:

$$P(\text{DCS}) = \frac{1}{1 + e^{-z}}, \quad (4)$$

where

$$z = \eta[\ln(ED_{50}) - \ln(D)]. \quad (5)$$

As shown in Eq. (5), the argument of the exponent,  $z$ , is a function of the parameter  $\eta$ , a dose  $D$  which is a measure of the decompression stress that causes DCS, and the  $ED_{50}$ . The latter is the value of the dose at which 50% of the diving population develops DCS.

After substitution of Eq. (5), Eq. (4) is readily transformed into the perhaps more familiar Hill equation:

$$P(\text{DCS}) = \frac{D^\eta}{D^\eta + ED_{50}^\eta}, \quad (6)$$

where the  $\eta$ , the  $ED_{50}$  and the parameters  $\beta_k$  in the function  $D = g(x_1, x_2, x_3, \dots, x_j)$  can be adjusted to fit the model to experience.

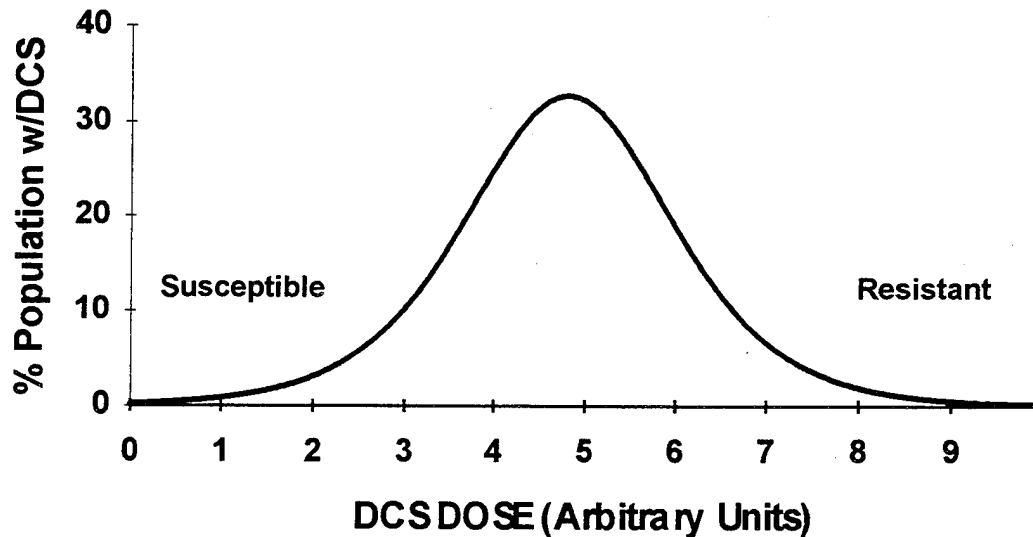


Figure 1. Frequency distribution of DCS incidence as a function of decompression stress or dose for a large population of individuals.

An essential feature of this formulation is that a given decompression profile is postulated to produce a certain stress or dose  $D$  to which different individuals are susceptible according to a bell-shaped frequency distribution. As schematized in Figure 1, different fractions of a large population of individuals will contract DCS after receiving various doses. Only a few susceptible individuals will bend at low doses. As the dose is increased, more individuals will be afflicted until a dose range is reached wherein most individuals will be afflicted. Finally, only few -- the most resistant -- individuals will require the highest doses to contract DCS. Integration of this distribution to give a cumulative distribution then yields the familiar sigmoidal dose-response curve of Equation (6) shown in Figure 2.

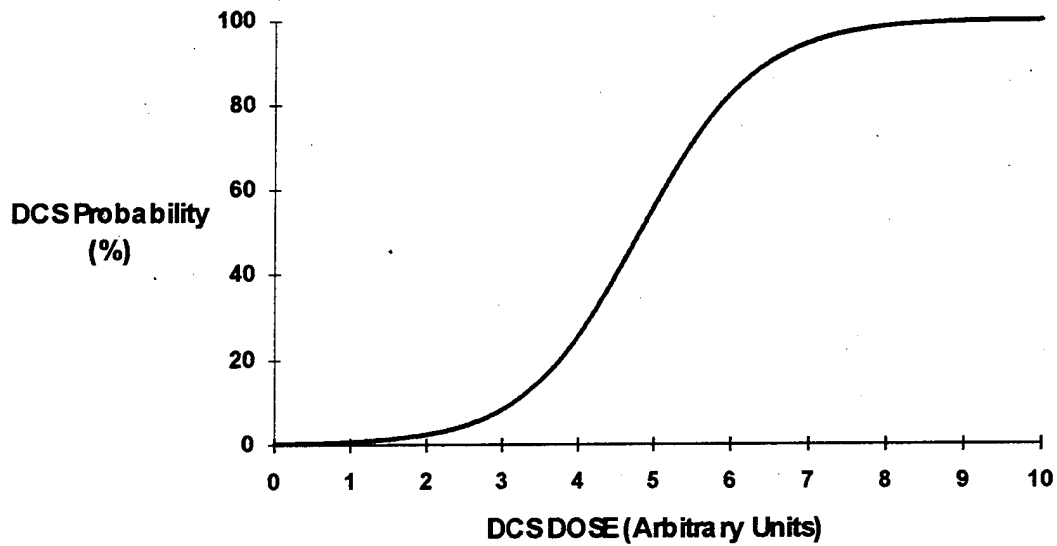


Figure 2. Cumulative dose-response distribution function obtained by integrating the frequency distribution shown in Figure 1.

The dose is given by another function,  $g$ , that embodies the dependence of the DCS probability on the hypothesized environmental and physiological effectors. This could be one of any number of different functions that incorporate particular notions of what constitutes decompression stress in a given decompression profile.

#### **2.1.1.2. Survival**

The logistic approach precludes any modeling of the time of DCS onset. As a result, model predictions provide a single  $P(\text{DCS})$  value for any profile without regard for when in the profile, no matter how complex, DCS is most likely to occur. Moreover, both model optimization and resultant model performance about any given profile are conditioned explicitly by only a single-valued dose parameter, and only indirectly by the shape of the dose-time curve. The shape of this curve, however, governs both the time-course of DCS risk accumulation and when in a profile DCS is most likely to occur, issues that are often of principal interest. These issues can be rigorously addressed by use of survival or failure time analysis. In this context, and assuming as before that DCS can either occur or not occur in any given profile, the probability  $P(S)_T$  that an individual remains free of DCS up to any time  $T$  in a profile is related to the probability  $P(\text{DCS})_T$  that the individual suffers DCS by that time:

$$P(S)_T = 1.0 - P(\text{DCS})_T. \quad (7)$$

The function  $P(S)_T$  is called the survivor function, and is given as a function of the instantaneous DCS risk  $r$  by [38]:

$$P(S)_T = \exp\left\{-\int_0^T r dt\right\}. \quad (8)$$

Hence, by substitution of Eq. (8) into Eq. (7):

$$P(DCS)_T = 1.0 - P(S)_T = 1.0 - \exp\left\{-\int_0^T r dt\right\}. \quad (9)$$

This expression is readily seen to replace the logistic distribution function [Eq.(4) or Eq.(6)] used in the simpler logistic approach. In turn, the risk function  $r = g'(x_1, x_2, x_3, \dots, x_j)$  with adjustable parameters  $\beta'_k$  replaces the dose function  $D = g(x_1, x_2, x_3, \dots, x_j)$  as the vehicle by which DCS probability is related to the various environmental and physiological effectors  $x_1, x_2, x_3, \dots, x_j$ . As with the dose function in the logistic approach, the instantaneous risk  $r$  can be given by any function that incorporates some measure or measures of decompression stress in a decompression profile. Importantly, however, the risk must be constrained to never assume negative values:  $r \geq 0$ . The cumulative risk is consequently a monotonically increasing function of time. The overall model is fit to experience by adjusting only the  $\beta'_k$  parameters. Unlike in the logistic approach, no other parameters arising from a probability distribution function appear.

### 2.1.2. Bubble Dynamics

Each of the models in present work was based on the well-accepted idea that DCS is caused by gas bubble growth that is caused in turn by decompression-induced gas-supersaturation. Measures of decompression stress that lead to the development of DCS were consequently postulated to be functions of modeled *in vivo* bubble volume(s).

A variety of quasi-physiological models had been developed and tested to model *in vivo* bubble dynamics before the present program was undertaken. Each assumed that the body consists of a number of parallel-perfused tissue compartments in which the kinetics of blood-tissue gas exchange are perfusion-limited, and in which a bubble can form if a sufficient gas supersaturation prevails. The earliest versions [3,7,29-31] used equations for bubble growth and resolution that neglected the effects of volume-dependent changes in bubble surface area and surface pressure, the latter arising from the well-known influence of surface tension. Each bubble in these models was effectively a cylinder, able to exchange gas with its surrounding tissue only through two parallel gas-tissue interfacial planes; one at either end of the cylinder. These "cylinder-slab" bubbles afforded the significant advantage that the equations describing their growth and resolution could be solved analytically to obtain the bubble volume at any given time in a profile. These models were similar in mathematical structure and performance to Thalmann's so-called Exponential-Linear (EL) model [22], on which the most recent USN DCS occurrence models are based [19]. In various implementations to compute the dose in logistic models of DCS incidence, however, these models were found to perform unsatisfactorily after optimization about highly heterogenous datasets that included diving, altitude and flying after diving data.

Present work was based on a second and more successful model class that had been developed using dynamic equations for bubbles of spherical geometry [11]. The equations include consideration of volume-dependent changes in bubble surface area and surface pressure. These models are schematized in Figure 3.

### n-parallel compartment Bubble Model

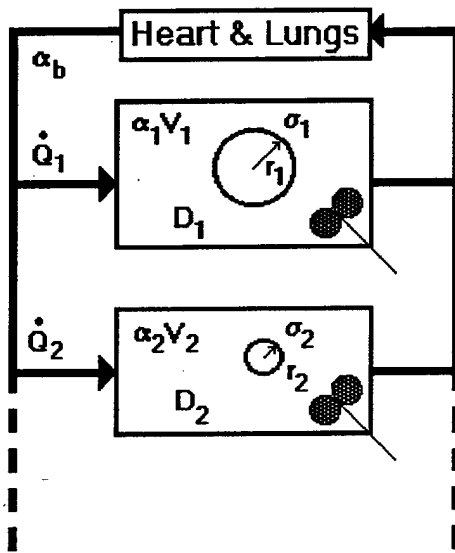


Figure 3. Schematic of the Bubble Dose/Risk Model. The volume of a spherical bubble in each of a number of tissue compartments is governed by modeled kinetics of gas exchange between blood, tissue and bubble. Gas exchange between tissue and blood follows perfusion-limited kinetics for which the tissue is considered "well-stirred." The growth and resolution of each bubble proceeds by gas diffusion between the bubble and its surroundings. With respect to the latter exchange, the tissue is **not** well-stirred. Bubble volume in each compartment was computed numerically as a function of the depth, inspired  $O_2$  fraction and time throughout a dive profile.

Arterial gas is assumed always equilibrated with alveolar gas as given by the alveolar gas equation. Thus, the arterial inert gas tension  $P_{aN_2}$  at ambient barometric pressure  $P_H$  is given by:

$$P_{aN_2} = FI_{N_2} \cdot \{ (P_H - P_{H_2O}) - P_{CO_2} (1 - 1/RQ) \}, \quad (10)$$

where  $FI_{N_2} = 1 - FI_{O_2}$  is the  $N_2$  fraction in inspired gas,  $RQ$  is the respiratory quotient,  $P_{H_2O}$  is the alveolar water vapor pressure, and  $P_{CO_2}$  is the alveolar carbon dioxide partial pressure.



Gas exchange between tissue and blood in each compartment  $i$  is governed by the gas solubility in blood ( $\alpha_b$ ) and by the compartment-specific gas solubility ( $\alpha_{t,i}$ ), blood flow ( $Q_i$ ) and compartmental volume ( $V_{t,i}$ ). When no bubble has nucleated in the compartment, only gas exchange between tissue and blood needs to be modeled. Such exchange occurs only after a change in the ambient pressure or inspired-oxygen fraction causes the arterial inert gas tension to change. The response at time  $t$  to an instantaneous change in arterial inert gas tension from  $P_{a,0}$  to  $P_{a,1}$  at time  $t=0$  is given by the well-known semi-exponential relation:

$$P_{t,i}(t) = P_{t,i}(0) + (P_{a,1} - P_{a,0}) \cdot \{1 - \exp(-t/\tau_i)\}, \quad (11)$$

where  $P_{t,i}(0)$  is the compartmental gas tension at time  $t=0$ , and  $\tau_i = (\alpha_{t,i} \cdot V_{t,i}) / (\alpha_b \cdot Q_i)$  is the compartmental gas exchange time constant. [It should be noted that the  $Q_i$  parameter is a blood flow in units of ml/min, *not* a perfusion rate in units of ml/ml/min. This definition is used to avoid implicit interdependence of the  $Q_i$  and  $V_{t,i}$  parameters.] Eq. (11), used in model implementations prior to the present program, does not provide an analytic solution for the tissue tension during or after a non-instantaneous, continuous change in arterial inert gas tension. In the present work, this deficiency was rectified by implementation of a more rigorous treatment that allows solutions to be found analytically when a given change in pressure or inspired-oxygen fraction is considered to occur linearly over a period of time from  $t_0$  to  $t_1$  [36]. The resultant change in arterial inert gas tension is modeled as a ramp with slope  $k$  given by:

$$k = \frac{(P_a - P_{a,0})}{(t - t_0)}. \quad (12)$$

The corresponding tissue inert gas tension at any time  $t$  in this ramp is:

$$P_{t,i}(t) = P_{t,i}(0) + k \cdot (t - t_0) - k\tau_i + k\tau_i \cdot \exp[-(t - t_0)/\tau_i]. \quad (13)$$

Accordingly, a given exposure profile is represented as a series of  $j=1, \dots, x, \dots, n$  ramps, each with starting time  $T_j$  and slope  $k_j$ . The dissolved inert gas tension in a given compartment at time  $t$  is then computed as the linear superposition of the responses to all ramps through time  $t$  in the prevailing ramp:

$$P_{t,i}(t) = P_{t,i}(0) + \sum_{j=1}^x k'_j (t - T_j) - \tau_i \sum_{j=1}^x k'_j + \tau_i \sum_{j=1}^x k'_j \cdot \exp[-(t - T_j)/\tau_i], \quad (14)$$

where  $k'_j = (k_j - k_{j-1})$  is the change in the arterial gas tension slope at  $T_j$ , and  $x$  is the subscript for the prevailing ramp.

With decompressions sufficient to produce gas supersaturation in any compartment, a bubble can "nucleate" and grow in the compartment by diffusion-limited exsolution of gas from its surroundings. Subsequent compression causes the bubble to dissolve with the same kinetic constraints. An expression for bubble growth and resolution derived by Van Liew and Hlastala [25,26] is used to model these processes:

$$dr_i/dt = -\alpha_{t,i} \cdot D_{t,i} \cdot (1 - P_{t,i}/P_{b,i}) (\lambda_i + 1/r_i), \quad (15)$$

where;  $\lambda_i = \sqrt{(\alpha_b Q_i) / (\alpha_{t,i} \cdot D_{t,i} \cdot V_{t,i})}$ ,

$D_{t,i}$  is the compartmental bulk diffusion constant of the gas, and  $P_{b,i}$  is the inert gas pressure in the bubble given by:

$$P_{b,i} = P_H - P_{mg} + 2\sigma_i/r_i + V_{b,i}M_i; \quad (16)$$

where  $P_{mg}$  is the sum of the tensions of the metabolic gases in the tissue, given by:

$$P_{mg} = P_{H_2O} + P_{CO_2} + P_{O_2},$$

and

$$V_{b,i} = 4\pi r_i^3/3.$$

Equation (15) gives the rate of change of the radius of a spherical bubble while accounting for: a) the divergence of the paths of gas molecules as they diffuse outward from the bubble, and; b) blood perfusion of the tissue around the bubble. This expression includes an implicit assumption that the tensions of the metabolic gases,  $P_{H_2O}$ ,  $P_{CO_2}$  and  $P_{O_2}$ , are always in equilibrium between tissue and bubble. Effects of gas-liquid surface tension,  $\sigma_i$ , and bubble-induced elastic deformation of the tissue are included via the last two terms in Equation (16). Because bubble nucleation *per se* is not modeled, inclusion of the surface pressure term,  $2\sigma_i/r_i$ , requires assumption of an ever-present nucleonic bubble of minimum or "critical" radius,  $r_i^{cr} > 0$ , for a bubble to grow in the compartment at reasonable model gas supersaturations. Thus, a bubble "nucleates" when  $r_i > r_i^{cr}$  and is extinguished when  $r_i < r_i^{cr}$ . The elastic recoil term,  $V_{b,i}M_i$ , is included with the assumption that the tissue is linearly elastic with an elastic modulus,  $M_i$ , given as a function of the Bulk Modulus,  $H_i$ :

$$M_i = H_i/v_i,$$

where  $v_i$  is the volume of tissue that is mechanically affected by the dynamics of a given bubble. Note that this volume is distinct from the compartmental volume,  $V_{t,i}$ , that appears in preceding expressions.

Effects of pressure changes on the volume of any supercritical bubble ( $r_i > r_i^{cr}$ ) are computed using Boyle's law, assuming instantaneous equilibration of metabolic gas tensions between tissue and bubble. Thus, in the absence of elastic forces ( $M_i=0$ ), the volume of a bubble after a pressure change from  $P_H^o$  to  $P_H$  is given by:

$$V_{b,i} = V_{b,i}^{\circ} \left( \frac{P_H^{\circ} - P_{mg}}{P_H - P_{mg}} \right), \quad (17)$$

where  $V_{b,i}^{\circ}$  is the volume of the bubble before the pressure change. In the presence of elastic forces ( $M_i > 0$ ), the expression for Boyle's Law resolves into a homogeneous quadratic equation in the bubble volume,  $V_{b,i}$ .  $V_{b,i}$  is thus the positive real root of this equation given by:

$$V_{b,i} = \frac{(P_H - P_{mg})}{2M} \left\{ -1 + \sqrt{1 + 4MV_{b,i}^{\circ} \left[ (P_H^{\circ} - P_{mg}) + MV_{b,i}^{\circ} \right] / (P_H - P_{mg})^2} \right\}. \quad (18)$$

It should be noted that Equations (17) and (18) neglect the effects of gas-liquid surface tension, which must be small except when considering pressure effects on very small bubbles.

As long as a supercritical bubble is present in a compartment, the dynamics of gas exchange between bubble and tissue and between tissue and blood cannot be modeled analytically using Eq. (14). The expression for  $P_{t,i}$  required to account for gas washin and washout via the blood and maintain mass balance between tissue and bubble is instead given in differential form as [24]:

$$dP_{t,i}/dt = \{(\alpha_b \cdot Q_i) \cdot (P_a - P_{t,i}) - P_{b,i} \cdot dV_{b,i}/dt - V_{b,i} \cdot dP_{b,i}/dt\} / (\alpha_{t,i} \cdot V_{t,i}), \quad (19)$$

which is solved numerically in conjunction with Eqs. (15-18) using Euler's method. The arterial inert gas tension,  $P_a$ , for each integration step in these calculations is obtained using:

$$P_a = k_x (t - T_x) + P_a^{\circ}, \quad (20)$$

where  $k_x$  is the slope of the prevailing arterial inert gas tension ramp [c.f., Eq. (12)] and  $P_a^{\circ}$  is the arterial inert gas tension at the beginning of the ramp.

In order to reduce computation time, the numerical integration interval,  $dt$ , is dynamically adjusted as a function of the rate of bubble growth or resolution,  $dr/dt$ , during isobaric stages. As the absolute value of  $dr/dt$  increases,  $dt$  is exponentially decreased, with a decay constant of  $\nu$ , from a maximum value of  $dt_{\max}$  to a minimum of  $dt_{\min}$ :

$$dt = (dt_{\max} - dt_{\min}) \cdot \exp(\nu \cdot |dr/dt|) + dt_{\min}. \quad (21)$$

The parameters  $dt_{\min}$ ,  $dt_{\max}$  and  $\nu$  are constants that are defined in a run parameterization file that is read at the outset of the calculations. Values used in the present work were:  $dt_{\min} = 0.01$  min,  $dt_{\max} = 1.0$  min and  $\nu = 0.0001$ . Boyle's Law effects greatly increase the sensitivity of results to changes in the integration interval, making use of a constant  $dt = dt_{\min}$  necessary during decompression or compression stages in which a bubble is present.

After the bubble dissolves, the compartmental inert gas tension is again computed by linear superpositioning the responses to the prevailing and subsequent ramps in arterial inert gas tension. Resumption of the calculations requires inclusion of the response to an additional "starting impulse" equal to the quantity  $(P_{t,i} - P_a)$  at the instant the bubble extinguished at time  $T_0$ . Thus, Equation (14) becomes:

$$P_{t,i}(t) = P_{t,i}(T_0) + \sum_{j=x}^n k'_j (t - T_j) - \tau_i \sum_{j=x}^n k'_j + \tau_i \sum_{j=x}^n k'_j \cdot \exp\left[-(t - T_j) / \tau_i\right] - (22)$$

$$(P_{t,i}(T_0) - P_a(T_0)) \cdot \{1 - \exp[-(t - T_0) / \tau_i]\}$$

Each dive profile to be processed is encoded as a sequence of nodes, with each node characterized by a pressure or depth, a respired  $O_2$  fraction, and a time elapsed since the preceding node. As described above, pressures and respired  $O_2$  fractions at successive nodes are connected in the time domain by straight lines to provide an unbroken description of the exposure profile. Each node can consequently be considered to describe the conditions prevailing at the end of a profile stage that may have been either a travel (compression or decompression) stage, an isobaric stage, a breathing gas switch stage, or a combination travel and breathing gas switch stage. The model is exercised on the profile by sequentially processing these stages, preserving the model state at the end of each stage as the initial state for the next. If a supercritical bubble is not present in a compartment when processing of a stage commences, the initial-state quantity  $(P_{t,i} + P_{mg} - 2\sigma / r_i^{cr})$  is first compared to the initial-state hydrostatic pressure to determine if bubble "nucleation" will occur in the stage. If this quantity exceeds the initial-state hydrostatic pressure, bubble nucleation will occur and processing is undertaken using Equations (15) - (20). If this first nucleation test fails, a provisional end-stage dissolved gas tension is evaluated for the compartment using Equation (14), or Equation (22) if a bubble had previously been present. An end-stage  $(P_{t,i} + P_{mg} - 2\sigma / r_i^{cr})$  in excess of the end-stage hydrostatic pressure also indicates that bubble nucleation will occur. With such a result, processing is undertaken from initial-state conditions using Equations (15) - (20). Otherwise the provisional end-stage dissolved gas tension is accepted and processing of the next stage is commenced.

### 2.1.3. Incorporation

In the logistic models, a single dose value must be specified for each exposure. This value was taken in present work as the largest volume attained by any bubble in any of the modeled compartments at any point in the profile. The adjustable  $\beta_k$  in the model function for the dose were consequently the  $\alpha_b Q_i$ ,  $\alpha_{t,i}$ ,  $V_{t,i}$ ,  $D_{t,i}$ ,  $r_i^{cr}$ , and  $M_i$  in the above gas exchange and bubble dynamics equations. Note that because of this dose definition, only a single compartment in these models governs the outcome of any given dive, despite the number of tissue compartments actually parameterized.

In the survival models, the instantaneous risk was taken as the weighted sum of the prevailing bubble volumes in all modeled compartments, with the compartmental weights given by an additional set of gain factors  $G_i$ :

$$r(t) = \sum_{i=1}^n \left\{ G_i \cdot \left( V_{b,i}(t) - v_i^{cr} \right) \right\} \quad (23)$$

where  $v_i^{cr}$  is the volume of the nucleonic bubble in compartment  $i$ . Thus, the adjustable parameters  $\beta'_k$  for the instantaneous risk  $r$  in Equations (8) and (9) included the  $\beta_k$  of the logistic models plus the gain factors  $G_i$ .

It is important to note that the models described to this point are theoretical constructs and that each provides only a framework for the processes that underlie development of a decompression dose or risk and the associated DCS probability. Relationships between various parameters are formalized into algebraic and logical expressions, but actual values of the parameters remain unspecified.

## 2.2. Model Parameterization

All models were parameterized using the method of maximum likelihood [34]. This method provides a means to find parameter values for a given model from actual experience. In so doing, it forces theory into best possible conformance with available data and provides quantitative measures of how well the data are described by the model for comparison of model performance to that of other models about the same data.

Similar to the definition of the individual outcome probability, the likelihood,  $l_i$ , of an individual decompression,  $i$ , is defined as the product of the probabilities of possible outcomes. Additionally, however, the contribution of each probability is conditioned by actual experience through the influence of an outcome variable,  $\chi$ . Thus, the definition of the likelihood under the present constraints, where DCS either does or does not occur, is given by:

$$l_i = P_i(1)^{\chi_i} * P_i(0)^{(1-\chi_i)}, \quad (24)$$

where  $\chi_i = 0$  if DCS does not occur in exposure  $i$  and  $\chi_i = 1$  if DCS occurs.

In logistic models,  $P_i(1)=P_i(\text{DCS})$  and  $P_i(0)=1-P_i(\text{DCS})$ . In survival models,  $P_i(0)$  is the probability that the entire exposure is completed DCS-free, given by Eq. (8) with  $T$  equal to a value  $T_3$  high enough for the risk  $r$  to decay to zero after the exposure, e.g., 24 hr [38]:

$$P_i(0) = P(S)_{T_3} = \exp\left\{-\int_0^{T_3} r dt\right\}. \quad (25)$$

The corresponding implementation of Eq. (9) for  $P_i(1)$  in these models is somewhat problematic, because there is often considerable uncertainty about the precise time of DCS onset. There is usually greater certainty, however, that an individual was DCS free at some time  $T_1$  before the time  $T_2$  at which DCS symptoms or signs were first reported. Accordingly, there is a probability  $P(S)_{T_1}$  that an individual remains DCS-free through time  $T_1$ , and a separate probability  $P(\text{DCS})_{T_1, T_2}$  that the individual develops DCS in the interval between times  $T_1$  and  $T_2$ . The joint probability  $P(S_{T_1}, \text{DCS}_{T_2})$  of these two outcomes is given as the product of the probabilities  $P(S)_{T_1}$  and  $P(\text{DCS})_{T_1, T_2}$ :

$$\begin{aligned} P(S_{T_1}, \text{DCS}_{T_2}) &= P(S)_{T_1} \cdot P(\text{DCS})_{T_1, T_2} \\ &= \exp\left\{-\int_0^{T_1} r dt\right\} \cdot \left[1.0 - \exp\left\{-\int_{T_1}^{T_2} r dt\right\}\right] \end{aligned} \quad (26)$$

Thus, Eq. (26) is used for  $P_i(1)$  in survival models when time of DCS-onset information is available for the exposure. Substituting Eq. (26) for  $P_i(1)$  and Eq. (25) for  $P_i(0)$  into Eq. (24), the likelihood of exposure  $i$  is given by:

$$\begin{aligned} l_i &= [P(S_{T_1}, \text{DCS}_{T_2})]^{\chi_i} \cdot [P(S)_{T_3}]^{(1-\chi_i)} \\ &= \left[\exp\left\{-\int_0^{T_1} r dt\right\} \cdot \left(1.0 - \exp\left\{-\int_{T_1}^{T_2} r dt\right\}\right)\right]^{\chi_i} \cdot \left[\exp\left\{-\int_0^{T_3} r dt\right\}\right]^{(1-\chi_i)} \end{aligned} \quad (27)$$

When DCS occurs in the exposure but time of onset information  $T_1$  and  $T_2$  is lacking, the likelihood is given by Eq. (27) with  $T_1=0$  and  $T_2=T_3$ :

$$l_i = \left[1.0 - \exp\left\{-\int_0^{T_3} r dt\right\}\right]^{\chi_i} \cdot \left[\exp\left\{-\int_0^{T_3} r dt\right\}\right]^{(1-\chi_i)} \quad (28)$$

Regardless of the model type, the likelihood,  $L$ , of a series of  $n$  decompressions is the product of the individual likelihoods:

$$L = \prod_{i=1}^n l_i = \prod_{i=1}^n \left\{ P_i(1)^{x_i} * [P_i(0)]^{(1-x_i)} \right\}. \quad (29)$$

Evaluation of Eq. (29) about a dataset of  $n$  exposures using a model with a given set of parameter values therefore yields a likelihood value that quantitatively embodies information from both theory (the model structure) and experience (the dataset outcomes).

Numerical difficulties occasioned by extremely small values of the likelihood *per se* are obviated by working with the logarithm of the likelihood,  $LL = \ln(L)$ . Equation (29) then becomes:

$$LL = \sum_{i=1}^n \left[ x_i \ln(P_i(1)) + (1-x_i) \ln(P_i(0)) \right]. \quad (30)$$

Datasets usually consist of a collection of different profiles, each of which describes the exposures of several subjects. The log likelihood of a dataset of  $n_j$  exposures on each of  $p$  different profiles ( $j=1, 2, \dots, p$ ) is computed using the following analog of Equation (30):

$$LL = \sum_{j=1}^p \left[ DCS_j \ln(P_j(1)) + (n_j - DCS_j) \ln(P_j(0)) \right], \quad (31)$$

where  $DCS_j$  is the number of exposures in which DCS occurred on profile  $j$  and  $(n_j - DCS_j)$  is the number of DCS-free exposures on profile  $j$ . The utility of Eq. (31) is limited in survival models. A separate summation element is required in Eq. (30) for each exposure in which DCS occurs on a given profile if, as is usually the case, the  $T_1$  and  $T_2$  times for DCS onset differ for the different occurrences. In such models, the condensation of Eq. (30) into Eq. (31) is consequently applicable for only those profiles in which no DCS occurred.

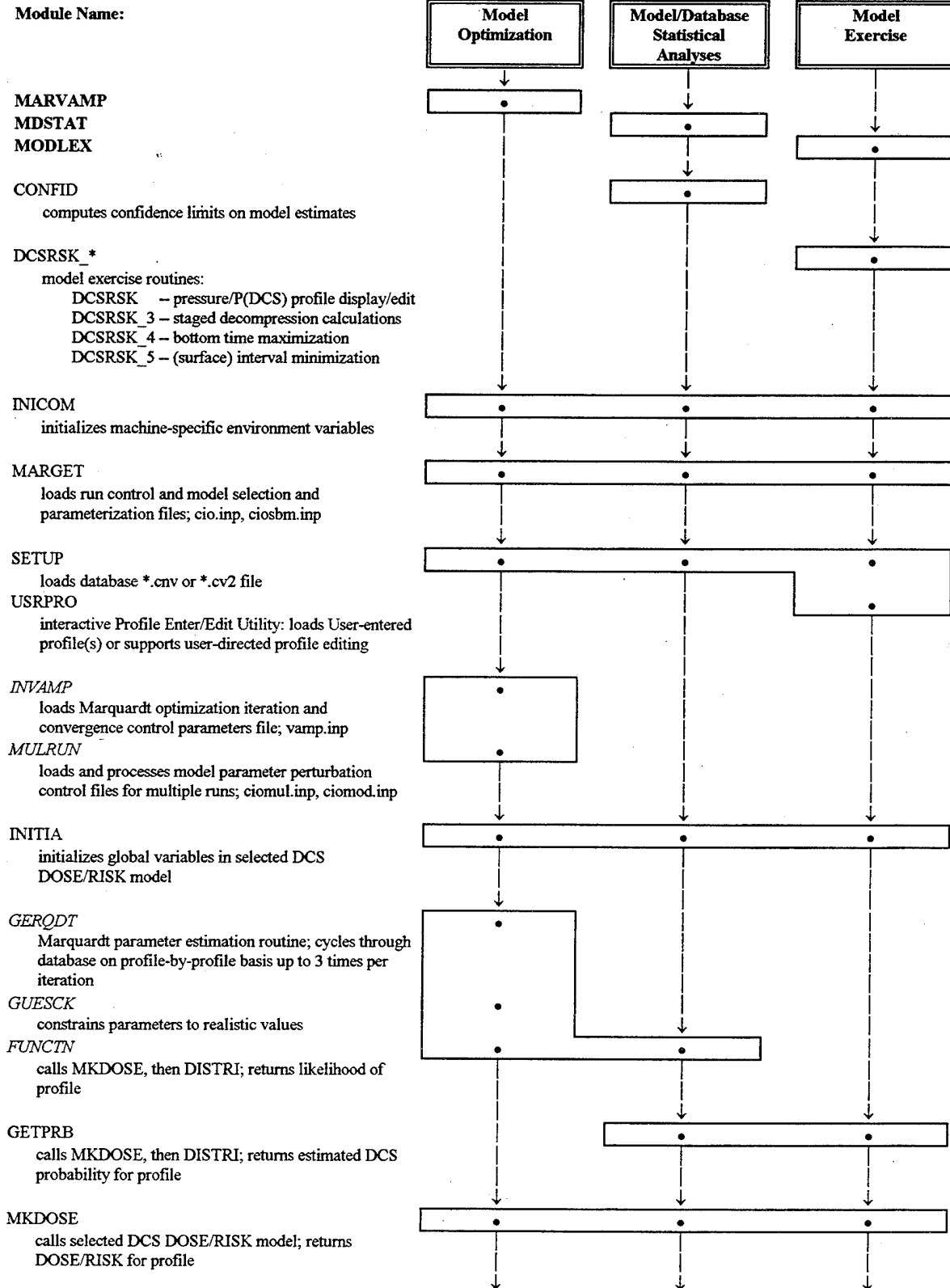
Importantly, as a measure of how well the dataset is correlated by the model, the likelihood is largest when the parameterized model best correlates the data. "Best fit" or optimized parameters for a model are consequently found by using an algorithm that systematically adjusts the parameter values until the likelihood is maximized. An iterative nonlinear parameter estimation routine based on Marquardt's algorithm [13,14] was modified to constrain parameters to positive values and used for parameter optimization. In order to ensure that parameters giving the global maximum likelihood were obtained, each of a series of separate optimizations were run from different sets of starting parameter values. The latter were obtained by systematic perturbation of those in various user-specified starting sets. This parameter reset/reoptimization recycling was rendered even more necessary by the presence of discontinuities in model behavior over certain regions of parameter space. In many instances, small changes in one or another parameter value could cause a given tissue compartment to "drop out" of the fit by no longer governing the outcome of any exposure in the dataset. Under such circumstances, further adjustments of the parameters for the compartment no longer took place, and the procedure would proceed to converge to the same likelihood attainable with the involved compartment omitted from the outset. Restart from a different set of initial parameter values was required to determine if inclusion of the compartment could indeed lead to higher final likelihoods.

### **2.3. Software Implementation**

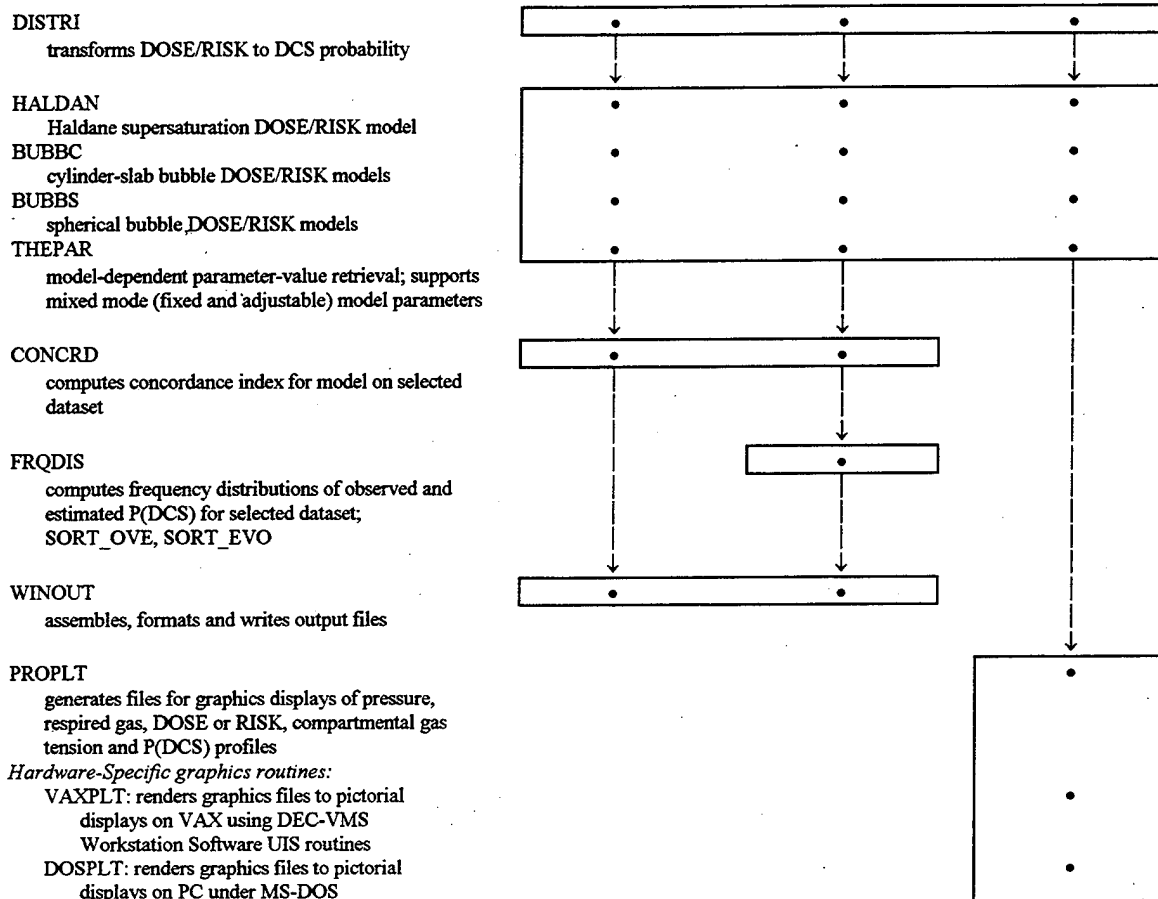
System software was implemented with several important features to enhance flexibility beyond that provided by the analytic approach *per se*. All code is written in FORTRAN-77, largely conforming to generic standards with only few widely supported DEC/VAX extensions to maintain portability among various computing environments. Thus, various system software components are routinely run in a variety of operating system environments (VAX/VMS, UNIX, MSDOS) on a variety of different machines. More importantly, an object-oriented software architecture was used that facilitates continued development and implementation of new model formulations. The three principal analytic/modeling functions of the present system: model optimization, calculation of model/dataset statistics and model exercise, are supported by various combinations of software modules as illustrated in Figure 4. Each module supports its respective subfunction without any context-dependent modifications. This object-oriented structure enhances developmental flexibility by minimizing coding requirements for implementation of new DCS DOSE/RISK models or even entire applications, such as the future transitioning of model exercise routines to support real-time decompression assessment and profiling. It also ensures that identical functionality is provided to the various applications in which any given module is used, thereby reducing error.



Figure 4. Model System Software Modules and Organization



## Statistical Bubble Dynamics Algorithms for DCS Incidence Assessment



The Model Exercise routines of the system for operation on personal computers running the DOS operating system were delivered to USAFAL on completion of the present program. Essential features of system use and operation were outlined in a **readme** file that was included with the release in both ASCII (**readme.**) and Microsoft® Word for Windows™ V.2.0 (**readme.doc**) format. A hardcopy of the contents of this file is appended to this report (APPENDIX B).

### 3. MODEL OPTIMIZATION

#### 3.1. Training Data

The parameters of a given model, and hence the performance of the model, can vary depending on the contents of the database to which the model is fit. This variation in model performance diminishes as the model embodies an ever more accurate and complete description of the processes that underlie the modeled outcomes. However, with a fully accurate and complete description of DCS etiology still beyond our grasp, it is important in "calibrating" a model for particular applications that the training dataset include as many profiles as possible that are typical of those to which the model will be applied. Accordingly, a training dataset compiled from the

USAFAL Hypobaric Decompression Sickness Database was used. The dataset consisted of profile descriptions and corresponding DCS incidences for 1194 person-exposures in experimental chamber-flights undertaken at USAFAL between 1983 and the present. A breakdown of the dataset in terms of gender and raw DCS incidence is given in Table 1. The summary description in the table does not reflect the relative homogeneity of the dataset contents. As illustrated in Figure 5, the dataset contained altitude exposures that consisted predominantly of single square ascents to one of relatively few altitudes between 8,000 and 30,000 ft. This homogeneity was reflected in results of the model fits. Model behavior about the USAFAL dataset combined with an additional more heterogeneous dataset obtained from the Naval Medical Research Institute (NMRI) in Bethesda, MD, was also examined. The NMRI dataset used was a subset, as described by Parker, *et al.* [19], of the Primary Air and Nitrox Database described in detail by Weathersby, *et al.* [37]. This subset was used to develop the USN LE1 DCS risk model for decompressions from hyperbaric exposures [19]. Summary information about these data are included in Table 1. In conformance with present model ability to accommodate breathing gases with only a single inert gas diluent, the datasets included only profiles in which oxygen, air or some other N<sub>2</sub>-O<sub>2</sub> mix was breathed.

Table 1. **TRAINING DATASETS: DESCRIPTIONS**

Source	# Profiles	Total # Person-Exposures	DCS Incidence (%)
USAFAL Hypobaric Decompression Sickness Database	= # Person-Exposures	1194 (1052 male) (142 female)	33.59 (37.26) (6.34)
USN/NMRI (Ref 19); Subset of Primary Air and N <sub>2</sub> O <sub>2</sub> Database (Ref 37)	799	2383	5.81*
USAFAL + USN/NMRI Combined	--	3577	15.08*

\* computed with 75 "marginal" cases each assigned an outcome  $\chi = 0.1$

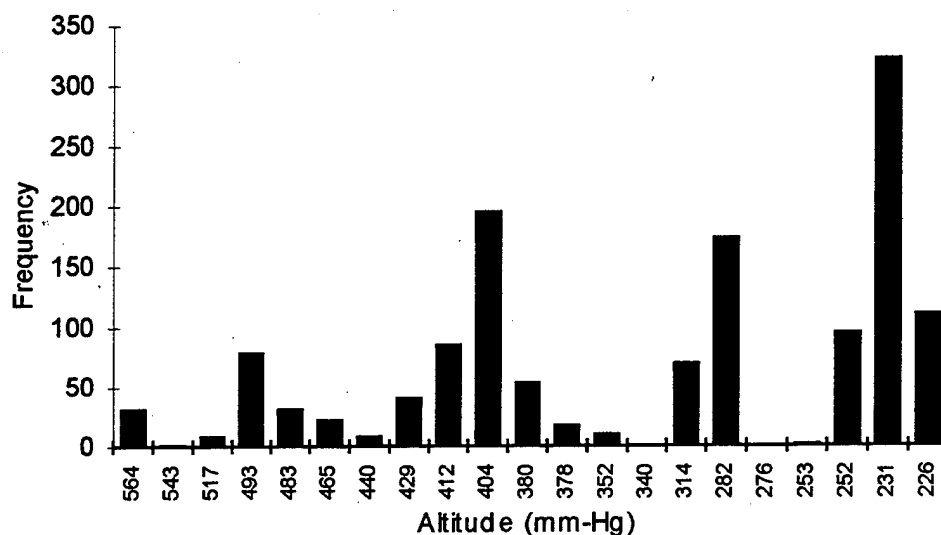


Figure 5. Altitude frequency distribution of stages of 5 minutes duration or more in the USAFAL dataset. Short ascents to 5,000 ft followed by return to ground for ear-and-sinus checks are not included. The total stage count exceeds the number of person-exposures by only 176 due to inclusion of profiles with inflight denitrogenation stages. Stages are clustered in frequency about altitudes of 404, 282 and 231 mm-Hg (16,500, 25,000 and 29,500 ft).

Compilation of the USAFAL dataset entailed off-loading required information from the USAFAL Hypobaric Decompression Sickness Database into an intermediate file, and transcription of this file into another file of format directly usable by present system software. The transcription process was performed by software written for this purpose, and included insertion of nodes in each profile description as required to complete any specified breathing gas switch within a certain maximum period of time.

Reflecting the content of the host USAFAL database, profile descriptions in the intermediate file contained only a single node for each breathing gas switch. This node specified the pressure and the time since the preceding node at which the breathing gas switch was effected, but a subsequent node specifying completion of the switch was lacking. For present work, the alveolar inert gas tension was nominally assumed to attain its post-switch steady-state value linearly over a period of 1 min after the breathing gas switch occurred at the mouth. This period usually completed within the time specified by the original gas switch end-node. In such cases, the transcription routine inserted a node for the 1 min point after the specified switch and decremented the time for the original end-node entry by 1 min. The pressure value for the added node was obtained by linear interpolation in native units (mm-Hg) between the pressure prevailing when the gas switch was begun and the pressure at the original gas switch end-node. The process is illustrated in Table 2, where data for a breathing gas switch is shown as originally specified and as transcribed. The original data specified a switch of inspired gas from air to 100% O<sub>2</sub> on

commencement of a 4-min ascent to 16,500 ft from ground-level at 500 ft. The transcribed data effect completion of the switch 1 min into the ascent without otherwise affecting the ascent. In rare cases where the original data specified completion of a breathing gas switch before expiration of the nominal 1 min switch period, the original data were not altered.

**Table 2. SAMPLE TRANSCRIPTION OF ORIGINAL USAFAL DATA  
FOR A BREATHING GAS SWITCH TO SPECIFY  
COMPLETION WITHIN 1 MIN**

<u>Original</u>			<u>Transcribed</u>		
Pressure (ft/10 <sup>3</sup> )	FIO <sub>2</sub>	Time (min)	Pressure (ft/10 <sup>3</sup> )	FIO <sub>2</sub>	Time (min)
0.5	0.21	-1.00	0.5	0.21	-1.00
16.5	1.00	4.00	3.8	1.00	1.00
			16.5	1.00	3.00

The data transcription routine also included provisions to write all last stages at ground level with time-indefinite (t=0) end-nodes and to automatically append: a) a time-indefinite node at ground level to any profile originally recorded with descent to ground in the last stage, and; b) any nodes required to ensure that air breathing was specified during all time-indefinite last stages. These provisions were not important for optimization of the logistic models about the dataset because bubble volume maxima that determined the doses were invariably attained during flight. However, provisions for precise specification of "post-flight" stages were vital for optimal results using survival models because bubble persistence after a flight causes continued DCS risk accumulation. Downloaded data did not contain any explicit time of DCS occurrence information, so the latter models were fit using the incidence-only forms of the risk integrations. These integrations were continued in each time-indefinite profile end stage until all bubbles resolved in the modeled compartments or until  $T_3$ =time of last arrival at ground + 5 days, whichever occurred first.

By default, calculations for any given profile were begun assuming subject saturation with air (FIO<sub>2</sub>=0.21) at 1 atmosphere absolute pressure (sea level), and that ground level was at sea level. The pressure of this reference surface condition could be reset on a profile-by-profile basis in the dataset by insertion of a first node entry with pressure equal to the new surface pressure and time equal to -1.0. Exercise of this reset option is illustrated by the data in Table 2, reflecting that the USAF Armstrong Laboratory is located in San Antonio, Texas, at an altitude of 500 ft above sea-level. The transcription routine inserted surface pressure reset nodes as required.

The USN/NMRI data were obtained in machine-readable form, which the transcription software was also written to recognize and render into format directly usable by present system software. The format of the original data is described in detail in Ref. 37.

Internal calculations were performed with all pressures in units of absolute atmospheres. Conversions from other units were performed using the relations given in Table 3.

Table 3. **PRESSURE CONVERSION FUNCTIONS.**

Pressure, P, in atmospheres = f(x); pressure, x, in various units.

Units of x	P=f(x)
mm-Hg	$P = x/760$
altitude, $10^3$ ft	$P = b_0 + b_1x + b_2x^2 + b_3x^3 + b_4x^4;$
	$b_0 = 1.0$
	$b_1 = -3.6174735 \times 10^{-2}$
	$b_2 = 5.3473326 \times 10^{-4}$
	$b_3 = -4.2249023 \times 10^{-6}$
	$b_4 = 1.8369812 \times 10^{-8}$
fswg	$P = x/33.066 + 1$
ffwg	$P = x/33.9139 + 1$
mswg	$P = x/10.337 + 1$
mfwg	$P = x/10.079 + 1$
psia	$P = x/14.7$

Coefficients for the altitude-to-atmosphere conversion polynomial were obtained by linear regression about the U.S. Standard Atmospheric Pressure Table. Where necessary for data display, internal pressures were inverted to any of the other units using the inverse of the appropriate function in Table 3. Atmosphere-to-altitude unit inversions were an exception. In these cases, the polynomial in Table 3 was numerically inverted to within  $\pm 100$  ft using Newton's method.

Model optimization about a given dataset was undertaken as specified in a run parameterization file that contained starting parameter values to initialize the Marquardt nonlinear parameter estimation process. A switch for each model parameter could be set in this file to either fix the value of the parameter at that specified in the file or allow the parameter to "float" so that its best-fit value could be found. Different model variants were thus created by fixing different sets of parameters while allowing the remaining parameters to float. The long computation times required for model optimization limited the number of models that could be tested to those defined in Tables 4 and 5 in the following section. Except as noted, three compartments were parameterized at each optimization startup with other model constants defined as follows:

$$\begin{aligned}
 RQ &= 0.85; & P_{O_2} &= 25 \text{ mm-Hg;} \\
 \sigma_i &= 30 \text{ dyne/cm; all } i & P_{CO_2} &= 45 \text{ mm-Hg;} \\
 & & P_{H_2O} &= 47 \text{ mm-Hg.}
 \end{aligned}$$

Note that consistent with the notation in Section 2.1.2, both the alveolar and compartmental  $P_{CO_2}$  were assumed equivalent.

### **3.2. Results and Evaluation**

Computation of the gradient of the parameter vector is an essential step in each iteration of the optimization process. This gradient is used to test for parameter convergence and, if the fit has not yet converged, to adjust the prevailing parameter values for the next iteration. It is also used to evaluate the standard errors of the parameters after convergence has been attained. Thus, the estimated standard error for a parameter is zero-valued when its element in the gradient is zero, as occurs when the parameter does not govern the outcome of *any* profile in the dataset. In logistic model fits to the USAFAL dataset, standard errors were invariably zero-valued for all parameters associated with more than one model compartment or tissue, indicating that only a single compartment in these models could be fit to these data.

How well any given model correlates or fits a dataset can be evaluated by comparing the likelihood (or log likelihood, LL) of the model about the dataset to the likelihoods of the perfect and appropriate null models for the dataset. The perfect model likelihood is that given when each exposure in the dataset is assigned a probability equal to the observed DCS incidence for that exposure. In contrast, the null likelihood is that given for the dataset using the most reduced version of the model being tested. For logistic models, the null likelihood is that obtained when the probability of DCS in each exposure is assigned a value equal to the mean DCS incidence for the entire dataset. Provided that the data are structured so that outcomes do not determine the risk, this null likelihood is applicable to incidence-only survival models as well. However, many profiles in the USAFAL dataset include altitude stages that were ended with recompression to ground level upon occurrence of DCS. The resultant profiles and their attendant DCS risks were consequently governed by the DCS outcomes. Stated another way, the USAFAL data implicitly include time of DCS occurrence information that biases the risks computed on an incidence-only basis.<sup>1</sup> The applicable null model is consequently one in which the instantaneous risk is constant throughout all hypobaric stages, regardless of the pressure. The constant risk value, and hence the null LL, must be found by optimizing the null model about the dataset. Survival null LL values are usually substantially lower than the corresponding incidence-only null LLs, but survival null LLs for the present datasets are unknown, pending implementation of the capability to calculate them in the present analytic system.

The logarithms of the perfect, incidence-only null and fitted model likelihoods for the USAFAL dataset are shown in Table 4. As indicated in the table, the perfect model LL is zero; a circumstance that arises because the dataset was configured with only a single exposure for each profile. This perfect model log likelihood is consequently a trivial value of limited utility in examination of model fits to this dataset or any composite dataset that includes the USAFAL

---

<sup>1</sup>This is a particularly important problem in altitude exposure profiles. In hyperbaric exposures, profiles usually end with the subject at surface and at continued risk of DCS undiminished by the last travel stages to surface. In contrast, final return to ground after a hypobaric exposure ameliorates or extinguishes continued accumulation of DCS risk.

dataset as a subset. Fitted model LLs, however, are substantially higher than the incidence-only null LL for all logistic models tested. Thus, each fitted logistic model describes the data significantly better than the null model ( $p < 0.000001$ ; likelihood ratio test and Chi-squared distribution [34]). Model III, in which both the nucleonic bubble size and tissue elasticity were included as adjustable parameters, correlated the data with the highest LL of the three logistic models examined.

In contrast, the LL of each of the two survival models tested is substantially lower than the incidence-only null LL, even though the models were fit in their incidence-only forms. This arises because, as noted above, the dataset contained implicit time of DCS occurrence information. Without explicit  $T_1$  and  $T_2$  values for completion of the calculations prescribed by Eq. (27), the 0 -  $T_3$  periods of the incidence-only calculations encompassed the 0 -  $T_1$  periods when subjects, later to develop DCS, were actually DCS-free. Moreover, DCS risk accumulation during  $T_2$  -  $T_3$  periods was averted with profile termination on occurrence of DCS, causing the 0 -  $T_1$  periods to constitute most of the time at which the subjects were at risk in the incidence-only calculations. As a result, falsely high estimated risks during "safe" periods in these profiles failed to register in the likelihood and condition that fits because the products,

$$\left( \exp \left\{ - \int_0^{T_1} r dt \right\} \right) \cdot \left( 1.0 - \exp \left\{ - \int_{T_1}^{T_2} r dt \right\} \right), \text{ could not be evaluated. With this situation prevailing by}$$

design in all profiles terminated due to DCS occurrence, the overall fits of the incidence-only survival models were degraded. Importantly, termination of the altitude exposures on occurrence of DCS and the aversion of continued DCS risk accumulation tended to make the effective  $T_3$  values used to terminate the risk calculations nearly equal to the  $T_2$  values -- the times of DCS onset. The resultant fits therefore approximate time-of-onset fits with high uncertainties in the  $T_1$  values. It is not unusual for a time of onset fit to have an LL value about its training dataset much lower than the incidence-only null while still exceeding the survival null LL. For example, the incidence-only null LL of the subset of the USN/NMRI dataset used in present work is -528.46. In comparison, the survival null LL of the same dataset is a reported -888.28, while the LL of the best fitting LE1 model tested about the dataset was -687.77 [19].

The two survival models differed from one another only in that the compartmental oxygen and carbon dioxide gas tensions were assigned zero values for model S-IIb, while they were assigned their nominal non-zero values for model S-IIa. Significantly, the elimination of these gases from participation in gas exchange and bubble dynamics in model S-IIb afforded a substantial improvement in model ability to correlate the USAFAL dataset.



Table 4. LOG LIKELIHOODS OF USAFAL TRAINING DATASET AND FITTED MODELS

Model	Parameters		Log Likelihood	c-index
	Fixed*	Fitted*		
Perfect	NA	NA	-0.0	--
Null, Incidence Only	NA	NA	-762.1	--
<b>Logistic:</b>				
I	$\sigma_i = 30.0$ dyne-cm $r_i^{cr} = 3.0$ $\mu$ m $M_i = 0.0$	$ED_{50}, \eta$ $\alpha_b Q_i, \alpha_{t,i}, V_{t,i}, D_{t,i}$	-675.7	0.788
II	$\sigma_i = 30.0$ dyne-cm $M_i = 0.0$	$ED_{50}, \eta$ $\alpha_b Q_i, \alpha_{t,i}, V_{t,i}, D_{t,i}$ $r_i^{cr}$	-673.2	0.796
III	$\sigma_i = 30.0$ dyne-cm	$ED_{50}, \eta$ $\alpha_b Q_i, \alpha_{t,i}, V_{t,i}, D_{t,i}$ $r_i^{cr}, M_i$	-645.8	0.759
<b>Survival:</b>				
S-IIa	$\sigma_i = 30.0$ dyne-cm $M_i = 0.0$	$G_i$ $\alpha_b Q_i, \alpha_{t,i}, V_{t,i}, D_{t,i}$ $r_i^{cr}$	-941.9	0.492
S-IIb <sup>②</sup>	$\sigma_i = 30.0$ dyne-cm $M_i = 0.0$	$G_i$ $\alpha_b Q_i, \alpha_{t,i}, V_{t,i}, D_{t,i}$ $r_i^{cr}$	-874.8	0.595

\* gas exchange compartment,  $i=1$

②  $P_{O_2}=0$ ;  $P_{CO_2}=0$

The c-index, which is the probability of concordance or agreement between predicted probability and observed response, provides a means for assessing the predictive ability of an incidence-only model [12]. In the present context, it is a measure of how well model predictions for a given dataset provide the same order,  $P(DCS) < P(\text{no-DCS})$  or  $P(DCS) > P(\text{no-DCS})$ , as was observed for each of all possible pairs of individual exposures in the dataset in which one

exposure resulted in DCS and the other did not. This measure is consequently similar to that obtained using discriminant analysis, but it obviates the need for arbitrary specification of a probability below which a prediction is taken as "negative" and above which a prediction is taken as "positive". The c-index is computed as:

$$c = \{(\# \text{ of concordant pairs}) + 0.5 \cdot (\# \text{ tied pairs})\} / \text{total \# of pairs.} \quad (32)$$

A given pair of exposures is a concordant pair when the subject with DCS has a higher P(DCS) than the subject without DCS. The pair is a tied pair when both subjects have the same P(DCS). Finally, the pair is a discordant pair when the subject without DCS has a higher P(DCS). With possible values ranging from 0 to 1.0, a computed c of 1.0 indicates perfect predictive ability, while a c of 0.5 indicates random prediction. A c-index greater than about 0.8 is considered to indicate that the model provides satisfactory predictions of the outcomes of individual trials.

Values of the c-index for the present logistic model variants on the USAFAL training dataset are included in Table 4. The c-indices for logistic models I and II are not appreciably different, and each nearly fulfill the acceptability criterion, suggesting that the models should have acceptable predictive ability. The c-index for model III, however, is lower than those for models I and II, despite having the highest LL.

A c-index for a survival model about a dataset can also be calculated by exercising the model in its incidence-only form on all profiles in the dataset. C-indices shown in Table 4 for survival models IIa and IIb about their training dataset were computed in this fashion. The relatively poor incidence-only correlations provided by these models are reflected in correspondingly low c-index values. The 0.492 value for model S-IIa indicates model predictive ability no better than random variation. The 0.595 value for model S-IIb is substantially better, but is well below the 0.8 acceptability criterion. These values can be compared to the incidence-only c-index of 0.69 presently calculated for our implementation of the USN LE1 model [19] on its USN/NMRI training dataset.

The log likelihoods and c-indices of logistic model variant I and survival model variant S-IIa fit to the combined USAFAL + USN/NMRI dataset are given in Table 5. The models are distinguished from those optimized about the USAFAL dataset alone by the addition of a "-C" suffix. As for its correlation of the USAFAL dataset alone, the logistic model I-C provides a good incidence-only correlation of the expanded and more heterogeneous combined dataset. Its LL about the dataset exceeds the incidence-only null LL by about 310 LL units. The c-index about this dataset, 0.83, also exceeds that achieved by any logistic model about the USAFAL dataset alone. Repeating the pattern evident for survival model fits to the USAFAL dataset, the LL of the survival S-IIa-C model is 225 LL units less than that of the incidence-only null LL. Notably, its 0.748 incidence-only c-index is substantially improved over that of the S-IIa model fit to the USAFAL data only.

Table 5. **LOG LIKELIHOODS OF COMBINED USAFAL + USN/NMRI TRAINING DATASET AND FITTED MODELS**

Model Variant	Parameters		Log Likelihood	c-index
	Fixed*	Fitted*		
Perfect	NA	NA	-24.4	--
Null, Incidence-Only	NA	NA	-1517.1	--
<b>Logistic:</b>				
I-C	$\sigma_i = 30.0$ dyne-cm $r_i^{cr} = 3.0$ $\mu$ m $M_i = 0.0$	$ED_{50}, \eta$ $\alpha_b Q_i, \alpha_{Li}, V_{Li}, D_{Li}$	-1197.6	0.831
<b>Survival:</b>				
S-IIa-C	$\sigma_i = 30.0$ dyne-cm $M_i = 0.0$	$G_i$ $\alpha_b Q_i, \alpha_{Li}, V_{Li}, D_{Li}$ $r_i^{cr}$	-1748.1	0.748

\* gas exchange compartments,  $i=1, 2, 3$

As originally conceived, the models can also be validated by comparing values of their optimized parameters to those that are expected or otherwise considered reasonable for the parameters. If the model structure provides a fully accurate and complete description of the processes leading to the observed outcomes, parameters that correspond to physically measureable quantities should assume values, when optimized, that agree with results of direct measurements of those quantities. Parameters for the present logistic model variants optimized about the USAFAL dataset are given in Table 6. As noted above, each of the models failed to show any variance about any more than one blood-tissue gas exchange compartment, even though fits to three compartments were attempted in all cases. Gas exchange half-times, as computed from the parameters for the single fitted compartment in each model, are also shown.

Table 6. PARAMETERS FOR LOGISTIC MODELS FIT TO USAFAL DATASET

Model Variant	Model Component	Parameter						
I	<i>Dose-Response function</i>	ED <sub>50</sub> (ml)	η (dimensionless)					
		0.02040	2.20420					
	<i>Tissue, i</i>	α <sub>t</sub> (ml/ml/atm) (x10 <sup>2</sup> )	V <sub>t</sub> (ml/bubble)	D <sub>t</sub> (cm <sup>2</sup> /min) (x10 <sup>2</sup> )	α <sub>h</sub> Q (x10 <sup>6</sup> )	r <sup>cr</sup> (μm)	M (atm/ml)	Gas Exchange Half-time (min)
	1	2.30003	0.28588	6.78027	2.52984	3.0*	0.0*	1801.6
II	<i>Dose-Response function</i>	ED <sub>50</sub> (ml)	η (dimensionless)					
		0.02027	2.04755					
	<i>Tissue, i</i>	α <sub>t</sub> (ml/ml/atm) (x10 <sup>2</sup> )	V <sub>t</sub> (ml/bubble)	D <sub>t</sub> (cm <sup>2</sup> /min) (x10 <sup>2</sup> )	α <sub>h</sub> Q (x10 <sup>6</sup> )	r <sup>cr</sup> (μm)	M (atm/ml)	Gas Exchange Half-time (min)
	1	2.37853	0.26890	6.51436	2.66111	2.30511	0.0*	1665.9
III	<i>Dose-Response function</i>	ED <sub>50</sub> (ml)	η (dimensionless)					
		0.05529	3.83096					
	<i>Tissue, i</i>	α <sub>t</sub> (ml/ml/atm) (x10 <sup>2</sup> )	V <sub>t</sub> (ml/bubble)	D <sub>t</sub> (cm <sup>2</sup> /min) (x10 <sup>2</sup> )	α <sub>h</sub> Q (x10 <sup>6</sup> )	r <sup>cr</sup> (μm)	M (atm/ml)	Gas Exchange Half-time (min)
	1	23.47162	2.96223	683.017	25.3157	19.4705	9.51127	19030.

\*Fixed

The computed gas exchange half-time of the single compartment in logistic model I is high at 1802 min, but compares in magnitude to the half-time obtained in a much different adynamic survival analysis of severe DCS incidence in altitude exposures [28]. The fitted value of the  $N_2$  solubility in this compartment also compares favorably to values of  $1.36 \times 10^{-2}$  ml(BTPS)/ml/atm and  $7.27 \times 10^{-2}$  ml(BTPS)/ml/atm for  $N_2$  in water and olive oil, respectively [6]. The tissue blood perfusion rate,  $Q'$  (ml/ml/min), can be computed from the  $\alpha_b Q$  and  $V_t$  parameters using a measured value for  $\alpha_b$  ( $\approx 1.41 \times 10^{-2}$  ml(BTPS)/ml/atm, [17]) and the relation:

$$Q' = (\alpha_b Q) / (V_t \alpha_b). \quad (33)$$

A value of  $Q' = 0.0006277$  ml/ml/min is obtained, which can be compared to a value for resting skeletal muscle of about 0.04 - 0.07 ml/ml/min. The high gas exchange half-time of the compartment in this model is consequently the result of a low  $Q'$  value, indicating involvement of a poorly perfused compartment. Similarly, the fitted value of the compartmental bulk diffusivity of  $N_2$  exceeds the expected value of about  $1.3 \times 10^{-3}$  cm<sup>2</sup>/min by over an order of magnitude. The high value in the latter case may arise from the model structural property that bubbles can grow or dissolve only via gas exchange with the tissue *per se*; not with the blood in the capillaries that perfuse the tissue. Gas exchange between bubbles and tissue perfusate may, in fact, proceed more directly than the model structure allows, forcing the effective diffusivity in neglect of such exchange to be as high as emerged in present results.

Parameters common to logistic model variants I and II do not vary by large amounts between the two models. Coupled with the near-equal LLs and c-indices of these models, no advantage could be substantiated for optimizing the bubble nucleonic radius in the logistic models. In contrast, all parameters in model III that also appear in models I and II vary widely in value from their correspondents in models I and II. The bulk  $N_2$  diffusivity in model III is two orders of magnitude greater than in either model I or II. The nucleonic bubble radius is nearly one order of magnitude greater than in model II. Finally, the  $\alpha_t$ ,  $V_t$  and  $\alpha_b Q$  parameters combine to give an implausible gas exchange half-time in excess of 13 days. The improved LL of model III over those of models I and II is thus attained through neglect of any tissue-blood gas exchange and the ascription of variance in the dataset entirely to pressure and elastic effects on bubbles of size only marginally greater than nucleonic size. This result is arguably an artifact of lack of variability in the dataset sufficient to constrain all the parameters in this more complex model. Results with this model cannot yet support the utility of adding tissue elastic recoil to the logistic models.

Parameters for the two survival models optimized about the USAFAL dataset are given in Table 7, including derivative compartmental gas exchange half-times. Notably, the gas exchange half-times for the single compartment in each model are low compared to those of the single compartments in each of the logistic models. This result is not driven by the emergence of high compartmental blood perfusion rates, which are physiologically reasonable at 0.021 ml/ml/min and 0.017 ml/ml/min for models S-IIa and S-IIb, respectively. The lower gas exchange half-times instead are more closely related to the relatively low compartmental volumes,  $V_t$ , which emerged from optimization with values more than two orders of magnitude smaller than their counterparts in the logistic models. The compartmental bulk  $N_2$  diffusivity is lower in model S-IIa than those obtained in the logistic models, but still appears unphysiologically high. The corresponding diffusivity in model S-IIb is greater than those for the logistic models. Coupled with the low

values of  $V_t$ , these diffusivities remain sufficiently high to allow very rapid bubble growth during or immediately after decompression when supersaturations are maximal.

Table 7. PARAMETERS FOR SURVIVAL MODELS FIT TO USAFAL DATASET

Model Variant	Parameter							
	$G_i$ ( $\text{min}^{-1}\text{ml}^{-1}$ )	$\alpha_t$ ( $\text{ml/ml/atm}$ ) ( $\times 10^2$ )	$V_t$ ( $\text{ml/bubble}$ )	$D_t$ ( $\text{cm}^2/\text{min}$ )	$\alpha_h Q$ ( $\times 10^8$ )	$r^{cr}$ ( $\mu\text{m}$ )	M ( $\text{atm/v}$ )	Gas Exchange Half-time (min)
S-IIa	52.5945	4.8549	0.00082	0.0263	23.8103	6.1493	0.0*	115.887
S-IIb <sup>②</sup>	146.8572	4.9418	0.00082	0.1123	19.3200	9.0555	0.0*	144.913

\*Fixed

②  $P_{O_2}=0$ ;  $P_{CO_2}=0$

Parameters for logistic model I-C optimized about the combined USAFAL + USN/NMRI dataset are given in Table 8. As indicated by the presence of parameter entries for three compartments, correlation of this larger, more heterogeneous dataset required three compartments. Gas exchange half-times computed from the parameters for each compartment are also shown. The highest half-time of the three compartments is notably lower at 443 min than the 1802 min half-time of the single compartment for this model optimized about the USAFAL dataset alone. The range of half-times for the three compartments spans the expected range. Fitted values of the  $N_2$  solubility in compartments 1 and 3 are also reasonable. Only the solubility value for compartment 2, with a very short gas exchange half-time, is unphysiologically high. Values of the compartmental blood perfusion rates are 0.00131 ml/ml/min, 95.0 ml/ml/min and 0.0303 ml/ml/min for tissues 1, 2 and 3, respectively. Thus, an unphysiologically high  $N_2$  solubility and perfusion rate for compartment 2 are the drivers for the short half-time of this compartment. Fitted values of the bulk diffusivity of  $N_2$  in the different tissues span a rather wide range of values from about three orders of magnitude lower than the expected value of  $1.3 \times 10^{-3} \text{ cm}^2/\text{min}$  to more than two orders of magnitude greater than this expected value.

Table 8. **PARAMETERS FOR LOGISTIC MODEL I-C FIT TO COMBINED USAFAL + USN/NMRI DATASET**

Model Component	Parameter						
<i>Dose-Response function</i>	$ED_{50}$ (ml)	$\eta$ (dimensionless)					
	0.00848	1.72538					
<i>Tissue, i</i>	$\alpha_t$ (ml/ml/atm) ( $\times 10^2$ )	$V_t$ (ml/bubble)	$D_t$ ( $\text{cm}^2/\text{min}$ ) ( $\times 10^2$ )	$\alpha_h Q$ ( $\times 10^4$ )	$r^{cr}$ ( $\mu\text{m}$ )	M	Gas Exchange Half-time (min)
1	1.17923	0.24078	46.59325	0.04446	3.0*	0.0*	442.7
2	257.76586	0.00366	0.00243	49.08610	3.0*	0.0*	1.3
3	4.37171	0.04600	1.10883	0.19681	3.0*	0.0*	70.8

\*Fixed

Fitted parameters for survival model S-IIa-C are given in Table 9. Compared to logistic model I-C, survival model S-IIa-C exhibits a notable lack of a gas exchange compartment with a half-time the order of 1 min. Accordingly, with the exception of compartment 1, compartmental perfusion rates of 0.00218, 0.00001 and 0.00012 ml/ml/min, respectively, are uniformly low. Again, compartmental diffusivities span an unphysiologically wide range. Nucleonic bubble sizes were optimized in this model and range in radius from 5 to 26  $\mu\text{m}$ .

Table 9. **PARAMETERS FOR SURVIVAL MODEL S-IIa-C FIT TO COMBINED USAFAL + USN/NMRI DATASET**

Tissue, i	Parameter							
	$G_i$ ( $\text{min}^{-1}\text{ml}^{-1}$ )	$\alpha_t$ ( $\text{ml/ml/atm}$ ) ( $\times 10^2$ )	$V_t$ ( $\text{ml/bubble}$ )	$D_t$ ( $\text{cm}^2/\text{min}$ ) ( $\times 10^3$ )	$\alpha_h Q$ ( $\times 10^7$ )	$r^{cr}$ ( $\mu\text{m}$ )	M ( $\text{atm/v}$ )	Gas Exchange Half-time (min)
1	94710.3	0.29926	0.00795	0.00067	2.43912	5.2805	0.0*	67.58
2	59079.4	0.00746	3.25132	0.00187	5.03285	4.6949	0.0*	333.99
3	35.8941	0.04352	0.08336	696.56849	1.41438	26.4806	0.0*	177.78

\*Fixed

In summary, no model emerged from optimization without one or more fitted parameters having a value outside of the physiological or expected range. The discrepancies between fitted and expected parameter values indicate that none of the models tested include a complete representation of the processes underlying DCS symptom onset. This is not surprising given that factors other than bubble volume, such as blood-bubble interactions, complement activation, etc., are also thought to play important roles in DCS etiology. However, such problems do not themselves render the optimized models unsuitable for predictive purposes. Rather, it must be recognized that the models emerging after optimization accommodate behavior that may not be included in the conceptual framework that was originally adopted to formulate their structure. Optimization overcomes some of the limitations of this structure by providing parameter values that force it to conform to experience nonetheless.

In addition to the above quantitative assessments, the fit of a model to any given dataset can also be illustrated as shown in Figures 6 through 10. In order to produce such illustrations, the training dataset is first sorted in order of increasing estimated DCS probability, and then divided into successive categories containing a fixed number of trials each that span consecutive ranges of estimated probability. Each graph is then constructed by showing the average observed DCS incidence for the trials in each category vs. the maximum probability in the respective categorical range of estimated probabilities. A so-called "perfect fit" results in observed incidences falling on the indicated line of identity [% DCS Observed = % DCS Estimated]. However, uncertainties in both the estimations and the observations can allow substantial non-significant deviations from the line of identity, which limits the utility of these presentations in assessing "goodness-of-fit" [18]. Such presentations are consequently useful principally for illustrative purposes.



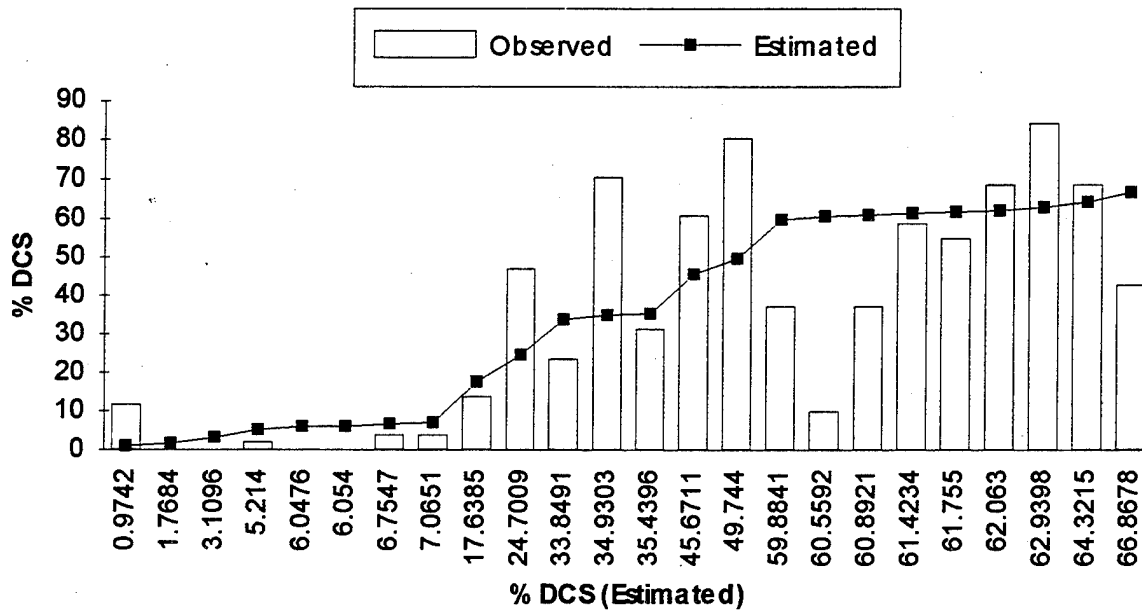


Figure 6. Distribution of observed vs. estimated DCS incidences for logistic model I on its USAFAL training dataset. The distribution shows the dataset after subdivision into categories of increasing estimated  $P(\text{DCS})$ , with approximately 50 trials/category. Only the maximum risk for each category is shown on the abscissa. The "Estimated" line is the identity line given by  $\% \text{ DCS Observed} = \% \text{ DCS Estimated}$ .  $P(\text{DCS})$  is over-estimated for categories with average observed DCS incidences below the identity line and under-estimated for categories with average observed incidences above the identity line.

Figure 6 shows the distribution of observed vs. estimated DCS incidences for logistic model I on its USAFAL training dataset. Estimated DCS incidence tends to increase with observed DCS incidence, but relatively large differences between observed and estimated incidences illustrate correspondingly severe limitations of model resolution. The model tends to overestimate DCS risk in profiles with average observed risks of less than about 12%.

The distribution of observed vs. estimated DCS incidences for this model (I-C) optimized about the combined USAFAL + USN/NMRI dataset is shown in Figure 7. A tighter and more satisfying correspondence between estimated and observed incidences is evident in this case. Altitude exposures with both high observed and high estimated DCS predominate in the right-most regions of the distribution.

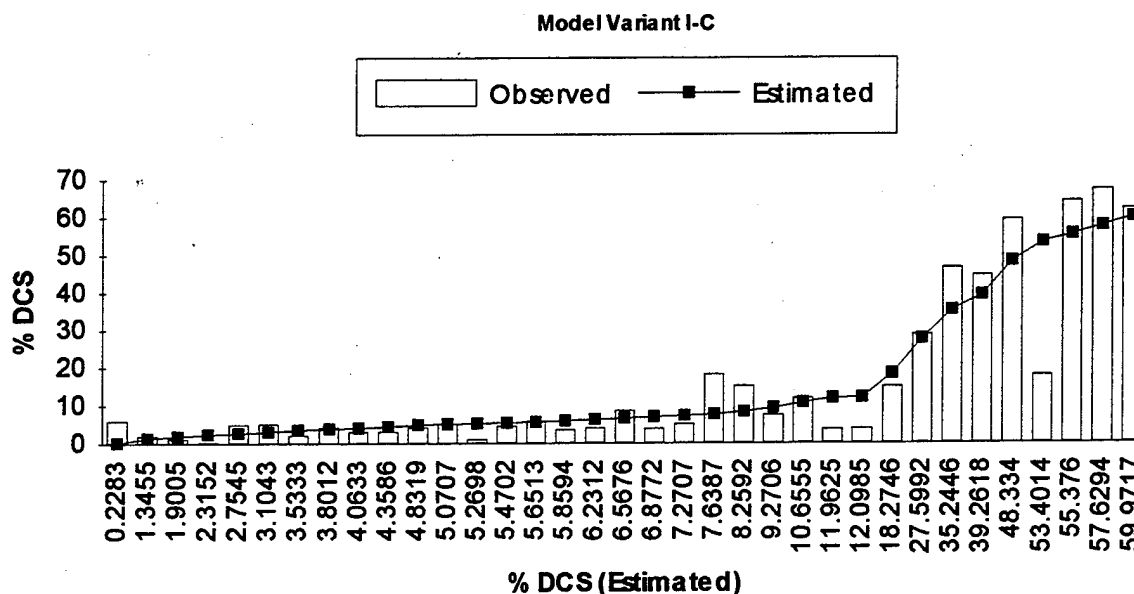


Figure 7. Distribution of observed vs. estimated DCS incidences for logistic model I-C on its combined USAFAL + USN/NMRI training dataset. The distribution shows the dataset after subdivision into categories of increasing estimated  $P(\text{DCS})$ , with approximately 100 trials/category. Only the maximum risk for each category is shown on the abscissa. The "Estimated" line is the identity line given by  $\% \text{ DCS Observed} = \% \text{ DCS Estimated}$ .  $P(\text{DCS})$  is over-estimated for categories with average observed DCS incidences under the identity line and under-estimated for categories with average observed incidences above the identity line.

The distribution of observed vs. estimated DCS incidences for model I-C about the USAFAL data subset shown in Figure 8 is similar to that shown in Figure 6 for model I, which was fit to only the USAFAL dataset. The c-index for model I-C about the USAFAL dataset, 0.780, is also comparable to that for model I about the same dataset. The model consequently correlates experience for both diving and altitude exposures very well, supporting the hypothesis that common etiological processes are responsible for DCS incidence in both hypo- and hyperbaric regimes. However, model I-C shows the same tendency as model I to overestimate DCS risk in altitude exposures with observed DCS risks below about 15%.

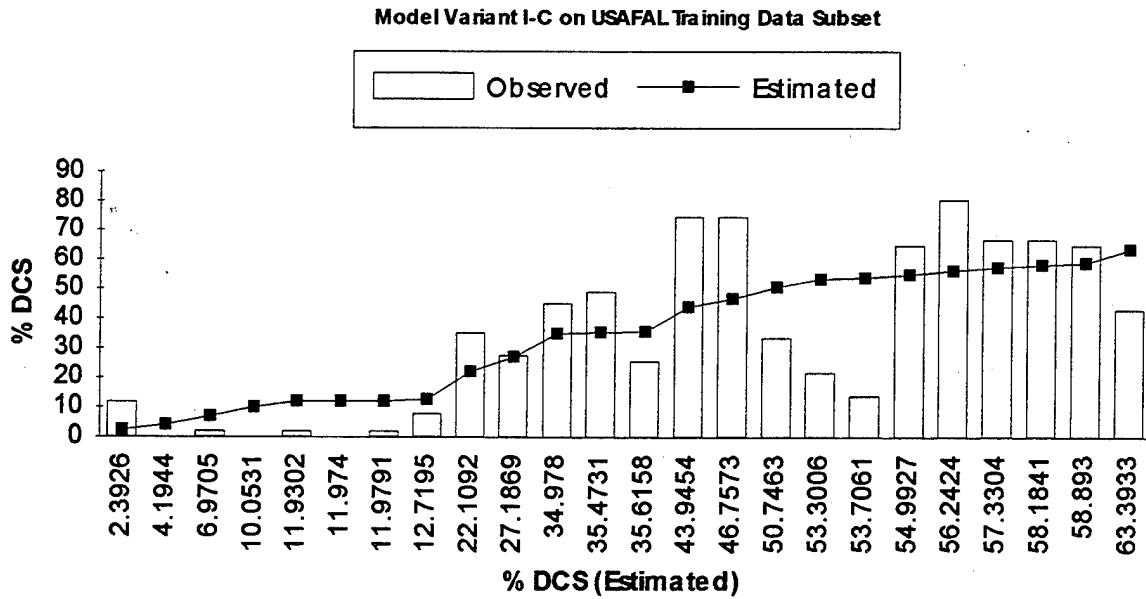


Figure 8. Distribution of observed vs. estimated DCS incidences for logistic model I-C on the USAFAL subset of its USAFAL + USN/NMRI training dataset. The distribution shows the dataset after subdivision into categories of increasing estimated  $P(\text{DCS})$ , with approximately 50 trials/category. Only the maximum  $P(\text{DCS})$  for each category is shown on the abscissa. The "Estimated" line is the identity line given by  $\% \text{ DCS Observed} = \% \text{ DCS Estimated}$ .  $P(\text{DCS})$  is over-estimated for categories with average observed  $P(\text{DCS})$  below the identity line and under-estimated for categories with average observed incidences above the identity line. The c-index for this model variant on the USAFAL dataset is 0.780.

The distribution of observed vs. estimated DCS incidences for survival model S-IIb about its USAFAL training data is shown in Figure 9. The poorer incidence-only correlation that this model provides of its training data is evident in the larger deviations from identity in a larger number of risk categories than appears in Figures 6 - 8. This model reproduces the tendency suggested in Figures 6 and 8 for models I and I-C, respectively, to produce bimodal distributions of observed vs. estimated DCS incidences about this dataset. Such bimodality arises in each case from extreme over-estimation of observed DCS risk for select groups of exposures in the dataset. The specific profiles about which these anomalies in performance occur for each model have yet to be identified.

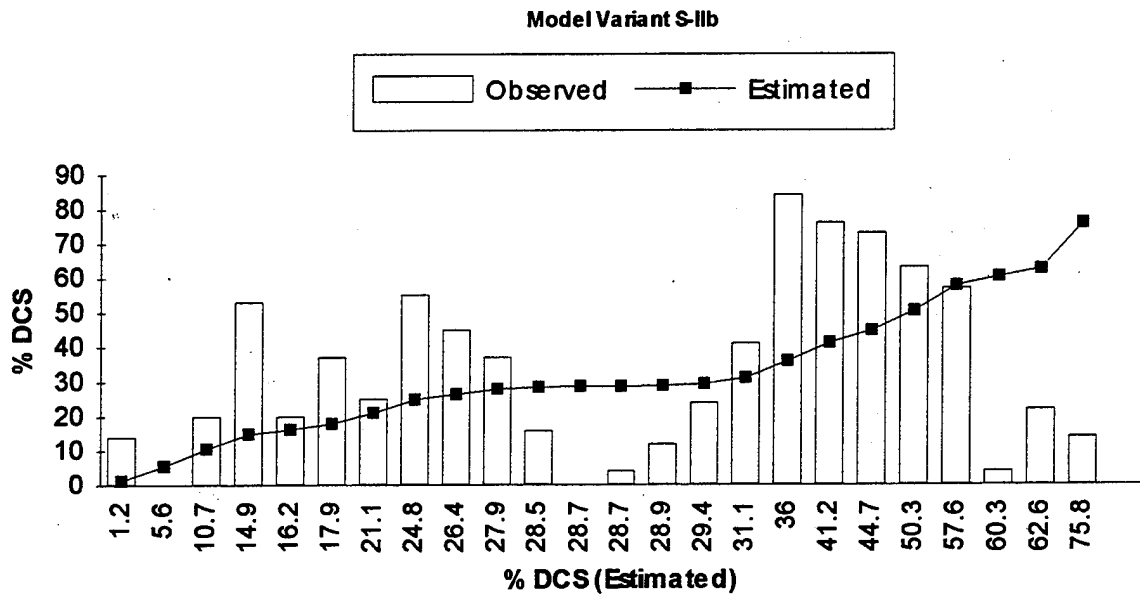


Figure 9. Distribution of observed vs. estimated DCS incidences for survival model S-IIb on its USAFAL training dataset. The distribution shows the dataset after subdivision into categories of increasing estimated  $P(\text{DCS})$ , with approximately 50 trials/category. Only the maximum  $P(\text{DCS})$  for each category is shown on the abscissa. The "Estimated" line is the identity line given by  $\% \text{ DCS Observed} = \% \text{ DCS Estimated}$ .  $P(\text{DCS})$  is over-estimated for categories with average observed  $P(\text{DCS})$  below the identity line and under-estimated for categories with average observed incidences above the identity line.

The distribution of observed vs. estimated DCS incidences for survival model S-IIa-C about the USAFAL subset of its USAFAL + USN/NMRI training data is shown in Figure 10. The pattern is similar to that in Figure 9 for model S-IIb, but with larger deviations from identity.

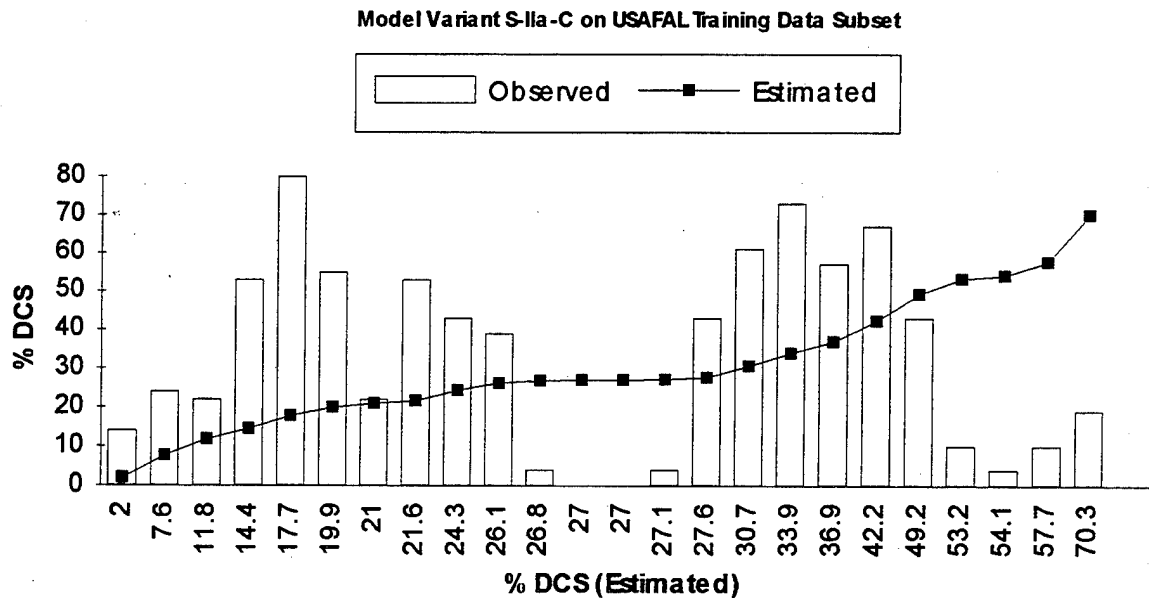


Figure 10. Distribution of observed vs. estimated DCS incidences for survival model S-IIa-C on the USAFAL subset of its USAFAL + USN/NMRI training dataset. The distribution shows the dataset after subdivision into categories of increasing estimated  $P(\text{DCS})$ , with approximately 50 trials/category. Only the maximum  $P(\text{DCS})$  for each category is shown on the abscissa. The "Estimated" line is the identity line given by  $\% \text{ DCS Observed} = \% \text{ DCS Estimated}$ .  $P(\text{DCS})$  is over-estimated for categories with average observed  $P(\text{DCS})$  below the identity line and under-estimated for categories with average observed incidences above the identity line. The incidence-only c-index for this model variant on the USAFAL dataset is 0.469.

## 4. APPLICATION

### 4.1. Specific Examples

Model performance can be illustrated by application to hypobaric exposures representative of those encountered in US Air Force training and flight operations. Descriptions of the profiles analyzed in the following sections are given in APPENDIX A using the node format used by the present modeling system. These descriptions include information about the inspired gases in the profiles that is omitted from the following figures for clarity.

#### 4.1.1. Type I Altitude Training Flight

Figure 11 shows results of analysis of a USAF Type I Altitude Training Flight using logistic model I-C. The light line traces the pressure profile of the exposure, while the heavy line shows the corresponding estimated  $P(\text{DCS})$ . Each  $P(\text{DCS})$  value shown was computed by transforming the largest bubble volume in the modeled compartments at the indicated time

The values are consequently *not* the cumulative values that are obtained using survivor or failure time analysis, but serve only to illustrate quantitative performance of the model about the particular profile. The only P(DCS) value of rigorous analytic significance is the maximum P(DCS) attained during the profile. This value in the present case is nearly 84%. Although it is attained during the short 2 min stage at 35,000 ft, it must be reiterated that this time of occurrence information is analytically meaningless in the logistic, incidence-only approach.

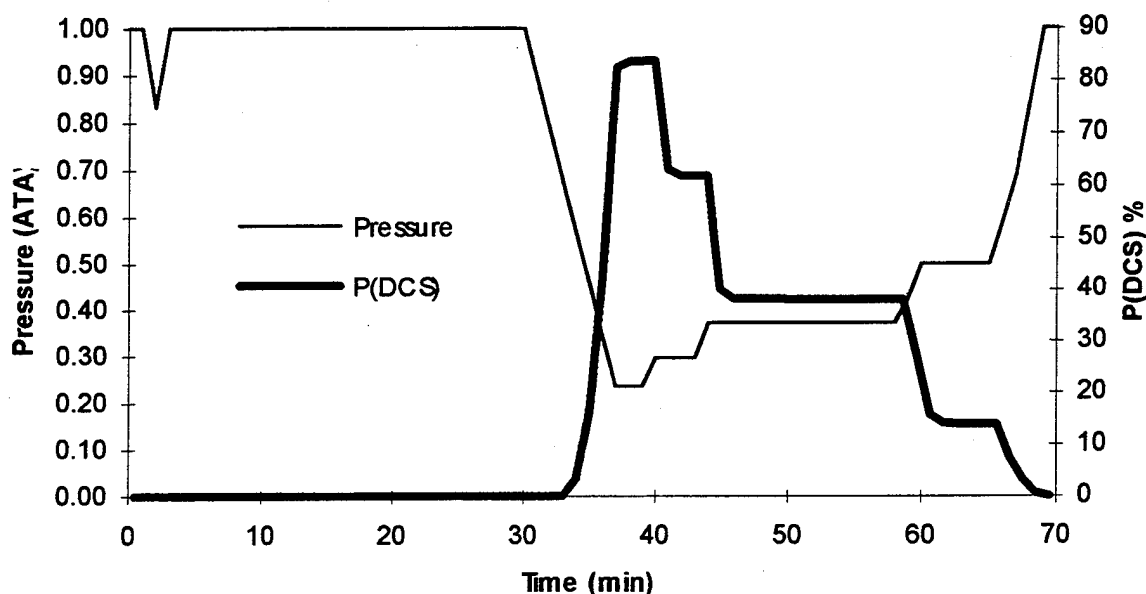


Figure 11. Analysis of USAF Type I Altitude Training Flight using logistic model I-C.

The predicted DCS probability for this profile is disconcertingly high, and is not decreased appreciably by addition of a 60 min O<sub>2</sub> prebreathe. Model performance underlying these estimations is made more clear by comparing the P(DCS) profile in Figure 11 to the corresponding compartmental dissolved N<sub>2</sub> profiles shown in Figure 12. The slowest gas exchange compartment, or that with the highest gas exchange half-time, governs the DCS outcome for this profile. Because of its high gas exchange half-time, the dissolved N<sub>2</sub> tension in this compartment, labeled T1 in Figure 12, decreases only slightly during O<sub>2</sub> breathing before ascent to 35,000 ft. The N<sub>2</sub> tension then momentarily exceeds the ambient pressure during the ascent from ground to 35,000 ft, causing a bubble to nucleate in the compartment. The ensuing fall in N<sub>2</sub> tension along with the rapid rise of DCS risk during the continued decompression are consequently caused by bubble growth that is accelerated by Boyle's law effects. The model overestimates the influence of such early and rapid bubble growth on DCS probability.

In having multiple altitude stages, this and most profiles to follow are of complexity that is poorly represented, if at all, in the USAFAL training dataset. Model performance about the profiles is consequently a considerable extrapolation from the experience embodied in this dataset.

Thus, despite their ability to correlate the training data, the logistic models prove to provide unreliable estimates in extrapolative contexts.

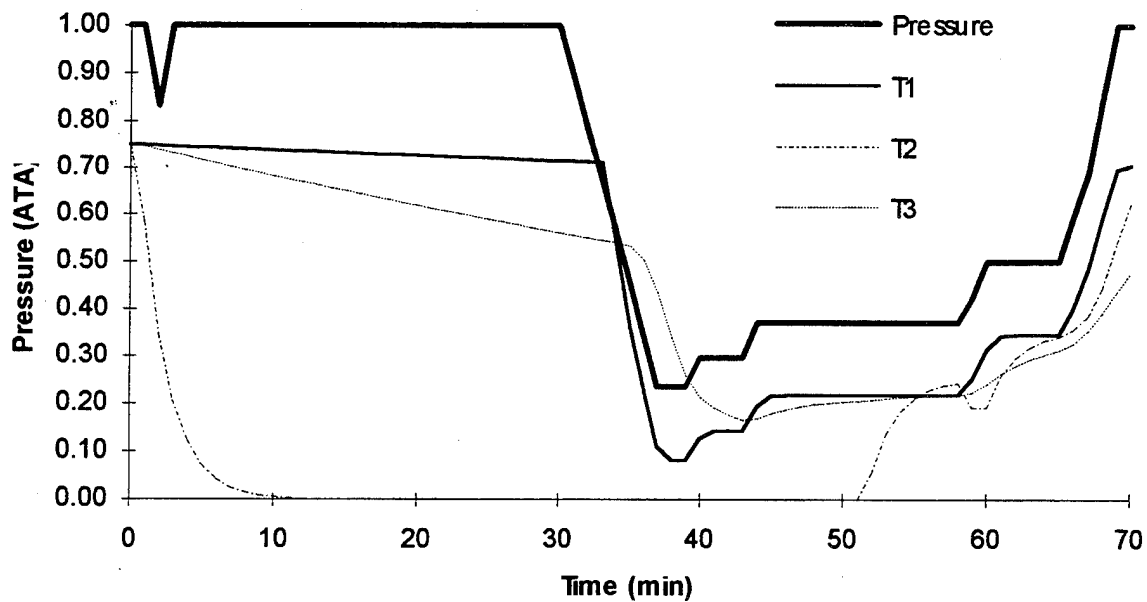


Figure 12. Calculated dissolved  $N_2$  tension profiles for the three tissue compartments in logistic model I-C during a USAF Type I Altitude Training Flight.

The influence of Boyle's law effects in the logistic models and their evident vulnerability to poor extrapolative performance are strengthened by their focus on a single point in any given profile, i.e., that at which the *maximum* bubble volume occurs. While this problem might be alleviated by definition of the dose as a time integral of bubble volume, this approach was not investigated in present work. Instead, survival models were adopted that use integrals of the bubble volume as measures of cumulative risk rather than overall risk. The cumulative probability at each point in time consequently depends explicitly on the shape of the preceding bubble volume/time profile.

Survival model S-IIa predictions of DCS risk during the Type I Altitude Training Flight are shown in Figure 13. The figure also includes the corresponding instantaneous risk profile. The entire computed  $P(\text{DCS})$  profile is of significance in this context, representing how DCS risk is accumulated throughout the exposure. The shape of this profile is accordingly quite different from the  $P(\text{DCS})$  profile in Figure 11. Note, however, that the instantaneous risk profile closely resembles the  $P(\text{DCS})$  profile in Figure 11. Most importantly, the cumulative  $P(\text{DCS})$  profile is seen to increase monotonically, reflecting that the actual probability of DCS in any profile can only increase. Interpretation of this behavior is clarified by reference to Eq. (26). As an individual progresses through the profile and remains DCS-free,  $T_1$  is the prevailing elapsed time and  $P(S)_{T_1}$ , or the probability that the individual remains DCS-free through  $T_1$ , is unity -- by stipulation. The corresponding probability of DCS *after* that time is thus given by Eq. (26) as only that portion of the overall  $P(\text{DCS})$  that is accrued during the remainder of the exposure, i.e.,

in the interval  $T_1$  to  $T_3$ . Thus, if the individual remains DCS-free through an elapsed time of about 68 min when he has reached ground level, his remaining risk of DCS is zero, although he has just successfully "beat" an estimated 12.9% risk of having had DCS beforehand. Survival models are consequently seen to provide quantitative information about DCS probability in specific time periods throughout an exposure, as well as information about the overall probability of DCS incidence. Logistic models, on the other hand, provide only the latter type of incidence-only information.

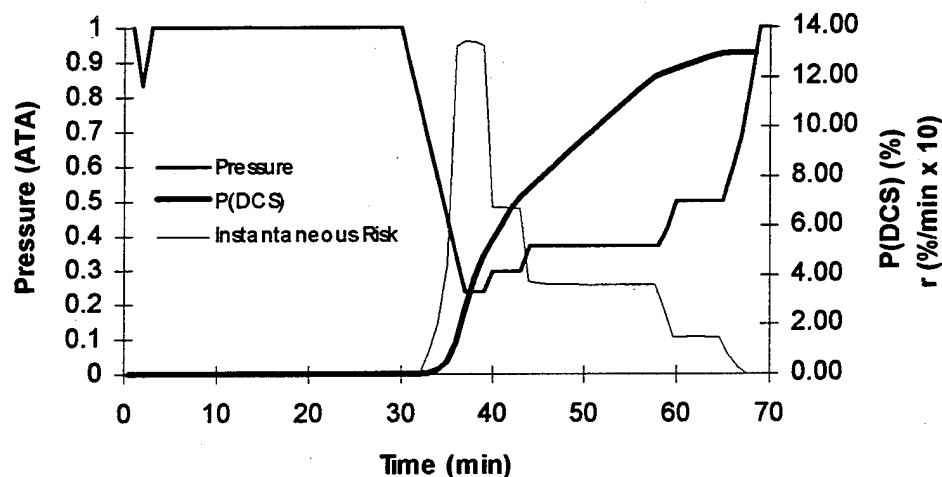


Figure 13. Cumulative P(DCS) during a USAF Type I Altitude Training Flight calculated using survival model S-IIa.

In the present case of the Type I Altitude Training Flight, survival model S-IIa yields predictions of DCS probability that are quantitatively more tenable than those provided by the logistic models. In particular, the influence of bubble growth during the initial decompression and subsequent short stage at 35,000 ft is reduced compared to that in the logistic model. However, the overall estimated DCS probability remains elevated due to this early and rapid bubble growth. The better-fitting survival model S-IIb estimates an even higher 18% cumulative DCS probability for this profile, with the same qualitative time course of instantaneous risk. As behavior allowed by the low compartmental volumes and high compartmental gas diffusivities in these models, it is expected that model reoptimization about the USAFAL dataset after time of DCS onset data are added will further reduce this remaining inordinate influence. Consistent with this expectation, survival model S-IIa-C fitted to the combined USAFAL+USN/NMRI dataset provides a lower 9.5% estimated P(DCS) for this profile [Figure 14]. Time of DCS occurrence data in the USN/NMRI subset of this dataset was used in the optimizations to obtain model S-IIa-C.



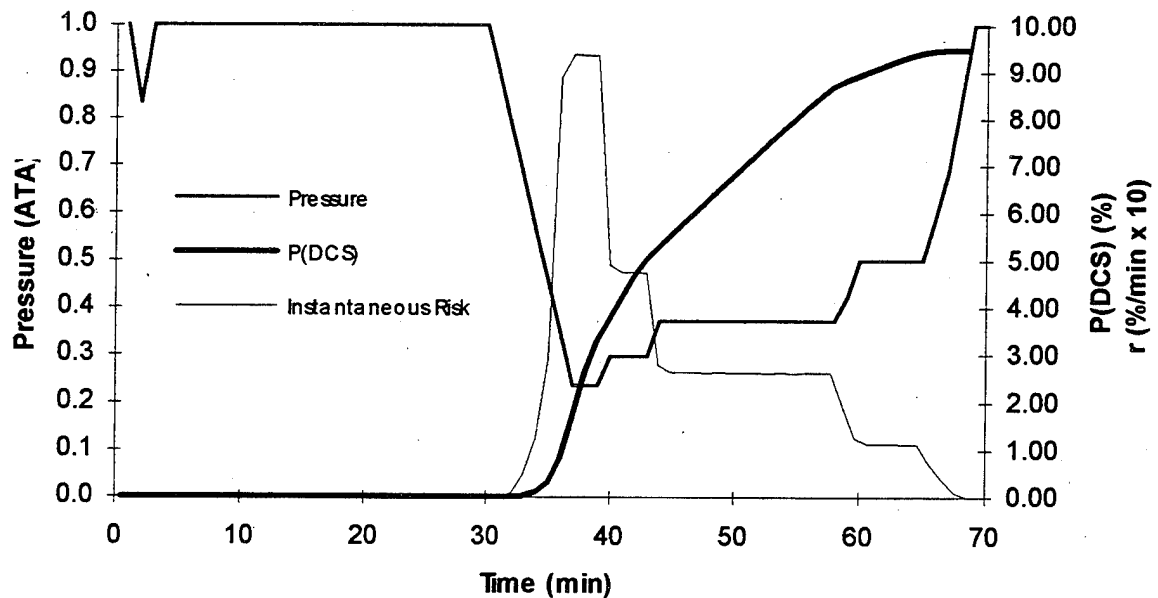


Figure 14. Cumulative P(DCS) during a USAF Type I Altitude Training Flight calculated using survival model S-IIa-C.

#### 4.1.2. Type II Altitude Training Flight

Survival model S-IIa-C predictions of DCS risk during a USAF Type II Altitude Training Flight are shown in Figure 15. The profile is similar to the Type I training flight, but with an initial excursion to 43,000 ft rather than 35,000 ft. The instantaneous DCS risk thus shows features similar to those evident in Figures 13 and 14 for the Type I flight profile. The instantaneous risk peaks sharply during the initial high altitude excursion, contributing substantially to the cumulative DCS probability. The preponderance of this risk arises from a relatively large bubble volume attained during ascent in compartment 3 with an unphysiologically high diffusivity (Table 9). Again, such rapid bubble growth is allowed by the extreme values of the optimized compartmental volumes and diffusivities, but is also exacerbated by a remaining inordinate influence of Boyle's law expansion during ascent. Such behavior will not likely be allowed by a model optimized about a dataset that includes explicit time of DCS onset information and that properly accounts for the nonequilibrium dynamics of tissue-bubble  $O_2$  and  $CO_2$  fluxes (Section 5.2.5.).

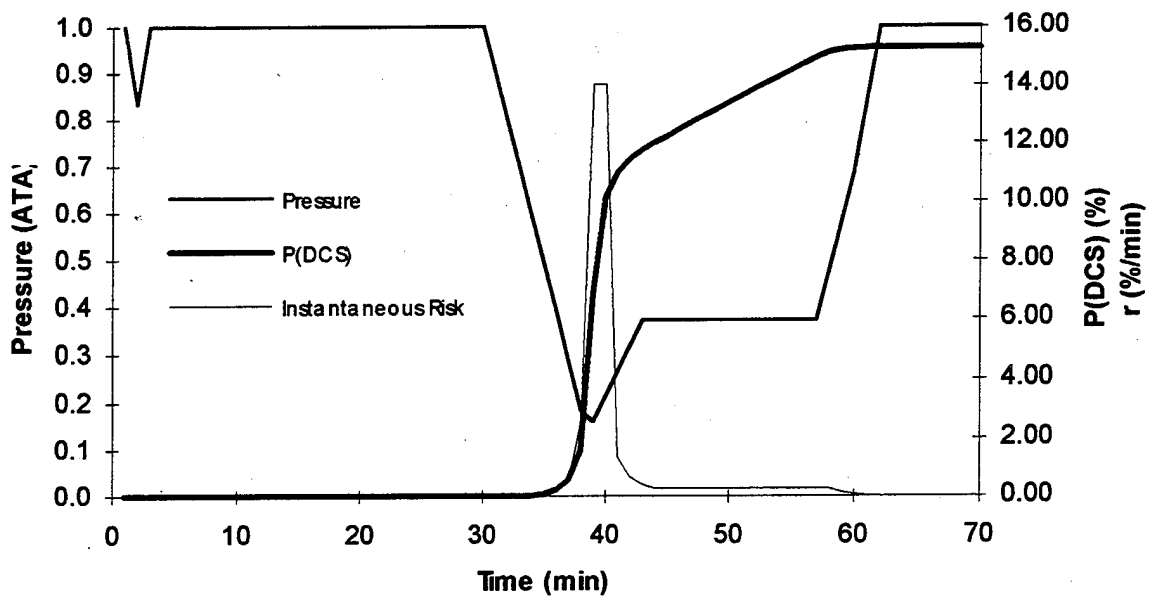


Figure 15. Cumulative P(DCS) during a USAF Type II Altitude Training Flight calculated using survival model S-IIa-C.

#### 4.1.3. USAF HALO Training Flight

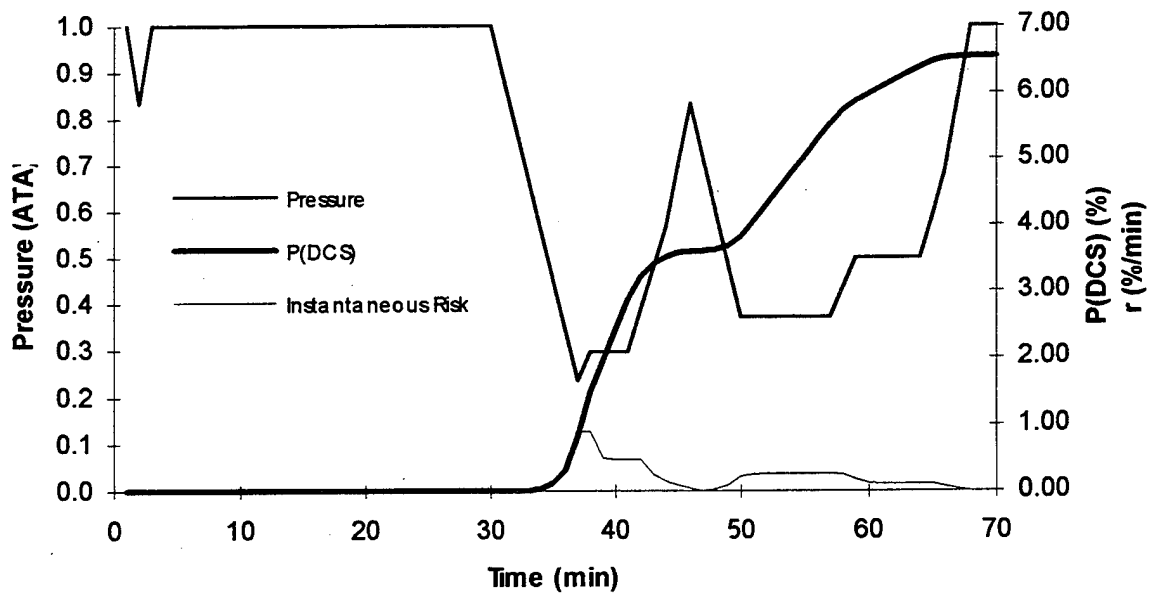


Figure 16. Cumulative P(DCS) during a USAF HALO Training Flight calculated using survival model S-IIa-C.

#### 4.1.4. Reconnaissance Flight

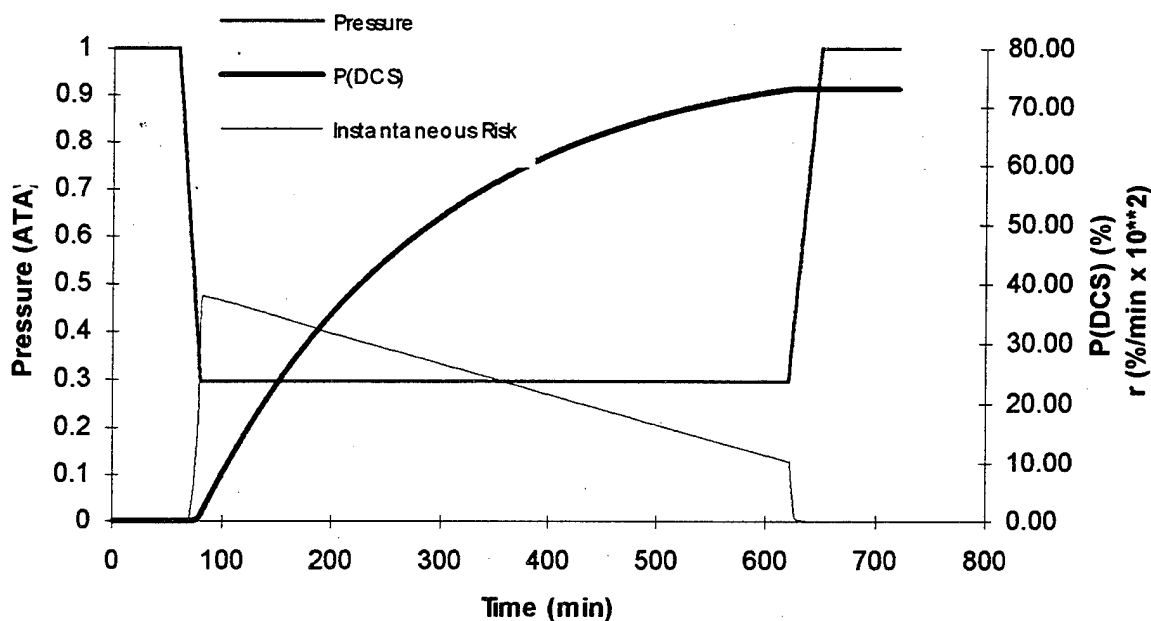


Figure 17. Cumulative P(DCS) during a USAF Reconnaissance Flight calculated using survival model S-IIa-C.

#### 4.1.5. T-37B Cross-Country Flight

Survival model estimates of DCS risk accumulation during a hypothetical cross-country flight in a T-37B aircraft with an unpressurized cabin is shown in Figure 18. The profile consists of multiple exposures at 25,000 ft with intermediate stages at ground for refueling, and includes a complicated breathing gas regime that is presented in detail in Appendix A. The instantaneous risk ramps during successive excursions at altitude decline in amplitude, reflecting the progressive elimination of the initial compartmental loads of dissolved inert gas. Despite this off-gassing, DCS risk continues to accumulate throughout each of the altitude excursions.

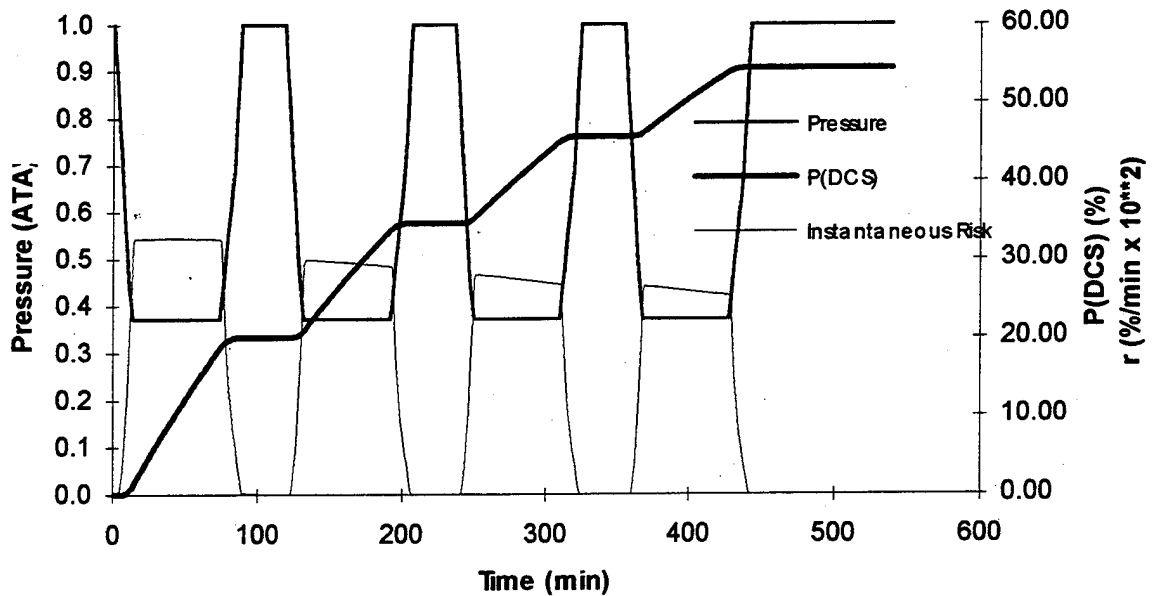


Figure 18. Cumulative P(DCS) during a USAF T-37B cross-country flight calculated using survival model S-IIa-C.

#### 4.1.6. Inflight Denitrogenation Study

Figures 19 -21 show P(DCS) profiles predicted by the two-tissue survival model for three exposure profiles tested in the USAFAL Inflight Denitrogenation Study. Study objectives were to substantiate earlier indications that a long preflight denitrogenation can be supplanted, at least in part, by oxygen breathing during a flight stage at an intermediate altitude before final ascent to a higher target altitude. The study control profile, shown in Figure 19, consisted of a 1 hr O<sub>2</sub> prebreathe followed by a 4 hr exposure at 29,500 ft. The predicted DCS probability for this profile is 53.5%.

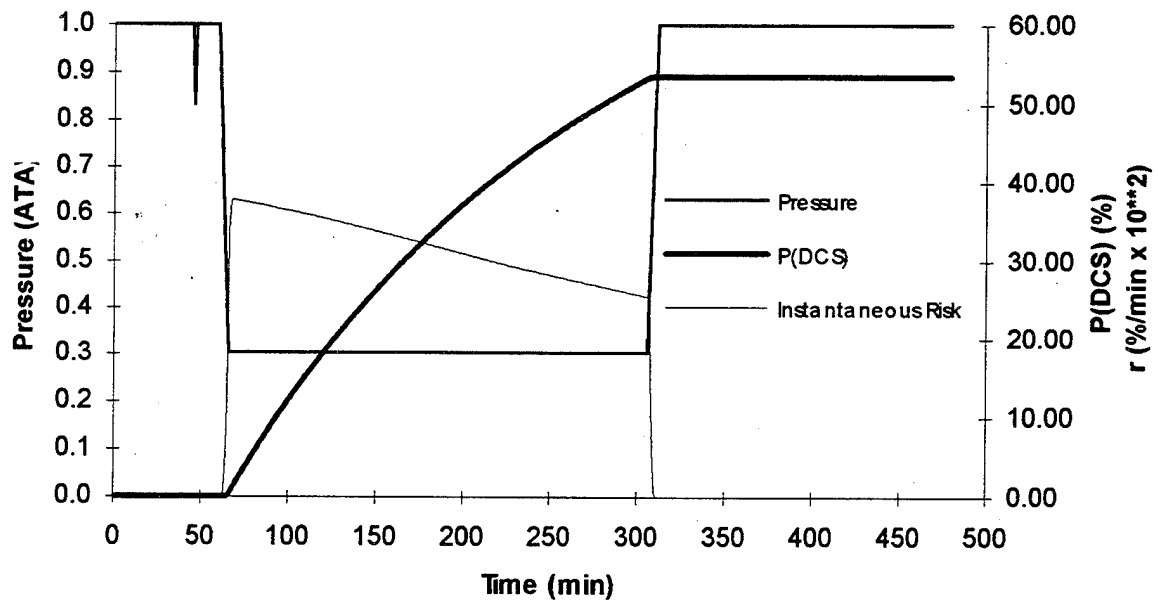


Figure 19. Cumulative P(DCS) during the profile used as an experimental control in the USAFAL Inflight Denitrogenation Study calculated using survival model S-IIa-C.

An experimental profile consisting of a 15-min O<sub>2</sub> prebreathe followed by a 1-hr O<sub>2</sub>-breathing stage at 12,000 ft and a 4-hr exposure at 29,500 ft is shown in Figure 20. The predicted DCS probability for this profile is 54.3%. Comparing Figures 19 and 20, model predictions indicate that after a 15-min O<sub>2</sub> breathing period at ground-level, a 60-min O<sub>2</sub> breathing stage at 12,000 ft is as effective as a 1-hr prebreathe in limiting DCS risk at 29,500 ft.

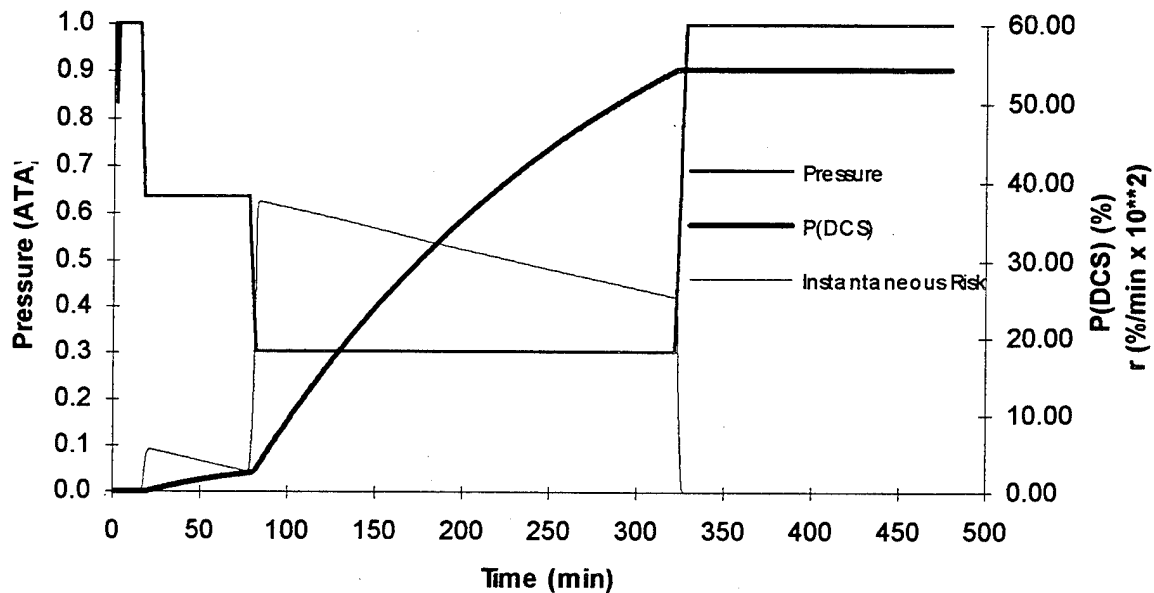


Figure 20. Cumulative P(DCS) during an experimental profile with a 12,000 ft denitrogenation stage in the USAFAL Inflight Denitrogenation Study calculated using survival model S-IIa-C.

A second experimental profile consisting of a 15-min O<sub>2</sub> prebreathe followed by a 1-hr O<sub>2</sub>-breathing stage at 16,000 ft and a 4-hr exposure at 29,500 ft is shown in Figure 21. The estimated DCS probability for this profile is 58.6%. The estimated DCS protection acquired during inflight denitrogenation at 16,000 ft is somewhat less than when the denitrogenation is performed at 12,000 ft.

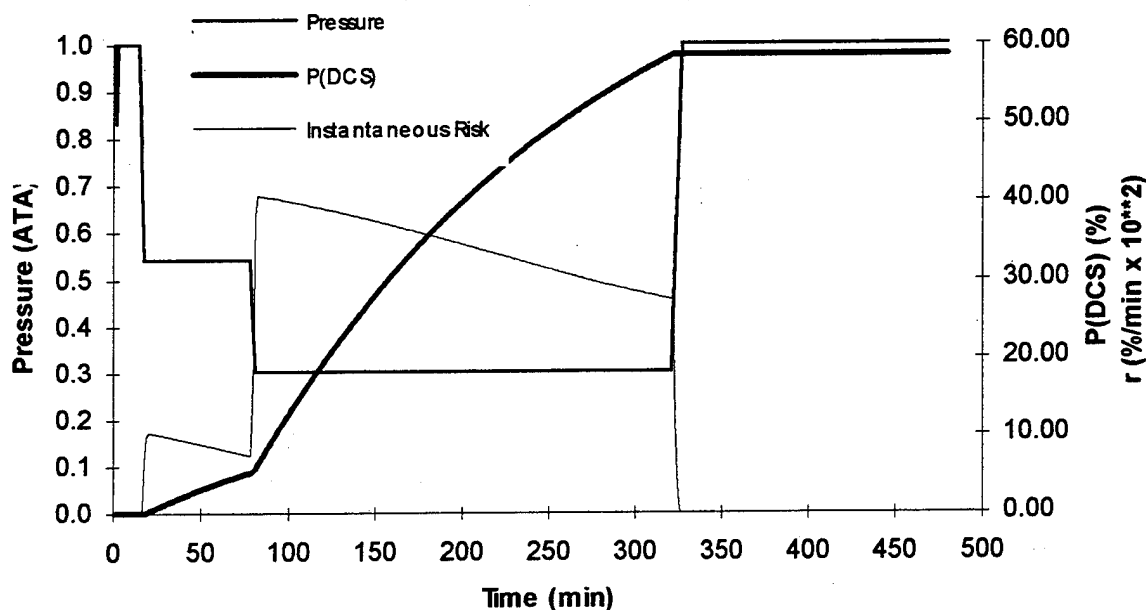


Figure 21. Cumulative P(DCS) during an experimental profile with a 16,000 ft denitrogenation stage in the USAFAL Inflight Denitrogenation Study calculated using survival model S-IIa-C.

## 4.2. Prescriptive Applications

The present statistical models can be readily used to plan decompression exposures so that associated DCS risks remain within certain acceptable levels. However, acceptable risks must be specified for such prescriptive calculations.

### 4.2.1. Acceptable Risk

Acceptable risks are best selected in accord with model predictions for profiles which experience indicates are acceptably safe. For example, the present two-compartment survival model provides an estimated DCS risk of about 10% for the USAF Type I and II altitude training flights. This is clearly an overestimate for profiles that are routinely undertaken with actual DCS incidences far below this value. Prescriptive predictions of this model can thus be scaled to conform with this experience by specification of 10% risk as acceptable.

#### **4.2.2. Prebreathe Minimization**

Figure 22 illustrates the process by which minimum O<sub>2</sub> prebreathe times are computed for a given altitude exposure using survival model S-IIa-C. Three pressure and corresponding DCS probability profiles are shown for ascent to a physiologic altitude of 30,000 ft. The profiles, similar to that shown in Figure 17, differ only in the length of the prebreathe time before the ascent. In each case, the instantaneous DCS probability rises from zero during and shortly after ascent, attains a maximum and then decays during the flight. The corresponding cumulative P(DCS) rises rapidly and reaches a maximum when the instantaneous risk decays to zero. As successive panels show, the cumulative P(DCS) rises to lower maximum values as the pre-flight O<sub>2</sub> breathing period is increased. By appropriate adjustment, a pre-flight pre-breathe interval is readily found that allows the cumulative DCS risk during flight to reach but not exceed any user-specified level of acceptable risk. The figure illustrates that for the present example, a minimum surface interval of 4.25 hr is required to keep DCS risk during flight within an acceptance level of 10%.

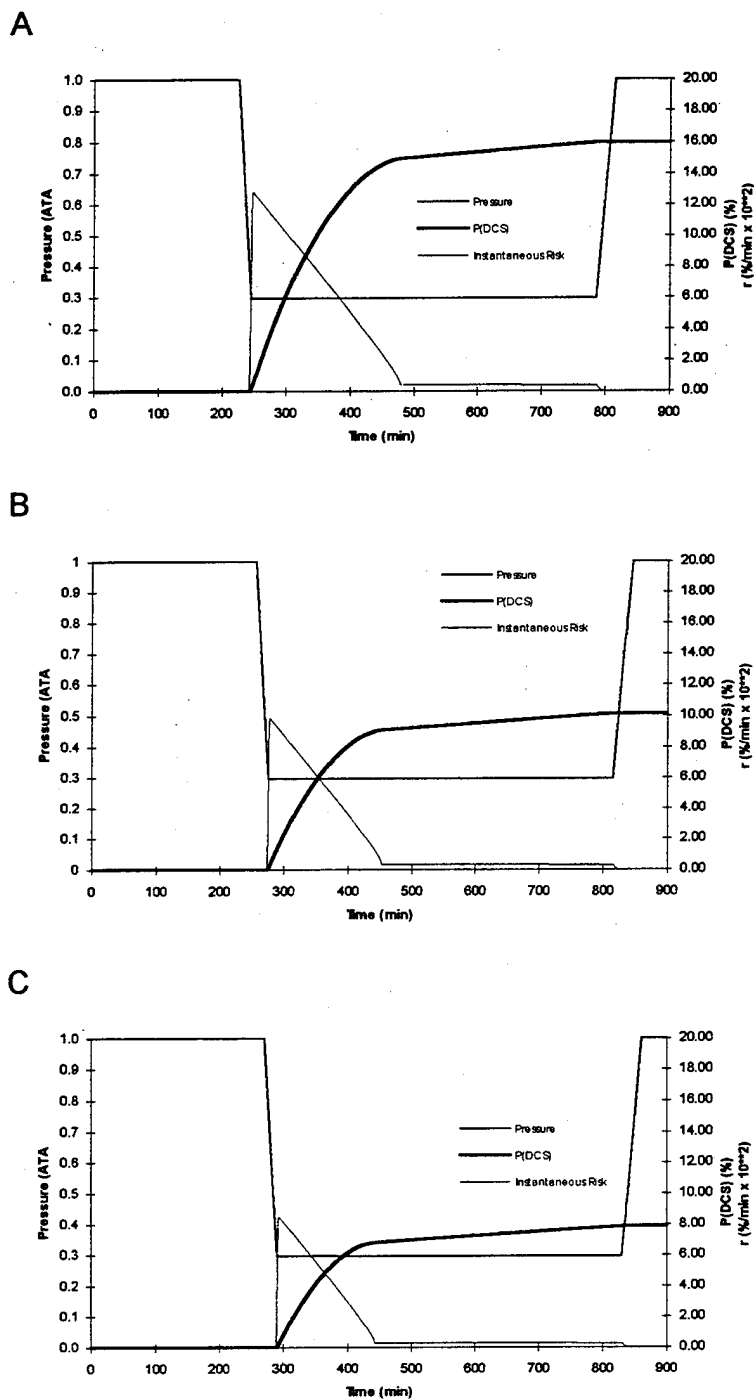


Figure 22. Pre-breathe minimization with 10% accepted DCS risk for ascent to FL300 (30,000 ft); 100% oxygen breathing throughout. A) Insufficient prebreath (3.75 hr) resulting in an unacceptably high DCS risk during flight; B) Minimum prebreath (4.25 hr) resulting in a maximum DCS risk during flight equal to the accepted risk; C) Conservative prebreath (4.75 hr) resulting in DCS risk during flight that remains below the accepted risk.



## **5. FUTURE WORK**

Present model structure supports a wide variety of model variants, each distinguished from the other by including different numbers of gas exchange compartments or by having different subsets of the available adjustable parameters fixed during optimization about given datasets. More of these variants, which could not be explored under the time constraints of the present program, must be tested in continued work to determine if they can provide better correlations of the training datasets. The survival models in particular require continued tuning and optimization to ameliorate their evident tendency to overpredict DCS risk for relatively safe low altitude exposures.

### **5.1. Time of DCS Onset**

Data downloaded from the USAF Hypobaric Decompression Database did not include explicit time of onset information for the DCS cases in the dataset. Such information was not needed and hence was not requested when data were initially retrieved from the database by USAFAL personnel to support work with the logistic models. Upon development of the survival models and the need for such information later in the program, time constraints precluded completion of work required to retrieve, validate and format the information. The survival models were consequently fit as incidence-only models, without constraint to perform in accord with known DCS onset time information. As discussed in Section 3.2, this lack of constraint, along with the time of DCS occurrence information implicitly included in the structure of many profiles, caused the incidence-only fits to approximate time-of-onset fits. Future optimization of these and other survival models about datasets that include explicit time of DCS onset data are expected to yield improved fits through relief of the present problem of inadequate accounting for known DCS-free periods in exposures which eventually culminated with DCS. Each of the present models was driven in optimization to have bubbles in all compartments that attained maximum volume during or very soon after decompression. As a result, the DCS dose in the logistic models and the instantaneous DCS risk in the survival models tended to be largest immediately after decompression when any supersaturations in the compartments were maximal. Such behavior, which is not in accord with experience in hypobaric decompression, will be discouraged in survival model optimizations that are conducted with DCS-free ( $0-T_1$ ) periods defined.

### **5.2. Model Enhancements**

While continued work with the present model system is indicated, further development and modification of certain structural and dataset features may improve model ability to correlate even larger and more heterogeneous datasets, increase the confidence that can be taken in model prescriptions for decompression profiles outside of the models' experience, and increase system utility in field applications. Results of the present program have suggested the most promising areas for attention in these regards.

### **5.2.1. Severity of DCS**

All present models treat DCS incidence as a binary all-or-nothing event. An exposure is consequently assigned a positive DCS outcome whether the incident involves mild to moderate joint pain or a more serious and debilitating Central Nervous System (CNS) disorder. Because of this ambivalence to the type or severity of DCS in these assignments, the models predict DCS incidence with the same ambivalence regarding the type or severity of the DCS incident that might actually occur. Moreover, DCS incidents in the training datasets are dominated in number by less severe occurrences at levels of decompression stress that are below those required to elicit substantial numbers of more severe DCS cases. Thus, conditioned by the type of data to which they were fit, the models tend to be better predictors of milder forms of DCS. In many operational contexts, however, high risks of relatively mild DCS are acceptable, while only more severe cases are to be avoided. DCS risk assessment in such contexts is not supported by present models, but can be accomplished by using different models optimized about datasets that have each been tailored to register only DCS incidents of consequence more serious than given acceptable levels. Undertakings of this sort will require expansion of present and future training datasets to include information about the type and severity of each DCS incident, as well as more data for the incidences of severe DCS in extreme exposures, but will yield models that are applicable to avoid severe DCS in operations which entail relatively high but acceptable risks of mild-to-moderate DCS.

### **5.2.2. Effects of Exercise**

Exercise during preflight oxygen breathing is known to improve the efficacy of denitrogenation and reduce subsequent DCS incidence, while exercise above certain minimum levels during and after decompression is known to potentiate DCS susceptibility. These influences, as well as those of high arterial oxygen tensions on perfusion [24], are not presently accommodated in present models. Such influences could be considered by making the compartmental blood flow  $Q_i$  an exercise- and arterial oxygen-dependent quantity and the nucleonic bubble size  $r_i^{cr}$  an exercise-dependent quantity. The latter modification would be in accord with evidence that exercise affects DCS susceptibility by promoting bubble nucleation *per se* [16,17].

### **5.2.3. Variable Bubble Number Density**

As formulated in Section 2.1.2., each compartmental volume,  $V_{t,i}$ , is a constant in the present bubble dynamics equations. The value of this parameter not only governs the tissue-blood gas exchange time constant,  $\tau_i$ , but also determines the compartmental bubble number density, which is an important governor of bubble-tissue mass balance. As  $V_{t,i}$  decreases and the bubble number density increases, a given incremental increase in bubble volume relieves the underlying supersaturation more quickly. The bubble-tissue system can consequently more readily attain a "clamped" condition in which the tissue tension remains at a constant minimal value that is governed only by surface tension and the prevailing hydrostatic pressure [27]. Under this condition, which prevails until the bubble is completely resorbed, gas washout from the

compartment proceeds according to time-linear rather than semi-exponential kinetics. The compartmental volume is therefore a very important parameter, but as it affects the bubble number density, it may not be appropriate to hold it constant from one profile to another.

Any pre-existing gaseous nuclei *in vivo* must have a distribution of sizes. If bubbles nucleate *in vivo* from such nuclei, bubbles must form first from only the largest of the nuclei. As decompression continues and the supersaturation is increased, bubbles must continue to form in increasing numbers as progressively smaller nuclei are recruited. As a result, the bubble number density must increase with the supersaturation when this nucleation mechanism is operative. This situation is accommodated to a first approximation by making  $V_{t,i}$  a monotonically decreasing function of the supersaturation. A compartmental volume decay factor,  $F_i$ , is defined:

$$\begin{aligned} F_i &= \exp(-k_{V,i} \cdot SSE_i), \quad SSE_i > 0; \\ F_i &= 1.0, \quad SSE_i \leq 0, \end{aligned} \quad (34)$$

where  $k_{V,i}$  is a compartment-specific decay constant, and  $SSE_i$  is the compartmental supersaturation in excess of that required to nucleate bubbles, given by:

$$SSE_i = (P_{t,i} + P_{mg} - 2\sigma / r_i^{cr}) - P_H. \quad (35)$$

The decay factor,  $F_i$ , ranges from unity at  $SSE_i \leq 0$ , to zero at  $SSE_i = \infty$ . This factor must be additionally constrained so that it may decrease as  $SSE_i$  increases, but may not increase thereafter until the bubble is resorbed. Changes in bubble number density are subsequently effected without changing  $\tau_i$ , the tissue-blood gas exchange time constant, by incorporating  $F_i$  into Eq. (19) as follows:

$$dP_{t,i}/dt = \{F_i \cdot (\alpha_b \cdot Q_i) \cdot (P_a - P_{t,i}) - P_{b,i} \cdot dV_{b,i}/dt - V_{b,i} \cdot dP_{b,i}/dt\} / (F_i \cdot \alpha_{t,i} \cdot V_{t,i}). \quad (36)$$

The  $F_i \cdot V_{t,i}$  term in the denominator effects the desired supersaturation-dependent change in the bubble number density, while the  $F_i \cdot Q_i$  term in the numerator effects a compensatory adjustment in the compartmental blood flow. This formulation accommodates the idea that more bubbles form with increasing supersaturation, but also assumes that these bubbles are homogeneously distributed and are all of the same size at any point in time. Because of this latter size uniformity, this formulation does not account for the fact that bubbles which nucleated later, i.e., not until higher supersaturations were attained, must be smaller than those which nucleated earlier. The approach offers the advantage of accommodating substantially more complex behavior with addition of only a single parameter for each modeled compartment. Support for this model enhancement was developed in the present program and implemented in system software, but optimization of this model about available training datasets remains for continued work. It is expected that this enhancement may enable the model to better correlate datasets which include both altitude and diving profiles, where the range of possible supersaturations is higher than in datasets including only altitude exposures.

#### **5.2.4. Bubble Damage/Repair**

Models in which DCS risk arises from a measure of bubble size alone are intrinsically limited. Other factors secondary to bubble formation and growth are also putatively important etiological factors in DCS. For example, late onset DCS occurring hours after hypobaric exposure and return to ground level are difficult to explain or model on the basis of bubble volume alone. The concept of bubble damage that can linger after bubbles have resolved can be accommodated by adopting a DCS DOSE or instantaneous risk equal to a time-varying damage (X), which is a function of the bubble volume (V) and a constant damage repair rate (c):

$$(dX/dt) = V - c \quad (37)$$

Use of this relation would uncouple the DCS DOSE or instantaneous risk from bubble volume *per se*, but it remains to be seen whether such uncoupling can afford better correlations of available data. It might be expected that any advantages of the approach would be most pronounced for survival models fit to datasets that include time of DCS onset information.

#### **5.2.5. Alternative Bubble Dynamics Models**

##### **Multiple Gas Dynamics**

Present models assume that the so-called metabolic gases  $P_{H_2O}$ ,  $P_{CO_2}$ , and  $P_{O_2}$  are always in equilibrium between bubble and tissue. This assumption causes overestimation of both the rates of diffusive bubble growth and resolution and the changes in bubble volume that arise from Boyle's law effects. The improved correlation of the USAFAL data afforded by survival model S-IIb over its S-IIa counterpart is apparently due to the absence in model S-IIb of erroneously potentiated Boyle's law effects that arise from this assumption in model S-IIa.

Burkhard and Van Liew [1] have developed an elaboration of the bubble dynamics equations used in the present models that account for diffusion-limited exchange of multiple gases between bubble and tissue. Model results indicate that diffusive nonequilibria of the metabolic gases between bubble and tissue can influence diffusion of the diluent inert gas and cause bubble dynamics to differ significantly from those obtained with the present equilibrium assumption, particularly in hypobaric exposures. The importance of these factors as governors of DCS risk accumulation must be examined by implementation of these more complex bubble dynamics equations in the present model system. The upgraded model system will also allow modeling of exposures in which diluent inert gases other than nitrogen are breathed.

##### **Diffusion Shell**

The performance of a spherical bubble dynamics model in which bubble growth and resolution are limited by diffusion through a "shell" at the bubble-tissue interface, rather than by bulk diffusion through tissue, should be assessed. In such a model, the tissue is well-stirred with respect to both blood-tissue and tissue-bubble gas exchange, in contrast to the present models in

which the tissue is not well-stirred with respect to tissue-bubble gas exchange and the latter occurs by gas diffusion through an unstirred tissue bulk phase. An important quantitative consequence of this difference is that the rate of bubble growth or resolution,  $dr/dt$ , is proportional to the inverse of the diffusion shell thickness  $1/h$  in the shell case, and to the inverse of the bubble radius  $1/r$  in the bulk diffusion case. With assumed constancy of the shell thickness, bubble growth rates are consequently overestimated in the shell case relative to the bulk diffusion case. Both Tikuisis [23] and Gernhardt [5] have developed bubble dynamics equations suitable for testing in this context, although the latter require modification to maintain mass balance between bubble and tissue.

### **5.3. Training Dataset Expansion**

As outlined in Section 3.1, the performance of any model is strongly conditioned by the data to which it is fit. Notwithstanding the needs outlined above for addition of DCS time of onset and severity information to existing training datasets, continued expansion of these datasets to include high-quality laboratory or field DCS occurrence data for profiles of increasing complexity and scope will be a perennial requirement of statistical DCS modeling. A large body of data for flying after diving exposures, for example, has been compiled and used in earlier work [9-11], but must yet be formatted for analyses using the present model/software structure. Conkin and coworkers [2] have also compiled a large body of altitude exposure data that should be incorporated into future model training datasets.

## **6. CONCLUSIONS**

Statistical bubble dynamics models have been shown able to correlate DCS incidence data for a wide variety of human altitude and diving exposures. The models track the dynamics of gas bubbles in hypothetical blood-tissue gas exchange compartments throughout the course of any given pressure/time profile and provide estimates of DCS risk based on the volumes that the bubbles achieve.

A variety of models using logistic probability distribution functions provide incidence-only correlations of both USAFAL and combined USAFAL+USN/NMRI data superior to those provided by the survival models tested. The logistic models, however, are severely constrained in performance by the nature of the data to which they are fit. This arises from their dependence on a single DCS dose value from a profile, irrespective of the complexity of the profile. In the present logistic implementations, for example, the dose is defined by a maximally sized bubble without regard for its persistence at any still-substantial size, whether for only moments or for hours. With the present USAFAL training dataset consisting predominantly of relatively long single-stage altitude exposures, fitted logistic models provide poor predictions of DCS risk for more complex profiles that include multiple altitude stages and short excursions to high altitude. These problems could potentially be mitigated by including ever more diverse types of profiles in the training dataset, but could then be expected to recur whenever the optimized models were applied to profiles beyond the experience embodied in those datasets. This overall lack of extrapolative reliability is caused by the failure of logistic models to capture essential temporal information about DCS risk accumulation from the profiles in their training datasets.

The above failure of logistic models is mirrored by their inherent inability to provide temporal information about DCS risk accumulation in predictive contexts. DCS probability profiles generated using the instantaneous bubble volume as an instantaneous dose provide an impression of such temporal information, but are, in fact, factitious and potentially deceptive renderings that are useful only to illustrate model performance. Ultimately, logistic models can provide only a single estimate of DCS probability for any given profile, regardless of its complexity and without regard to when in the profile DCS is most likely to occur.

Survival models ameliorate the above problems of the logistic models by explicitly incorporating temporal information about DCS risk during optimization. In turn, they provide legitimate estimates of the time courses of DCS risk accumulation during application, and consequently emerge as those with the most utilitarian promise. Time constraints, and the undertaking of the survival approach later in the program, limited the number of survival models that could be tested in present work. Their poor incidence-only correlation of the USAFAL data was found to arise from the implicit inclusion of time of DCS occurrence information in the dataset and the absence of information required to define DCS-free periods in profiles that eventually ended with a DCS event. Despite these problems, the survival models provided more uniformly tenable predictions of DCS risk in test and evaluation profiles than any logistic model. The models require optimization about the USAFAL dataset updated to include the time of DCS onset for each recorded DCS event before they can emerge able to support USAF operational requirements for DCS risk assessment.

## 7. REFERENCES

- 1) Burkard ME and Van Liew HD: Simulation of exchanges of multiple gases in bubbles in the body. *Resp. Physiol.*, 95: 131-145, 1994.
- 2) Conkin J, Bedahl SR and Van Liew HD: A computerized databank of decompression sickness incidence in altitude chambers. *Aviat. Space Environ. Med.*, 63: 819-824, 1992.
- 3) Fawcett TA, Vann RD and Gerth WA: Surface interval oxygen: Rationale and study design. In: Lang MA and Vann RD (eds.), Proceedings of AAUS Repetitive Diving Workshop. Duke University, March 1991. AAUS Costa Mesa, CA, 1991, pp. 293-298.
- 4) Fife CE, Pollard GW, Mebane GY, Boso AE and Vann RD: A database of open water, compressed air, multi-day repetitive dives to depths between 100 and 190 FSW. In: Lang MA and Vann RD (eds.), Proceedings of AAUS Repetitive Diving Workshop. Duke University, March 1991. AAUS Costa Mesa, CA, 1991, pp. 45-54.
- 5) Gernhardt ML: Development and Evaluation of a Decompression Stress Index Based on Tissue Bubble Dynamics. Dissertation, University of Pennsylvania, 1991.
- 6) Gerth WA: Applicability of Henry's Law to Hydrogen, Helium, and Nitrogen Solubilities in Water and Olive Oil at 37°C and Pressures Up to 300 Atmospheres. *Archiv. Biochem. Biophys.*, 241: 187-199, 1985.
- 7) Gerth WA, Vann RD and Southerland DG: Quasi-physiological decompression sickness incidence modeling. In: Lang MA and Vann RD (eds.), Proceedings of AAUS Repetitive Diving Workshop. Duke University, March 1991. AAUS Costa Mesa, CA, 1991, pp. 253-262.
- 8) Gerth WA, Vann RD and Southerland DG: No-stop repetitive N<sub>2</sub>O<sub>2</sub> diving with surface interval O<sub>2</sub> (SIO<sub>2</sub>): Calculation of schedules. *Undersea Biomed. Res.*, 19(Supplement): 79, 1992.
- 9) Gerth WA, Vann RD, Southerland DG and Hasselblad V: Calculation of Schedules for Diving and Flying After Diving Using a Statistical Bubble Dynamics Model. Universities Space Research Association Contract #905-72, Final Report, 1992.
- 10) Gerth WA, Vann RD, Southerland DG and Hasselblad V, "Calculation of Schedules for Flying After Diving Using a Statistical Bubble Dynamics Model." 1993 Annual Meeting of the Aerospace Medical Association, Toronto, Canada, May 23-27, 1993.
- 11) Gerth WA, Vann RD and Southerland DG: Quasi-Physiological Models for Calculating Flying After Diving Guidelines. Recreational Diving Research Foundation, Inc., Final Report, March, 1993.

- 12) Harrell FE, Califf RM, Pryor DB, Lee KL and Rosati RA: Evaluating the yield of medical tests. *J. Am. Med. Assoc.*, 247: 2543-2546, 1982.
- 13) Homer LD and Bailey RC: An analogy permitting maximum likelihood estimation by a simple modification of general least squares algorithms. Bethesda, MD: NMRI Technical Report 77-55, 1977.
- 14) Marquardt DW: An algorithm for least-squares estimation of nonlinear parameters. *J. Soc. Indust. Appl. Math.* 11: 431-441, 1963.
- 15) McDonough PM and Hemmingsen EH: Bubble formation in crustaceans following decompression from hyperbaric gas exposures. *J. Appl. Physiol.: Resp. Envir. Exercise Physiol.*, 56: 513-519, 1984.
- 16) McDonough PM and Hemmingsen EH: Swimming movements initiate bubble formation in fish decompressed from elevated gas pressures. *Comp. Biochem. Physiol.*, 81:209-212, 1985.
- 17) Ohta Y, Ar A, and Farhi LE: Solubility and partition coefficients for gases in rabbit brain and blood. *J. Appl. Physiol.: Resp. Environ. Exercise Physiol.*, 46:1169-1170, 1979.
- 18) Parsons YJ, Weathersby PK, Survanshi SS and Flynn ET: Statistically based decompression tables V: Haldane-Vann models for air diving. Bethesda, MD. NMRI Technical Report 89-34, 1989.
- 19) Parker EC, Survanshi SS, Weathersby PK, and Thalmann ED: Statistically based decompression tables VIII: Linear-exponential kinetics. Bethesda, MD. NMRI Technical Report 92-73, 1992.
- 20) Thalmann ED: Testing of decompression algorithms for use in the U.S. Navy Underwater Decompression Computer. NEDU Report No. 11-80, 1980.
- 21) Thalmann ED: Phase II testing of decompression algorithms for use in the U.S. Navy Underwater Decompression Computer. NEDU Report No. 1-84, 1984.
- 22) Thalmann ED: Air-N<sub>2</sub>O<sub>2</sub> decompression computer algorithm development. NEDU Research Rep. No. 8-85, 1986.
- 23) Tikuisis P, Gault KA and Nishi RY: Prediction of decompression illness using bubble models. *Undersea and Hyperbaric Med.* (In press).
- 24) Tikuisis P and Nishi RY: Role of oxygen in a bubble model for predicting decompression illness. Defence and Civil Institute of Environmental Medicine, Ontario, Canada, DCIEM No. 94-04, 1994.
- 25) Van Liew HD and Hlastala MP: Influence of bubble size and blood perfusion on absorption of gas bubbles in tissues. *Resp. Physiol.* 7: 111-121, 1969.



- 26) Van Liew HD: Simulation of the dynamics of decompression sickness bubbles and the generation of new bubbles. *Undersea Biomed. Res.* 18: 333-345, 1991.
- 27) Van Liew HD and Burkhard ME: Density of decompression bubbles and competition for gas among bubbles, tissue and blood. *J. Appl. Physiol.* 75(5): 2293-2301, 1993.
- 28) Van Liew HD, Conkin J and Burkhard ME: Probabilistic model of altitude decompression sickness based on mechanistic principles. *J. Appl. Physiol.* 76(6): 2726-2734, 1994.
- 29) Vann RD, Gerth WA, Leatherman NE and Feezor MD: A likelihood analysis of experiments to test altitude decompression protocols for Shuttle operations. *Aviat. Space and Environ. Med.*, 58(9, Suppl.): A106-A109, 1987.
- 30) Vann RD: A likelihood analysis of decompression data using haldane and bubble growth models. In: Bove AA, Bachrach AJ and Greenbaum LJ, eds. Underwater and Hyperbaric Physiology IX. Undersea and Hyperbaric Medical Society, Bethesda, MD, 1987. pp. 165-181.
- 31) Vann RD: Decompression risk in flying after diving. In: Sheffield, P.J., ed. *Flying after diving. Proceedings of the thirty-ninth UHMS Workshop*. Bethesda, MD: Undersea and Hyperbaric Medical Society, 1989.
- 32) Vann RD, Fawcett TA, Currie MS, Fife CE, Zhang J and Piantadosi CA: No-stop repetitive N<sub>2</sub>/O<sub>2</sub> diving with surface interval O<sub>2</sub> (SIO<sub>2</sub>): Phase I. *Undersea Biomed. Res.*, 19(Supplement): 79, 1992.
- 33) Vann RD, Gerth WA, Southerland DG, Stanton GR, Pollock N, Kepper W and Heinmiller R: No-stop repetitive N<sub>2</sub>/O<sub>2</sub> diving with surface interval O<sub>2</sub> (SIO<sub>2</sub>): Phase II. *Undersea Biomed. Res.*, 19(Supplement): 80, 1992.
- 34) Weathersby PK, Homer LD and Flynn ET: On the likelihood of decompression sickness. *J. Appl. Physiol.: Respirat. Environ. Exercise Physiol.* 57(3): 815-825, 1984.
- 35) Weathersby PK: Human decompression trial in nitrogen-oxygen diving. Bethesda, MD. NMRI Technical Report 86-97, 1986.
- 36) Weathersby PK, Survanshi SS and Nishi RY: Relative decompression risk of dry and wet chamber air dives. *Undersea Biomed. Res.* 17: 333-352, 1990.
- 37) Weathersby PK, Survanshi SS, Nishi RY, and Thalmann ED: Statistically based decompression tables VII: Selection and treatment of primary air and N<sub>2</sub>O<sub>2</sub> data. Bethesda, MD. NMRI Technical Report 92-85, 1992.
- 38) Weathersby PK, Survanshi SS, Homer LD, Parker E and Thalmann ED: Predicting the time of occurrence of decompression sickness. *J. Appl. Physiol.* 72(4): 1541-1548, 1992.

## APPENDIX A

## APPENDIX A. NODE DESCRIPTIONS OF PROFILES IN TEXT

USAF_PRO.DAT	USAF flight profiles for evaluation			
ALT.	FO2	PO2	TIME	DCS DIVES /COMMENTS
	F:4		6.	*=6 Altitude & Alternate: Ft/10**3
0.0	1.0	0.0	1.0	1) Type I Altitude Chamber Training Flt
5.0	1.0	0.0	1.0	
0.0	1.0	0.0	1.0	
0.0	1.0	0.0	27.0	
35.0	1.0	0.0	7.0	
35.0	1.0	0.0	2.0	
30.0	1.0	0.0	1.0	
30.0	1.0	0.0	3.0	
25.0	1.0	0.0	1.0	
25.0	1.0	0.0	7.0	
25.0	0.21	0.0	1.0	
25.0	0.21	0.0	6.0	
22.0	1.0	0.0	1.0	
18.0	0.21	0.0	1.0	
18.0	0.21	0.0	5.0	
10.0	0.3	0.0	2.0	
0.0	0.21	0.0	2.0	
0.0	0.21	0.0	0.	
0.0	1.0	0.0	1.0	2) Type II Altitude Chamber Training Flt
5.0	1.0	0.0	1.0	
0.0	1.0	0.0	1.0	
0.0	1.0	0.0	27.0	
40.0	1.0	0.0	8.0	
43.0	1.0	0.0	1.0	
25.0	1.0	0.0	4.0	
25.0	1.0	0.0	7.0	
25.0	0.21	0.0	1.0	
25.0	0.21	0.0	6.0	
10.0	0.4	0.0	3.0	
0.0	0.21	0.0	2.0	
0.0	0.21	0.0	0.	
0.0	1.0	0.0	1.0	3) USAF HALO Training Scenario
5.0	1.0	0.0	1.0	
0.0	1.0	0.0	1.0	
0.0	1.0	0.0	27.0	
35.0	1.0	0.0	7.0	
30.0	1.0	0.0	1.0	
30.0	1.0	0.0	3.0	
15.0	1.0	0.0	3.0	
5.0	0.35	0.0	2.0	
25.0	0.6	0.0	4.0	
25.0	0.21	0.0	5.0	
25.0	1.0	0.0	2.0	
18.0	0.21	0.0	2.0	
18.0	0.21	0.0	5.0	
10.0	0.3	0.0	2.0	
0.0	0.21	0.0	2.0	
0.0	0.21	0.0	0.	
0.0	1.0	0.0	1.0	4) Reconnaissance Flt
0.0	1.0	0.0	59.0	
30.0	1.0	0.0	20.0	
30.0	1.0	0.0	540.0	
0.0	1.0	0.0	30.0	

# Statistical Bubble Dynamics Algorithms for DCS Incidence Assessment

0.0	0.21	0.0	1.
0.0	0.21	0.0	0.

0.0	0.21	0.0	1.0
20.0	0.55	0.0	10.0
25.0	0.6	0.0	3.0
25.0	0.6	0.0	60.0
10.0	0.3	0.0	10.0
0.0	0.21	0.0	5.0
0.0	0.21	0.0	30.0
20.0	0.55	0.0	10.0
25.0	0.6	0.0	3.0
25.0	0.6	0.0	60.0
10.0	0.3	0.0	10.0
0.0	0.21	0.0	5.0
0.0	0.21	0.0	30.0
20.0	0.55	0.0	10.0
25.0	0.6	0.0	3.0
25.0	0.6	0.0	60.0
10.0	0.3	0.0	10.0
0.0	0.21	0.0	5.0
0.0	0.21	0.0	30.0
20.0	0.55	0.0	10.0
25.0	0.6	0.0	3.0
25.0	0.6	0.0	60.0
10.0	0.3	0.0	10.0
0.0	0.21	0.0	5.0
0.0	0.21	0.0	0.

5) T-37 Cross-country Flt

0.0	1.0	0.0	1.0
0.0	1.0	0.0	44.0
5.0	1.0	0.0	1.0
0.0	1.0	0.0	1.0
0.0	1.0	0.0	13.0
29.5	1.0	0.0	6.0
29.5	1.0	0.0	240.0
0.0	1.0	0.0	6.0
0.0	0.21	0.0	1.
0.0	0.21	0.0	0.

6) In-Flight Denitrogenation: Control

0.0	1.0	0.0	1.0
5.0	1.0	0.0	1.0
0.0	1.0	0.0	1.0
0.0	1.0	0.0	12.0
12.0	1.0	0.0	3.0
12.0	1.0	0.0	60.0
29.5	1.0	0.0	4.0
29.5	1.0	0.0	240.0
0.0	1.0	0.0	6.0
0.0	0.21	0.0	1.
0.0	0.21	0.0	0.

7) In-Flight Denitrogenation: 12,000 ft

0.0	1.0	0.0	1.0
5.0	1.0	0.0	1.0
0.0	1.0	0.0	1.0
0.0	1.0	0.0	12.0
16.0	1.0	0.0	3.0
16.0	1.0	0.0	60.0
29.5	1.0	0.0	3.0
29.5	1.0	0.0	240.0
0.0	1.0	0.0	6.0

8) In-Flight Denitrogenation: 16,000 ft

Statistical Bubble Dynamics Algorithms for DCS Incidence Assessment

0.0	0.21	0.0	1.
0.0	0.21	0.0	0.

**APPENDIX B. README.DOC** file included with USAF release Version 2.1 of the Duke University DCS Incidence Modeling System.

## Statistical Bubble Dynamics Algorithms for DCS Incidence Assessment

README

WAG; October 18, 1994

This diskette contains all files required to install and use Version 2.1 of the Duke University Decompression Sickness Incidence Modeling System on a DOS-based computer. This is a limited distribution release of the system for experimental use only. Please do not distribute any copies.

No warranty, express or implied, including any warranty of merchantability, fitness for a particular purpose or functionality, is offered in relation to this software. Neither Duke University nor the authors will be liable for any special, incidental, consequential, indirect or similar damages that may occur due to use of this software or any other reason.

### INSTALLATION -----

To install the system, close all other running programs, such as Windows, load the distribution diskette into drive a: and type

```
a:\setup
```

The system will be installed on drive c: under the following directories:

```
c:\dcs
c:\dcs\init
c:\dcs\data
c:\dcs\results
```

If the system was previously installed on your machine, setup updates the previous installation. Only those files on the distribution diskette(s) which were not included in the previous distribution or which supercede an earlier version are loaded. In order to perform a complete system re-installation, all files and subdirectories in the c:\dcs directory tree must be deleted before running setup.

If the DOS error message "Out of environment space" appears, be sure that you are not running Windows. If Windows is not running, consult your system DOS manual about increasing the environment space. The latter is set at boot-time by a SHELL statement in the CONFIG.SYS file similar to:

```
SHELL=C:\DOS\COMMAND.COM C:\DOS\ /e:1024 /p
```

Ensure that adequate environment space is allocated by adding or editing the /e:nnnnn switch to increase the value of nnnnn, the environment size in bytes. If such a statement is not present, add it to your CONFIG.SYS file. Reboot your computer and repeat the DCS Incidence Modeling System installation.

If the system is to be installed from a device other than a: or onto a device other than c:, setup can be invoked with the optional command parameters drive1 and drive2 using the following syntax:

```
drive1:setup [drive1] [drive2]
```

where:

[drive1] specifies the device location of the distribution diskette;

[drive2] specifies the destination device onto which the system is to be installed.

## Statistical Bubble Dynamics Algorithms for DCS Incidence Assessment

Both drive1 and drive2 must be specified in the command line to provide an alternate specification for drive2. However, if the system is to be installed on the default drive c:, then only drive1 need be specified in the command line.

Although the system can be installed onto any user-specified drive, setup will only place files on that drive according to the default directory structure given above. The present documentation of system features assumes that the system is installed on your machine as per these installation defaults. Drive and path specifications must be reinterpreted in accord with any changes made from these defaults.

If the system is installed on a drive other than c: or reconfigured after installation to reside in a directory structure other than the default, the IOPATHS.DAT file must be edited after installation to reflect any changes. Installed by default in the c:\dcs directory, this file should always reside in the same directory as the system \*.EXE files. The file contains instructions for editing, if required.

To conserve disk space and simplify installation, some files are compressed on the distribution diskette(s). These files are automatically decompressed during installation. When a previous installation of the system is being updated, answer affirmatively to queries about overwriting pre-existing versions of the \*.EXE files. The file c:\dcs\install2.bat remaining after completion of the installation should be deleted.

### USAGE -----

The system consists of the following executable modules installed in the c:\dcs directory:

c:\dcs\dcsrsk.exe	-- draws pressure/P(DCS) vs. time profiles
c:\dcs\dcsrsk_4.exe	-- bottom time maximization
c:\dcs\dcsrsk_5.exe	-- (surface) interval minimization
c:\dcs\convert2.exe	-- datafile format conversion

Software in this release will operate only on computers with a math co-processor or a 486 cpu. Proper operation of the modules also requires support of the device driver ANSI.SYS which should be loaded at computer boot-time by inclusion of the command

DEVICE=[path]ANSI.SYS

in your CONFIG.SYS file.

The DCSRSK\* routines in this distribution require at least 490 Kb of DOS memory to run. Additional memory is required when the graphics package executes and loads the graphics fonts. Thus, even if there is sufficient memory to start a given routine, the graphics package may malfunction by failing to generate embedded text if the routine loads at the limit of available memory. If this should occur, execute the routine after closing as many other concurrent jobs as possible (including Windows). If this fails, ensure that as much free conventional memory as possible is available by configuring your system to run DOS in high memory and device drivers and other memory-resident programs in upper memory. Execution of the MemMaker utility enclosed with MS-DOS(R) 6.0 is one way to accomplish this easily. If all of these measures fail, contact the author listed below for a down-sized version of the software which will alleviate this problem on your system.



## Statistical Bubble Dynamics Algorithms for DCS Incidence Assessment

NOTE: This README file is not a comprehensive User's Manual for the system. Many system features and capabilities are not documented here. It is recommended that a null response ('<Enter>') be provided to program queries for which an appropriate response is not clear.

### DCSRSK\*.exe Routines -----

All of the DCSRSK\* routines startup by presenting a common series of queries to the user to obtain essential setup information.

The system incorporates several DCS incidence models. The model actually used is determined by information read from a run control and parameterization file specified by the user in response to a run-time query, usually the first issued after startup of any given DCSRSK\* module. The query is of the form,

"Optimization filename for model and parameters = ?"

This distribution contains several such files, all with ".out" filename suffixes, which were placed during installation in the c:\dcs\results directory. Other parameterization files may be included with future system releases.

If the above query is answered with a null response ('<Enter>'), the default file, c:\dcs\init\CIO.INP, will be used. In this distribution, this file is simply a copy of c:\dcs\results\NA4S313.OUT. If a parameterization file other than that copied into c:\dcs\init\CIO.INP is to be used, the query should be answered by entering the appropriate filename. No path is required if the file resides in the c:\dcs\results directory.

Each module then can process pressure/respired gas/time profiles as read from one or more user-specified data files, or as user-entered interactively from the keyboard. When exercise of the former option is desired, enter '{Y|y}<Enter>' in response to the program query,

"Process profile from existing dataset ?"

Data files must be in the format produced by CONVERT2.EXE. Sample files of proper format are located in the c:\dcs\data directory with \*.cv2 filenames. Any such filename can be entered in response to the subsequent query,

"Dataset name = ?"

Again, no path is required if the file resides in the c:\dcs\data directory. (The file session.log, written on execution of the 'W' command, is also of proper format for specification in response to this query. A path specification must usually be included with this selection. See Graphics Displays section following in this documentation.) The next query,

"Profile number to process = ?"

should be answered with the decimal number giving the ordinal position of the desired profile in the specified dataset. An entry that calls a nonexistent profile in the dataset, a null entry, or an entry that is otherwise erroneous causes the query for profile number to be presented again. A '{Q|q}<Enter>' response forces exit from this loop with opportunity to either exit the program or restart the Q&A series for profile selection/definition.

When you wish to process a pressure/gas/time profile entered from the keyboard, enter '{N|n}<Enter>', or more simply, '<Enter>', in response to

## Statistical Bubble Dynamics Algorithms for DCS Incidence Assessment

"Process profile from existing dataset ?"

A menu of system-supported pressure units will then be presented from which those for use in keyboard entry must be selected. Following entry of your selection, the profile Enter/Edit screen will be presented for node-by-node entry of the profile description.

### Interactive Profile Enter/Edit

-----

Each dive profile to be processed is encoded as a sequence of nodes, with each node characterized by a pressure or depth, an inspired O2 fraction, and a time elapsed since the preceding node. The modeling system connects the pressures and respired O2 fractions at successive nodes with straight lines in the time domain to provide an unbroken description of the exposure profile. Each node can consequently be considered to describe the conditions prevailing at the end of a profile stage that may have been either a travel (compression or decompression) stage, an isobaric stage, a breathing gas switch stage, or a combination travel and breathing gas switch stage. The present system configuration can accommodate a profile with up to 900 nodes.

The Enter/Edit screen provides for interactive entry of numeric values for pressure, inspired oxygen fraction (FIO2) and time elapsed since the preceding node for one or more successive nodes in a profile. Values must be entered within the indicated field using floating point syntax and spaces to separate the field entries\*. For example, the screen format for entry of node 1 data will appear as follows, where the underscore indicates the initial cursor position:

Stage	PRESSURE (FSWG)	FIO2	Time (min)
-----			
	XXXX.XXX	XXXX.XXX	XXXX.XX
1	_		

The "XXXX.XX" row indicates the columns for the respective data entry fields, with default decimal positions. After user-entry of node 1 data, terminated by '<Enter>' after the Time entry, the screen will appear similar to that following for entry of node 2 data:

Stage	PRESSURE (FSWG)	FIO2	Time (min)
-----			
	XXXX.XXX	XXXX.XXX	XXXX.XX
1	60.	0.21	2.
2	_		

The node data in the above example indicate a 2 min compression/travel stage to 60 fswg (30 fsw/min) with air as the respired gas. Note that explicit specification of a decimal within any given entry, as in the above example, overrides the corresponding default decimal position. The profile is terminated by either a null node or a node with a 0.0 Time entry, indicating a stage of indefinite duration.

\*NOTE: Field entries may also be TAB-delimited; i.e., separated by a SINGLE '<TAB>' character. However, because ANSI.SYS does not support soft TAB resets, the system cannot reset your screen TAB settings to ensure that a '<TAB>' moves the cursor to the first position in the "XXXX.XX" column of the next field. Consequently, field entries separated by a TAB will probably not appear on screen properly column-aligned as they

## Statistical Bubble Dynamics Algorithms for DCS Incidence Assessment

are typed. Although the data are echoed in proper alignment after data entry for each node is completed, column-alignment of the entries as they appear during typing MUST BE IGNORED if TAB-separators are used.

Some profiles, such as those for flying after diving, are most conveniently entered using two sets of pressure units; one for diving stages and another for altitude stages. The system accommodates such situations using the pressure units initially chosen as the default, or "primary", units. These are as indicated in the "PRESSURE" column label. However, a given pressure entry is interpreted in so-called "alternate units" when it is followed by an asterisk (\*). This asterisk can be typed within the "PRESSURE" field limits, or in place of one of the two blank spaces between the "PRESSURE" and "FIO2" fields. Alternate units are as indicated in the screen header. This header is shown for the following annotated example of node entries for a dive to 60 fswg, followed immediately by a flight to 18,000 ft altitude, with air breathing throughout:

```
[ Alternate pressure units, e.g. for altitude, are Thft, (6).      ]
[ Use "*" after entry to invoke; Enter "A" for any PRESSURE to change. ]
```

Stage	PRESSURE (FSWG)	FIO2	Time (min)	
	XXXX.XXX	XXXX.XXX	XXXX.XX	
1	60.	0.21	2.	<-- 2 min descent to 60 fswg
2	60.	0.21	60.	<-- 60 min isobaric stage @ 60 fswg
3	0.	0.21	1.	<-- 1 min ascent to surface
4	10.*	0.21	2.	<-- 2 min ascent to 10,000 ft alt
5	10.*	0.21	15.	<-- 15 min isobaric @10,000 ft
6	18.*	0.21	2.	<-- 2 min ascent to 18,000 ft alt
7	18. *	0.21	120.	<--120 min isobaric @18,000 ft
8				

Alternate units can be changed at any time during profile entry by entering '{A|a} <Enter>' for the pressure at any node. The menu of system-supported pressure units is then presented. After a selection has been made, data entry for the node is resumed with the new alternate units indicated in the screen header. Data entered using the units prevailing before the change was effected remain unchanged. Alternate pressure units can be changed as many times during profile entry as desired.

Primary pressure units can also be changed during profile entry by entering '{P|p} <Enter>' for the pressure at any node. The procedure is otherwise identical to that for changing alternate pressure units. After a selection has been made, data entry for the node is resumed with the new primary units indicated in the PRESSURE column header.

If an error in the data for a given node is discovered after the node has been entered, typing '{E|e} <Enter>' at any position in the next node's data fields will allow re-entry of the preceding node data. The following example illustrates use of this feature to re-enter erroneous node 2 data (decimal for FIO2 entry omitted):

Stage	PRESSURE (FSWG)	FIO2	Time (min)
	XXXX.XXX	XXXX.XXX	XXXX.XX
1	60.	0.21	2.
2	60.	21	58.
3	e		

An FIO2 entry is not required unless the FIO2 for the node differs from that for the preceding node. Thus, the default FIO2 is that for the preceding node, with the default for stage/node 1 equal to that for air, FIO2=0.21. When an FIO2 entry is not required, the FIO2 field must be null-filled or skipped using an extra TAB strike after the PRESSURE entry.

In many instances, inspired O2 data is more conveniently entered in terms of O2 partial pressure, or PIO2, rather than in terms of O2 fraction, or FIO2. Data entry is toggled between FIO2 and PIO2 modes by entering the command, '{O|o} <Enter>' as the first entry for any new node. Data entry is then resumed for the node with the new FIO2/PIO2 context indicated in the column header. In PIO2 mode, the default PIO2 is the PIO2 for the preceding node, with the default for stage/node 1 equal to that for air, PIO2=0.21 ATA.

Inspired gas is always assumed dry when interpreting inspired FIO2 entries [ $\text{PIO2} = \text{FIO2} \times \text{Pamb}$ ]. This is also the default when entering data in constant O2 partial pressure mode. However, exercise of the '{W|w} <Enter>' command causes entries in the latter mode to be interpreted for inspired gas saturated with water vapor at body temperature (37 C) [ $\text{PIO2} = \text{FIO2} \times (\text{Pamb} - \text{PH2O})$ ]. Successive invocations of this command toggle the PIO2 data entry mode between 'wet' and 'dry' inspired gas. The prevailing interpretation mode is reflected in the column header. Invocation of this command in constant FIO2 mode results in issuance of an error message and request to reenter current node data. Note that the 'W' command is a context-sensitive command that has a different function than described above when issued from a graphics display screen (c.f., Graphics Displays section below).

By default, calculations for any given profile are begun assuming subject saturation with air (FIO2=0.21) at 1 atmosphere absolute pressure (sea-level). The pressure of this reference surface condition can be changed when entering node 1 data, or when editing a completed profile from the Review/Edit Utility; c.f., 'R' and 'S' commands described subsequently in the Graphics Displays section of this documentation. This capability is useful for processing flying from altitude and diving at altitude profiles.

During interactive profile entry, entry of '{S|s}' for the node 1 PRESSURE value elicits prompts for changing the reference surface pressure from the sea-level default (1 ATA) to any user-specified value less than or equal to sea-level pressure. The query for the new surface pressure must be answered with a value in the pressure units indicated. These units can be changed by responding with the '{P|p}' command described subsequently in the Graphics Displays section. After the pressure units have been changed, the query for a new surface pressure value is repeated using the new units.

NOTE: Surface pressure resets are accomplished by inserting a profile node 1 with PRESSURE equal to the new surface pressure and Time equal to -1.0. Profile entry consequently resumes with a prompt for node 2 data after the surface pressure has been reset.

A summary of commands available in the Enter/Edit Utility is as follows:

- {H|h} - Invoke HELP. Presents a list of available commands with summary descriptions;
- {S|s} - Change surface pressure (Available when entering node 1 data only);
- {E|e} - Re-enter preceding profile node data;
- {P|p} - Change primary pressure units;
- {A|a} - Change alternate pressure units;
- {O|o} - Toggle between FIO2 (oxygen fraction) and PIO2 (oxygen partial pressure) for inspired oxygen entries;

## Statistical Bubble Dynamics Algorithms for DCS Incidence Assessment

- {W|w} - Toggle between 'dry' and 'wet' gas for inspired PIO2 entries (Available only when entering oxygen partial pressures in PIO2 mode);
- {Q|q} - Quit Interactive Enter/Edit Utility. If entering a new profile, previously entered data are cleared. If editing an existing profile, the profile remains unchanged.

### DCSRSK\_4. Bottom-Time Maximization

The bottom-time maximization routine, DCSRSK\_4, computes the duration(s) of diving stages in a given pressure/gas/time profile that cause DCS risk during subsequent decompression(s) to reach but not exceed a user-specified DCS risk limit. After the run parameterization file has been specified, the user is queried for the limiting or "acceptable" DCS risk. The profile to process is then established and the user is queried to determine which profile stages are to be time maximized. The routine has a limited capability to locate and process all dive stages automatically, or the user can specify the stages manually. The alternative taken is governed by the user response to the query,

"Enable manual selection of stages for time maximization ?"

A '{Y|y} <Return>' response invokes manual stage selection and the prompt,

"Enter stage number(s) for time maximization (<Return> to finish):  
> \_"

where the underscore indicates the position of the screen cursor. A '{R|r} <Return>' response clears the screen and causes the Review/Edit numeric listing of the profile node data to be presented (c.f., '{R|r}' command under Graphics Displays). The stages to be time maximized should be located in this listing and their numbers noted for subsequent entry. The listing is closed by a null response to the 'Return to CONTINUE -->' prompt at the bottom of the screen. (Any of the list/profile edit commands described below for the Review/Edit Utility may also be issued.) After the listing is closed, the '>' prompt for stage number entry is then reproduced. The number of the first stage to be time maximized should be entered in response to this prompt. Another '>' prompt will then be presented on the next line, to which another stage number can be given to continue stage entry. Successive '>' prompts are given on successive lines until a null response is given to complete stage entry. The program then continues with the calculations.

Manual selection of stages for time maximization is recommended for profiles with two or more consecutive stages at depth. The algorithm for locating dive stages automatically will select each of the consecutive stages, leading to unpredictable results.

### DCSRSK\_5. Surface/Preflight Interval Minimization

Operation of the surface/preflight interval minimization routine, DCSRSK\_5, is similar to that of DCSRSK\_4. After the run parameterization file has been specified and the acceptable DCS risk and the profile to process have been established, one or more queries are presented to determine the stage or stages that are to be time minimized. As in the bottom time maximization routine, DCSRSK\_5 has a limited capability to locate and process all surface intervals automatically, or the user can specify the intervals manually. The

## Statistical Bubble Dynamics Algorithms for DCS Incidence Assessment

procedures for executing either alternative are identical to those described for DCSRSK\_4, except stages are selected for time minimization and must be surface interval stages in which no breathing gas switch occurs. Once these have been selected, the program continues with calculations to minimize the times in these stages so that the user-specified DCS risk is achieved, but not exceeded, during the decompressions that follow them.

### Graphics Displays

All DCSRSK\* modules produce a graphical display of pressure, FIO2, and estimated P(DCS) vs. time for each processed profile. Upon completion of each display, the message

"<Return> to CLOSE WINDOW and CONTINUE"

is presented at the bottom of the screen. If this prompt is answered with '<Enter>', the display is closed and the user is queried regarding graphics data disposition and processing of another profile. However, several other commands are available that, if entered in response to the above prompt, achieve the various actions outlined following:

- '{H|h} <Enter>' - Invoke HELP. Presents a list of available commands with summary descriptions. The display is restored unchanged after execution of this command.
- '{G|g} <Enter>' - Draw compartmental gas tension profile(s). Clears the graphics screen and produces a new graphics display of the computed compartmental dissolved gas tension profile(s). Any of the main display commands (H, G, W, E, R) can also be issued in response to the "<Return> to CLOSE WINDOW and CONTINUE" prompt presented at the bottom of this display. The original PDCS vs time display is restored after completion of this command.
- '{W|w} <Enter>' - Write present profile to SESSION.LOG in User's default directory. If the file SESSION.LOG already exists in the current default directory, the user is queried about whether to append the present profile to the existing file or to overwrite the existing file to create a new SESSION.LOG. The default is to append. Profiles in SESSION.LOG are written in format suitable for later recall/processing by any of the DCSRSK\* routines. This feature is thus useful for saving profiles that have been entered or edited using the Interactive Enter/Edit utility. The current display is restored unchanged after execution of this command.

session.log can be renamed and saved after program termination for later recall and processing under the new name. Valuable data is thus protected from being inadvertently overwritten and lost. Because the user default directory is usually not c:\dcs\data, the filename must include the path when session.log or a descendant is later specified as the dataset for processing; e.g., c:\dcs\session.log in a default system installation.

- '{E|e} <Enter>' - Edit present profile node data. Equivalent to '{R|r} <Enter>' below.

'{R|r} <Enter>' - Review/Edit present profile node data. Clears the graphics screen and presents a list of the profile stage/node data in numeric format for review. Pressures are shown by default in units of feet seawater gauge (FSWG) when in excess of the reference surface pressure (defaulted at sea-level; c.f., '{S|s}' command below). Pressures less than the reference surface pressure; i.e., those indicating an altitude exposure; are shown in alternate units which, by default, are thousands of feet equivalent altitude. Each such use of alternate pressure units is flagged by an '\*' after the pressure entry. Primary or alternate pressure units can be changed by issuing the respective '{P|p}' or '{A|a}' command described below.

The prompt, "<RETURN> to Continue -->", is presented at the bottom of each screen. When answered with a simple '<Enter>', the display is advanced to the next screen of data, if unreviewed data remain from a long profile, or the Review/Edit utility is exited and the current graphics display is restored. Alternatively, the prompt can be answered with one of the following list and profile editing commands:

- {H|h} - Invoke HELP. Presents a list of available commands with summary descriptions;
- {P|p} - Change primary pressure units. Opens the pressure unit menu. After a selection has been made, the profile numeric listing is regenerated using the selected units;
- {A|a} - Change alternate pressure units. Similar to the '{P|p}' command, but acts on the units used to express altitude pressure entries;
- {O|o} - Toggle between FIO2 (oxygen fraction) and PIO2 (oxygen partial pressure) for inspired gas oxygen composition entries;
- {S|s} - Change surface pressure. Prompts the user to change the reference surface pressure from the sea-level default (1 ATA), or the otherwise prevailing surface pressure for the profile, to any user-specified value less than or equal to sea-level pressure. Useful for processing flying from altitude and diving at altitude profiles. [The query for the new surface pressure must be answered with a value in the pressure units indicated. These units can be changed by responding with a '{P|p}' command as described above. After the pressure units have been changed, the query for a new surface pressure value is repeated using the new units.] After the surface pressure has been changed, the Review/Edit numeric listing is restored with entries reflecting the new surface pressure. Note: The process for changing

the surface pressure differs from that for editing a single node. A new node 1 entry is inserted with Pressure equal to the new surface pressure and Time equal to -1. If the new surface pressure is less than the old surface pressure, the pressure entries for all profile nodes greater than the new surface pressure are adjusted. If the new surface pressure is greater than the old surface pressure, the pressure entries for all profile nodes greater than the old surface pressure are adjusted. In either case, the pressure entries for all nodes at altitude; i.e., at pressures less than the new surface pressure; are always expressed in reference to sea-level pressure (1 ATA). Remember that entries for dive nodes in gauge pressure units are expressed with reference to the prevailing surface pressure. Such entries will consequently appear unchanged after a surface pressure change unless viewed using one of the absolute pressure units options;

{D####|d####} - Delete profile node number ####;  
{E####|e####} - Edit data for profile node number ####;  
{I####|i####} - Insert new profile node before existing node number ####;  
{Q|q} - Exit Review/Edit utility.

In the above commands, #### is an integer giving the number of the stage/node, as given in the preceding profile listing, where the desired edit is to occur. If an undefined stage/node is specified in the command, the Review/Edit numeric listing is restored with no action taken on the profile data.

The Delete, 'O' and 'Q' commands are summarily executed. However, if the Edit or Insert command is issued, the screen is cleared, the Interactive Enter/Edit screen is presented, and node data are entered interactively in a fashion similar to that used to keyboard-enter a complete profile.

The numeric listing is reproduced after each edit to reflect any changes that were made. Additional edits can be made, as before, by entry of the appropriate command in response to the prompt, "<RETURN> to Continue -->". A null or "{Q|q} <Enter>" response terminates the Review/Edit utility.

If the profile was modified, the newly edited profile is processed and a new display of pressure, FIO2 and estimated PDCS vs. time is presented. The prompt to close the display and continue is presented again at the bottom of the display, to which the '{W|w}' command can be issued to save the edited profile in SESSION.LOG, and/or the Review/Edit command, '{R|r}' or '{E|e}', can be issued to further edit the profile. A null response causes normal program continuation.



## Statistical Bubble Dynamics Algorithms for DCS Incidence Assessment

If the profile was not modified, the Review/Edit utility is exited, the graphics display is restored, and the original prompt to close the display and continue is presented again. Again, a null response causes normal program continuation.

Upon normal program continuation, graphics data can be retained in ASCII files for import into other analytic and graphics packages, such as MS-EXCEL, by entering '{Y|y} <Enter>' in response to the query

"Save graphics data in file ?"

The graphics scratch files, PROPLT.DAT and GEXPLT.DAT, will then be retained in the directory from which the routine was run. Because these files are overwritten for each profile plotted, PROPLT.DAT and GEXPLT.DAT will contain data for only the last profile drawn. PROPLT.DAT will consist of unlabeled columns of the following information:

[Elapsed time]	[Pressure]	[FIO2]	[DOSE]	[ P(DCS) ]
[ (min) ]	[ (ATA) ]			[fraction(%/100)]

Data in the DOSE column are model dependent. For logistic incidence-only bubble models, D is the maximum bubble volume (ml) attained in the compartment during the period between the indicated elapsed time and that of the preceding entry. For survival models, DOSE is the instantaneous risk prevailing at the indicated elapsed time.

GEXPLT.DAT will consist of unlabeled columns of the following information for generation of compartmental gas tension profiles:

[Elapsed time]	[Pressure]	[ PN2 ]	[ D ]	[ PN2 ]	[ D ]	...
[ (min) ]	[ (ATA) ]	[tis 1]	[tis 1]	[tis 2]	[tis 2]	...
		[ (ATA) ]		[ (ATA) ]		...

Again, data in the second column for each compartment, indicated "D" above, is model dependent. For bubble models, D is the maximum bubble volume (ml) attained in the compartment during the period between the indicated elapsed time and that of the preceding entry. Similarly, for LE models, D is the compartmental relative supersaturation at the indicated elapsed time.

Elapsed time is recorded in each file at 1 minute resolution or better, so these files can become quite large for longer profiles.

The DCSRSK# routines will also save stage data, with calculated surface interval minima or bottom time maxima, for selected processed profiles. After each profile is processed, its results are appended to the ASCII file, STAGE.DAT, when '{Y|y} <Enter>' is entered in response to the query

"Save STAGING/RESULTS in data file ?"

STAGE.DAT is located in the user's default directory and is overwritten each time any DCSRSK# routine is run.

If profiles are being processed from a datafile, DCSRSK.EXE presents the following query after the "Save graphics data in file ?" query is presented:

"Process next profile in \*.\* ?"

## Statistical Bubble Dynamics Algorithms for DCS Incidence Assessment

where the filename of the datafile being processed appears in place of the \*.\* string. Processing proceeds as expected for a 'Y|y' or 'N|n' response. Alternatively, the number of any profile in the dataset may be entered instead to invoke processing of that profile.

CONVERT2.exe -----

Profiles are processed most conveniently when read from a pre-configured datafile, rather than from the keyboard. CONVERT2.exe renders user-generated ASCII datafiles into the format required by other system modules for file-entered profiles. CONVERT2 recognizes several user-generated file formats. The "Mixed diving & altitude w/DCS onset times" format is described here for use as a template for new files that you may wish to create.

Each file contains a three-line header, followed by records that describe successive stages in pressure/time profiles. The header and first two profiles from the ASCII datafile, FAD01.DAT, are shown following:

FAD01.DAT Flying-after-diving, from Vann 1989.

DEPTH	FO2	PO2	TIME	DCS	DIVES	SOURCE/COMMENTS
	F:4		1.	*=7		DEPTHS: FSW; ALTITUDES: FL
100.*	0.21	.0	1.667			1) (K&D 1) [Kiessling and ...
180.*	1.00	.0	1.333			
180.*	1.00	.0	27.			Workload D <5.0>
0.	1.00	.0	3.			
0.	0.21	.0	.5			
0.	0.21	.0	0.	1.	11.	
100.*	0.21	.0	1.667			2) K&D 2
180.*	1.00	.0	1.333			
180.*	1.00	.0	57.			Workload D
0.	1.00	.0	3.			
0.	0.21	.0	.5			
0.	0.21	.0	0.	0.	6.	

The first and second lines of the header are free-form comment fields. The third header line contains information that is used to define the file format (optional) and the default (required) and alternate (required only if used) pressure units for all of the profiles recorded in the file. The file format is defined by the index number immediately following the string 'F:'. The index for the "Mixed diving & altitude w/DCS onset times" file format is 4. The system pressure index number for the default pressure units must appear in column 25. Supported pressure indices are:

- 1 -- FSWG, feet seawater gauge
- 2 -- MSWG, meters seawater gauge
- 3 -- FFWG, feet freshwater, gauge
- 4 -- MFWA, meters freshwater absolute
- 5 -- PSIA, pounds per square inch absolute
- 6 -- ThFt, Altitude: Feet/10\*\*3
- 7 -- FL, Altitude: FL or Flight Level, Feet/10\*\*2
- 8 -- ThM, Altitude: Meters/10\*\*3
- 9 -- ATA, atmospheres absolute

Alternate pressure units are defined by the system pressure index number immediately following the string '\*' anywhere in the third header line. The remainder of header line 3 can be used for additional comments.

## Statistical Bubble Dynamics Algorithms for DCS Incidence Assessment

Remaining records in the file describe successive profiles, with each line describing a single profile stage. The format for each stage record is as follows:

12345678901234567890123456789012345678  
XXXX.X XX.XX X.XX XXXXXX XXX XXXXX

```
col 1- 6: Pressure (in units specified by header line 3, col 25 entry,
           or in alternate units if '*' follows the entry)
col 1- 8: field searched for '*' to trigger use of alternate pressure
           units (Note: '*' is required after each pressure entry that
           is to be interpreted in alternate pressure units)
col 9-13: FIO2, inspired oxygen fraction
col 14-15: field separator; blank
col 16-19: PIO2, inspired oxygen partial pressure in ATA
col 20-21: field separator; blank
col 22-27: time in stage (min)
col 28-29: field separator; blank
```

col 40- \*: DCS onset time data and COMMENTS (optional)

Note that for any given record, an entry is required for either FIO2 OR PIO2, not for both. The unused field should be assigned a 0.0 value as in the above examples. The FIO2 field is most convenient for profiles in which a constant oxygen fraction gas mix is breathed. The PIO2 field is convenient for profiles in which constant oxygen partial pressures are breathed, such as when a rebreather is used.

Entries in the remaining fields are optional. When DCS incidence data are available for the profile, these fields should be filled only for the last stage in the profile:

```
col 30-32: number of DCS positives on profile; floating decimal
col 33: field separator; blank
col 34-38: number of person-exposures on profile; floating decimal
```

A stage is recognized as the last in a profile when either of following occurs:

- a) a nonzero entry is present for the number of person-exposures on the profile;
- b) a zero or null entry is present for the stage time/duration;
- c) the stage record is followed by a blank record, or;
- d) the string 'End' or 'END' is present anywhere in the stage record.

A user-generated file is rendered suitable for processing by the DCSRK\* routines by CONVERT2. Simply run CONVERT2 and provide the filename of your file in response to the query

```
"Name of file to be converted = ?"
```

Appropriate drive and path specifications should be included with this filename. When the query

```
"New name for converted file [*] = ?"
```

is answered with '<Enter>', CONVERT2 will write the reformatted file to the same drive and path using the same filename but with a 'CV2' extension. (The default path\filename will be indicated in place of the '\*' within the brackets of the above query.) This default is overridden when the query is answered with any other filename string.

## Statistical Bubble Dynamics Algorithms for DCS Incidence Assessment

CONVERT2 can also reformat and concatenate a series of user files into a single converted \*.CV2 file. This is accomplished manually by affirmatively answering the query,

"Convert and append another file ?"

that is presented after each file is processed. The affirmative response is followed by a query for the path\filename of the next user file to be reformatted and appended to the currently open \*.CV2 file. This process can be repeated to convert and append as many user files as desired. A negative or null response to the "Convert and append another file ?" query terminates user file processing and CONVERT2 operation.

Alternatively, a series of user files can be processed automatically from a so-called BUILD-LIST file by affirmatively answering the query,

"Build compilation of converted files from a LIST file ?"

that is presented at the outset of CONVERT2 operation. The affirmative response is followed by the query,

"BUILD-LIST filename = ?"

to which the path\filename of a text file containing sequential entries of the successive files to be reformatted and concatenated should be given.

-----  
For assistance or further information, contact:

Wayne A. Gerth, Ph.D.  
Box 3823; F.G. Hall Hypo-Hyperbaric Center  
Duke University Medical Center  
Durham, NC 27710  
Tel. (919) 684-3305  
FAX. (919) 684-6002  
E-mail: wgerth@bubble.mc.duke.edu

## APPENDIX C. SYSTEM SOFTWARE PARAMETERIZATION FILES

Training Dataset	Model Variant	Parameters		Filename
		Fixed	Fitted	
USAFAL	<b>Logistic<sup>①</sup>:</b>			
	I	$\sigma_i = 30.0$ dyne-cm $r_i^{cr} = 3.0 \mu\text{m}$ $M_i = 0.0$	$ED_{50}, \eta$ $\alpha_h Q_i, \alpha_t i, V_{t i}, D_{t i}$	a7S311.out
	II	$\sigma_i = 30.0$ dyne-cm $M_i = 0.0$	$ED_{50}, \eta$ $\alpha_h Q_i, \alpha_t i, V_{t i}, D_{t i}$ $r_i^{cr}$	a7S311b.out
	III	$\sigma_i = 30.0$ dyne-cm	$ED_{50}, \eta$ $\alpha_h Q_i, \alpha_t i, V_{t i}, D_{t i}$ $r_i^{cr}, M_i$	a7S411b.out
	<b>Survival<sup>①</sup>:</b>			
	S-IIa	$\sigma_i = 30.0$ dyne-cm $M_i = 0.0$	$G_i$ $\alpha_h Q_i, \alpha_t i, V_{t i}, D_{t i}$ $r_i^{cr}$	a7S341.out
	S-IIb <sup>②</sup>	$\sigma_i = 30.0$ dyne-cm $M_i = 0.0$	$G_i$ $\alpha_h Q_i, \alpha_t i, V_{t i}, D_{t i}$ $r_i^{cr}$	a7S341c.out

①  $i=1$

②  $P_{O_2}=0; P_{CO_2}=0$

## APPENDIX C

**APPENDIX C. SYSTEM SOFTWARE PARAMETERIZATION FILES (Continued)**

Training Dataset	Model Variant	Parameters		Filename
		Fixed	Fitted	
USAFAL + USN/NMRI	Logistic* :			
	I-C	$\sigma_i = 30.0$ dyne-cm $r_i^{cr} = 3.0$ $\mu$ m $M_i = 0.0$	$ED_{50}, \eta$ $\alpha_h Q_i, \alpha_{t\ i}, V_{t\ i}, D_{t\ i}$	na4S313.out
	Survival* :			
	S-IIa-C	$\sigma_i = 30.0$ dyne-cm $M_i = 0.0$	$G_i$ $\alpha_h Q_i, \alpha_{t\ i}, V_{t\ i}, D_{t\ i}$ $r_i^{cr}$	na4S343.out

\*  $i=1, 2, 3$ **Undocumented inclusions:**

The present software release also includes the following parameterization files to exercise the authors' implementation of the USN LE1 survival model which the system also supports. The USN LE1 model is not documented in this report, but is described in detail in Reference 19 and its precursors.

**Duke Implementations of USN LE1 Model**

Training Dataset	# Compartments	Parameters		Filename
		Fixed	Fitted	
USAFAL	1	---	$G_1$ , $TC_1$ $PXO_1$ , $THR_1$	a7N1x1
USAFAL + USN/NMRI	3	$PXO_1$ , $PXO_3$ $THR_1$ , $THR_2$	$G_i$ , $TC_i$ ( $i=1,2,3$ ); $PXO_2$ , $THR_3$	na4N1x3

APPENDIX D



## APPENDIX D. SUPPLEMENTAL UPDATE TO MODEL DEVELOPMENT JULY 1995

The foregoing work clearly indicated that model optimization using DCS time of occurrence information would be required to obtain an operationally useful model of DCS risk during hypobaric decompressions. Continued work has substantiated this indication and yielded a model considerably superior in performance to those described in the Final Report. This progress motivated the following attachment of preliminary descriptions of the improved model and its performance on the hypobaric decompression profiles analyzed in Section 4.1 of the Final Report.

### Model Structure

The model is based on the S-IIa gas and bubble dynamics survival model described earlier, with enhancements to include tissue elastic resistance to bubble growth ( $M_i \neq 0$ ) and variable bubble number density from recruitment of bubble nuclei during decompression. Elastic resistance to bubble growth was incorporated as described in Equations (16) - (18) in Section 2.1.2. Other work conducted in parallel with the present effort, but beyond the scope of this attachment, indicated that such a factor was required for gas and bubble dynamics survival models to best correlate air and nitrox (oxygen-enriched air) diving DCS incidence data [2].

Bubbles were assumed to nucleate from a population of pre-existing nuclei in each of the modeled compartments. As described by Yount [4], the nuclei were assumed to be stabilized against extinction by skins of adsorbed amphiphilic molecules, and have an integral distribution of sizes given by:

$$N = N_o \exp\left(-\frac{r_{\min}}{\beta_f}\right), \quad (D.1)$$

where  $N$  is the number of nuclei of radius greater than or equal to  $r_{\min}$  per unit compartmental volume,  $N_o$  is a constant overall number of nuclei, and  $\beta_f$  is a slope factor to be described subsequently. Substituting the expression

$$r_{\min} = 2\sigma / SSE$$

into Equation (D.1), where  $SSE$  is the supersaturation required to cause a nucleus of radius  $r_{\min}$  to grow [c.f., Equation (35), Final Report], the number of bubbles nucleated (or recruited) per unit of compartmental volume at  $SSE$  is:

$$N = N_o \exp\left(-\frac{2\sigma}{SSE \cdot \beta_f}\right). \quad (D.2)$$

The distribution of nuclear sizes was assumed to be affected by pressure, under the constraints that: a) no nuclei are extinguished by any overpressures; b) the original ordering of nuclear sizes is always preserved, and; c) the adsorbed skins on the nuclei remain ever-permeable to dissolved gases. The slope factor in the logarithmic distribution of Equation (D.1) or (D.2) is then given as a function of the maximum overpressure,

$P_{\text{crush}} = P_H - (P_t + P_{\text{mg}})$ , to which the compartment has been exposed [4]:

$$\beta_f = \frac{2\sigma_c \beta_o}{2(\sigma_c - \sigma) + P_{\text{crush}} r_{\text{min}}^o}, \quad (\text{D.3})$$

where  $\sigma_c$  ( $>\sigma$ ) is a "skin compression" that acts to counter the tendency for surface tension to extinguish small bubbles,  $\beta_o$  is a constant, and  $r_{\text{min}}^o$  is a reference nuclear radius.

Increasing values of  $P_{\text{crush}}$  decrease  $\beta_f$  and shift the population of nuclei towards smaller sizes. The bubble of largest size in the distribution governs the inception of bubble formation. The radius of this bubble is given by Equation (D.1) with  $N=1$ :

$$r_{\text{min}} = \beta_f \ln(N_o). \quad (\text{D.4})$$

Supersaturations of magnitude smaller than required to recruit a nucleus of  $r_{\text{min}}$  radius are sustained metastably; i.e., without bubble formation. Larger supersaturations are accompanied by bubble nucleation and growth from increasing numbers of nuclei recruited as given by Equation (D.2). Increasing  $P_{\text{crush}}$  consequently increases the threshold supersaturation for bubble inception and reduces the number of nuclei recruited to become macroscopic bubbles at given supersaturations larger than this threshold. In the present model implementation, compartmental  $\beta_f$  was updated throughout a given profile except when one or more bubbles were present in the compartment, during which time  $\beta_f$  was held constant.

Increasing  $N$  with increasing supersaturation causes corresponding increases in the compartmental bubble number density. This in turn causes the compartmental volume governing the dynamics of any one bubble to differ from  $V_{t,i}$ , the compartmental volume governing blood-tissue gas exchange kinetics, by a factor:

$$F_i = \frac{1}{N_i}. \quad (\text{D.5})$$

As described in Section 5.2.3 of the Final Report, this factor was re-evaluated for each integration step and incorporated into the numerical expression for the compartmental dissolved inert gas tension to yield:

$$dP_{t,i}/dt = dt(P_a - P_{t,i})/\tau_i - (P_{b,i} \cdot dV_{b,i}/dt - V_{b,i} \cdot dP_{b,i}/dt)/(F_i \cdot \alpha_{t,i} \cdot V_{t,i}). \quad (\text{D.6})$$

The compartmental bubble number density,  $1/(F_i V_{t,i})$ , was allowed only to remain constant or increase once the compartmental threshold supersaturation for bubble inception had been exceeded.

Finally, the bubble number density was also incorporated into the compartmental contribution to the instantaneous DCS risk,  $r(t)$ , so that Equation (23) of the Final Report was used in the following form:

$$r(t) = \sum_{i=1}^n \left\{ \frac{G_i (V_{b,i}(t) - V_i^{cr})}{F_i V_{t,i}} \right\} = \sum_{i=1}^n \left\{ \frac{G_i \cdot N_i(t) (V_{b,i}(t) - V_i^{cr})}{V_{t,i}} \right\}, \quad (D.7)$$

where  $V_i^{cr} = \frac{4}{3} \pi r_{min}^3$ , with  $r_{min}$  given by Equation (D.4).

This model of bubble nucleation is more complex than that outlined in Section 5.2.3 of the Final Report, but affords the advantage via Equation (D.3) of added consideration of the influence of any preceding pressure history on bubble nucleation events. Although hyperbaric exposures did not occur in the present applications,  $P_{crush}$  increases with pre-flight oxygen breathing, causing corresponding shifts of bubble nuclei to smaller, more difficult to recruit, sizes. Thus, this nucleation model adds another factor to the mechanisms by which oxygen breathing reduces DCS risk during subsequent decompression.

The nucleation model was incorporated into the overall DCS risk model with  $r_{min,i}^o$ ,  $N_{o,i}$  and  $\beta_{o,i}$  as adjustable parameters, and  $\sigma_{c,i}$  as a fixed parameter of value equal to  $2\sigma$  for each modeled compartment. The  $r_{min,i}^o$  parameter replaced the fixed nucleonic radius,  $r_i^{cr}$ , of earlier models. The resultant overall model is designated as S-V to distinguish it from other model variants in the Final Report, and to reflect the model's basis on a survival dose-response function, inclusion of elastic resistance to bubble growth, incorporation of a different model of bubble nucleation than used in any earlier model, and use of a risk function defined in terms of both bubble volume and bubble number density.

### Training Data

The model was optimized about a version of the USAFAL dataset that was augmented by arbitrarily defining DCS onset  $T_1$  and  $T_2$  times for each exposure that culminated with a DCS incident. In such cases,  $T_1$  and  $T_2$  were defined to bracket the last 15 min of the isobaric stage preceding final descent to ground level. This was equivalent to assuming that the subject remained DCS-free until 15 min before reporting DCS, which then caused immediate termination of the exposure with descent to ground. These  $T_1$  and  $T_2$  assignments are consistent with the use of DCS onset as the experimental end-point for the exposures in the USAFAL data. Thus, with the exception of DCS cases that might have occurred after final

return to ground, the assumed  $T_1$  and  $T_2$  values probably did not differ substantially from the actual values.

### Optimization Results

Only a single gas exchange compartment was parameterized in the first model optimizations about the augmented USAFAL dataset. The resultant maximum log likelihood is shown in Table D.1. Addition of a second compartment, with nine additional adjustable parameters, resulted in only an insignificant 2 unit improvement of maximum log likelihood over that shown. Thus, as for earlier models, model S-V requires only a single gas exchange compartment to correlate the augmented USAFAL data.

As expected, the maximum likelihood of model S-V about the augmented USAFAL data is considerably lower than the maximum likelihoods of models optimized about the same data but without time of DCS occurrence information. As discussed in the Final Report, the model likelihood is diminished by estimated DCS risk that is accumulated during the  $T_0$ - $T_1$  periods of profiles in which DCS occurred [*c.f.*, Equation (27)]. This influence is absent when models are optimized in incidence-only form or when  $T_1$  data are undefined ( $T_1=T_0$ ), resulting in a higher model log likelihood maxima. However, such optimizations are indifferent about whether the risk function manifests most of its time integral over the period in which DCS actually occurred -- the  $T_1$ - $T_2$  interval. In contrast, optimization using  $T_1$  and  $T_2$  data constrains the risk function to manifest as much of its integral as possible in the  $T_1$ - $T_2$  periods, so that it emerges providing its best possible indications of both *whether*, but also *when*, DCS occurs.

Table D.1. MAXIMUM LOG LIKELIHOODS OF MODELS ABOUT AUGMENTED USAFAL TRAINING DATASET

Model	Parameters		Log Likelihood	c-index
	Fixed*	Fitted*		
Perfect	NA	NA	-0.0	--
Null, Incidence Only	NA	NA	-762.1	--
<b>Survival:</b>				
S-V	$\sigma_i = 30.0$ dyne-cm	$G_i$	-1742.0	0.560
	$\sigma_{c,i} = 60.0$ dyne-cm	$\alpha_b Q_i, \alpha_{t,i}, V_{t,i}, D_{t,i},$ $M_i$ $r_{min,i}^o, N_{o,i}, \beta_{o,i}$		

\* gas exchange compartment,  $i=1$

As shown in Table D.1, the c-index for model S-V about its augmented USAFAL training data is only 0.560. This is an apparent improvement over the c-index of the earlier S-IIa model about the same data, and probably indicates a better model fit than suggested by simple comparison to the 0.8 minimum c acceptance criterion cited in the Final Report. Survanshi, *et al.*, [3] have recently shown that the expected value for the c-index depends on the nature of the dataset about which it is evaluated, and that this expected c can be considerably lower than the above 0.8 acceptance criterion. Model c-indices near the expected value indicate good model correlation of the data, while values either above or below the expected c indicate poorer correlations. For example, a model c equal to 0.69 about the USN/NMRI data, with an expected c of about 0.69 [3], provides a very favorable indication about goodness of fit to this data. Because the expected c for the USAFAL data has not been determined, the significance of the present model c remains unclear.

Optimized values of the model parameters, all determined to within a coefficient of variation of 25% or better, are given in Table D.2. The  $\alpha_t$ ,  $\alpha_b Q$  and  $V_t$  parameters specify a gas exchange half-time of 667.3 min for the single modeled compartment. Using Equation (33) of the Final Report, model  $\alpha_b Q$  and  $V_t$  parameters specify a perfusion rate of 0.00482 ml/ml/min for the compartment. This is a physiologically reasonable value about 10% of that for resting skeletal muscle. Similarly, the solubility parameter,  $\alpha_t$ , compares favorably to the value cited in the Final Report for  $N_2$  solubility in olive oil. The elastic modulus,  $M$ , is a lumped parameter, the value of which is determined by the bulk modulus and the volume of

tissue per bubble that mechanically influences bubble dynamics. If the latter volume is assumed equal to  $V_t$ , the volume governing compartmental gas exchange with blood, the present elastic modulus transforms to a bulk modulus of 11.1 atm. This value is intermediate between reported measured bulk moduli of about 0.02 and 247 atm for connective tissue and articular cartilage, respectively [Final Report reference 5]. The optimized value for the compartmental bulk  $N_2$  diffusivity is low compared to the diffusivity of  $N_2$  in water, but is not below some values estimated for  $N_2$  diffusivity in tissue and used in other *in vivo* bubble dynamics models [Final Report reference 5].

**Table D.2. PARAMETERS OF SURVIVAL MODEL S-V FIT TO AUGMENTED USAFAL DATASET**

$G_i$ ( $\text{min}^{-1}$ )	$\alpha_t$ ( $\text{ml/ml/atm}$ ) ( $\times 10^2$ )	$V_t$ ( $\text{ml}$ )	$D_t$ ( $\text{cm}^2/\text{min}$ ) ( $\times 10^5$ )	$\alpha_b Q$ ( $\times 10^8$ )	$r_{\min,i}^o$ ( $\mu\text{m}$ )	$M$ ( $\text{atm/ml}$ )	$N_o$ ( $\#/\text{V}_t$ )	$\beta_o$ ( $\mu\text{m}$ )
0.02883	6.5414	0.01398	5.7046	95.013	0.13579	797.25	340.96	0.29631

### Model Applications

Model S-V applications to flight profiles analyzed in Section 4.1 of the Final Report show features of model performance not exhibited by earlier models. Most notable among these are consistent model predictions of increasing instantaneous DCS risk during often long periods after decompression. This behavior results in a latency in DCS risk accumulation that greatly diminishes the importance of Boyle's law effects from bubble nucleation during decompression that is a prominent feature of earlier models. Additionally, this latency is mirrored by slower decay of risk after it has attained its maximum value. DCS risk often continues to accumulate for a time after final return to ground, as bubbles which nucleated and grew at hypobaric pressures fail to fully resolve with final descent. This behavior is in accord with delayed onset DCS cases that are relatively common after hypobaric exposures.

The importance of DCS risk latency is evident in the estimated instantaneous DCS risk profile for the USAF Type I Altitude Training Flight shown in Figure D.1. Unlike the performance of earlier models about this profile, where instantaneous risk increases to a maximum value during the initial ascent (*c.f.*, Figures 11, 13 & 14; Final Report), the latency of risk accumulation prescribed by model S-V attenuates the impact of the initial decompression and 2 min stage at 35,000 ft. DCS risk increases from near zero at the end of the initial ascent and continues to increase throughout the ensuing stages-- interrupted by only a slight decrease during the second short ascent stage -- to a reach maximum value at the end of the third isobaric altitude stage at 25,000 ft. DCS risk decays with subsequent descents, but requires about 1 hr after final descent to complete its decay to zero. The overall cumulative estimated P(DCS) of 5.1% for the profile is lower than estimated by earlier models, but still appears to be excessive for this profile that is routinely undertaken in training exercises without incident.

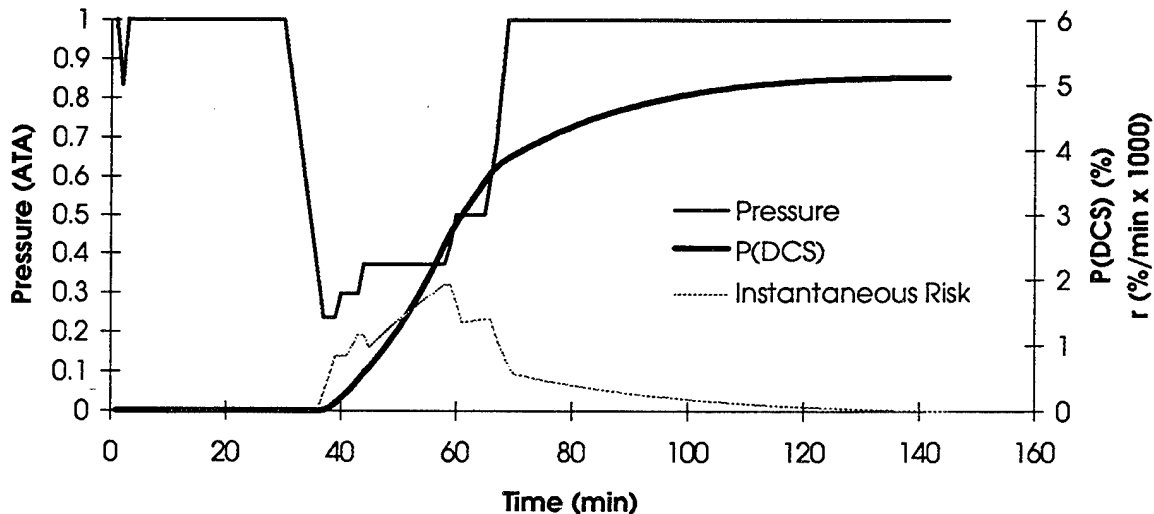


**Figure D.1.** Model S-V performance on USAF Type I Altitude Training Flight. DCS risk increases throughout the profile despite decreasing compartmental gas-supersaturations caused by partial descents. Risk decays to zero only after about 1 hr has elapsed at ground level after final descent. The cumulative DCS probability, P(DCS), for the profile is 5.1%.

Model performance about the USAF Type II Altitude Training Flight profile shown in Figure D.2. illustrates that sufficiently stressful decompressions can shorten the latency for DCS risk accumulation. In this case, the initial ascent to 43,000 ft is accompanied by achievement of the highest instantaneous risk in the profile. The risk drops during subsequent ascent to 25,000 ft, then resumes increasing until the final descent. As in the Type I profile of Figure D.1., bubbles fail to fully resolve during the final descent and risk continues to accumulate for about 1 hr after the flight.

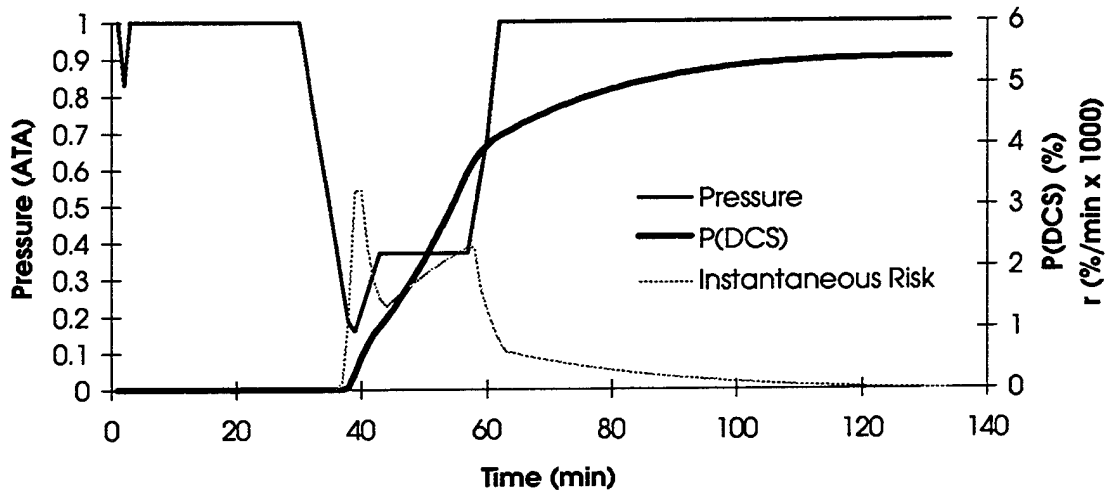


**Figure D.2.** Model S-V performance on USAF Type II Altitude Training Flight. The cumulative DCS probability,  $P(\text{DCS})$ , for the profile is 5.4%.



Model S-V performance on the hypothetical HALO training flight of Final Reprot Figure 16 is shown in Figure D.3. The instantaneous DCS risk is predicted by this model to attain its maximal value later in the profile than predicted by model S-IIa-C.

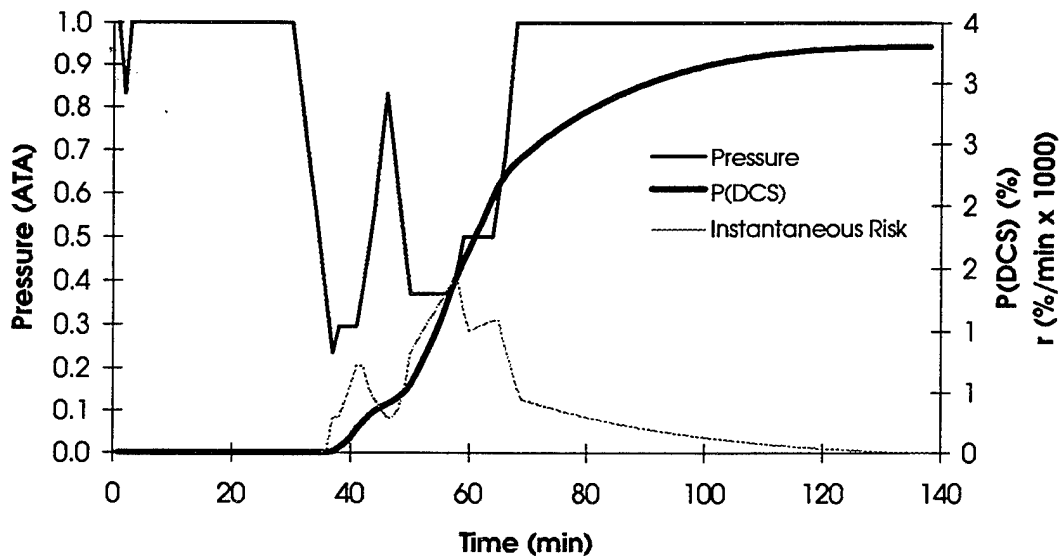


**Figure D.3.** Model S-V performance on USAF HALO Training Flight. The cumulative DCS probability,  $P(\text{DCS})$ , for the profile is 3.3%.

The DCS onset latency typical of model S-V predictions is clearly evident in the hypothetical reconnaissance flight profile of Figure D.4. The near-zero DCS risk on arrival at 30,000 ft contrasts sharply with the maximum DCS risk at this point predicted by earlier models (c.f., Figure 17, Final Report). The model S-V prediction of increasing risk to a maximum at about 1.5 hr into the exposure at 30,000 ft is also in far better accord with observed latencies of DCS onset in this type of exposure than earlier model predictions.

Because this profile is representative of cabin pressures in operational profiles flown by USAF U-2/TR-1 aircraft, the estimated overall cumulative  $P(\text{DCS})$  of over 80% appears high. Crew members in these flights, however, do not engage in the exercises that were performed during most of the hypobaric exposures in the USAFAL training data, so their DCS risk would be expected to be overestimated by the present model. Nevertheless, the overestimation may not be severe: Ainscough, *et al.* [1], report that the career occurrence of DCS symptoms in U-2/TR-1 pilots is much higher than previously reported.

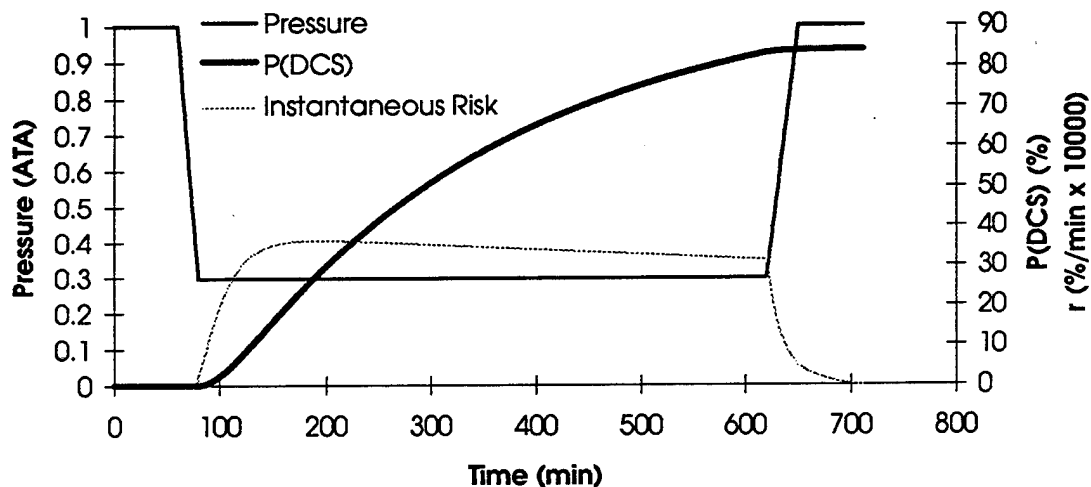


**Figure D.4.** Model S-V performance on hypothetical reconnaissance flight profile of Final Report Figure 17. DCS risk begins to increase from near zero on arrival at 30,000 ft to attain a maximum value about 1.5 hr later, in accord with DCS onset latencies usually observed in this type of exposure.

Model S-V performance on the hypothetical USAF T-37B cross-country flight of Final Report Figure 18 is shown in Figure D.5. Note that contrary to indications of earlier model S-IIa-C, instantaneous DCS risk increases throughout each altitude leg of the flight. Risk increases to a maximum value early during descent from the second altitude leg, aided by Boyle's law expansion of bubbles that formed during the first altitude leg and failed to completely resolve before the second ascent. Peak risk decreases in the third and fourth altitude legs from continued net washout of compartmental inert gases.

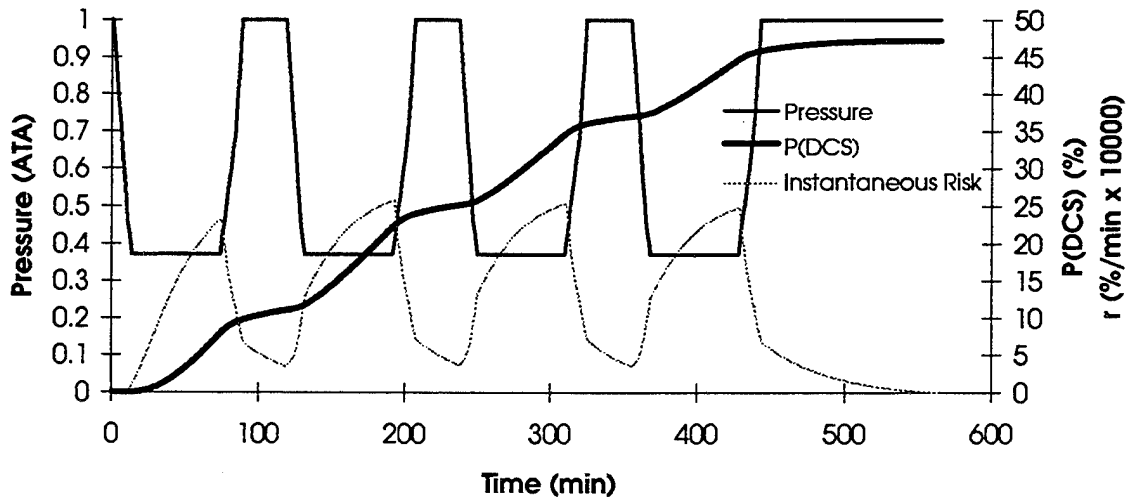


**Figure D.5.** Model S-V performance on hypothetical USAF T-37B cross-country flight of Final Report Figure 18. The cumulative DCS probability,  $P(\text{DCS})$ , for the entire profile is 47.2%.

Profiles from the USAFAL Inflight Denitrogenation Study that were analyzed in the Final Report are re-examined using model S-V in Figures D.6 - D.8. As shown in Figure D.6, model S-V predicts an overall DCS probability of 55.2% for the control profile in this study, similar to the earlier model S-IIa-C prediction of  $P(\text{DCS})=53.5\%$ .

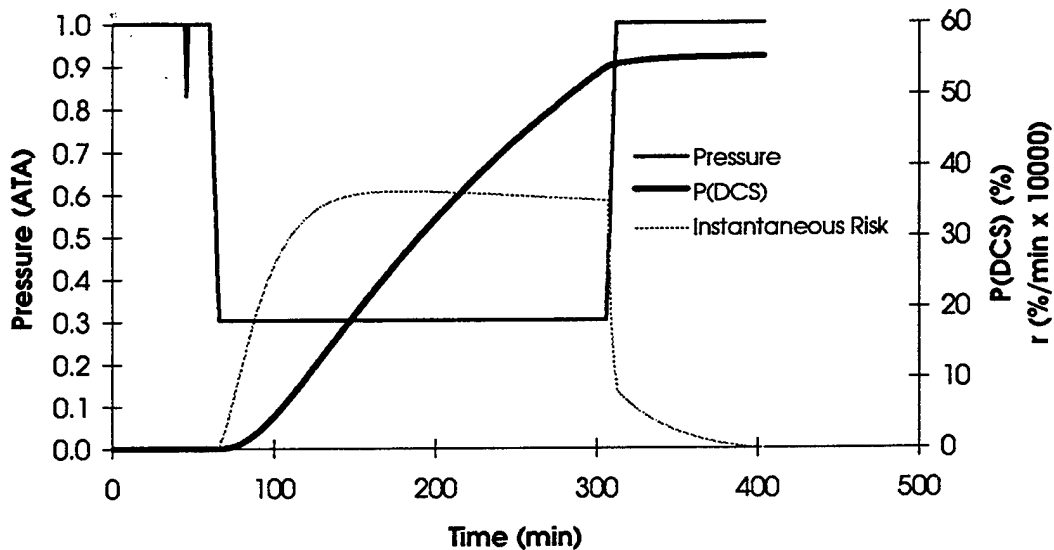


**Figure D.6.** Model S-V performance on USAFAL Inflight Denitrogenation Study control profile of Final Report Figure 19. The cumulative DCS probability,  $P(\text{DCS})$ , for the profile is 55.2%.

The experimental profile, in which a 1hr inflight denitrogenation stage at 12,000 ft is added in place of the last 45 min of ground-level O<sub>2</sub> breathing in the control profile, is shown in Figure D.7. The presently estimated overall DCS probability in this profile exceeds that in the above control profile by about 6%, indicating that the inflight denitrogenation is somewhat less effective than the ground-level prebreathe segment it replaces. Although cumulative DCS risk during the 12,000 ft stage is satisfyingly low, unlike that predicted by model S-IIa-C, the expansion of bubbles formed during this stage with ascent to 29,500 ft potentiates subsequent risk accumulation. As shown in Figure D.8, model S-V predicts the same trend, with even greater DCS risk potentiation on ascent to 29,500 ft, when the inflight denitrogenation stage is performed to 16,000 ft. The model predicts that bubbles will fail to form during the inflight denitrogenations tested in this series of profiles only when performed at altitudes of about 9,000 ft or less. The predicted DCS protection acquired during such denitrogenations is then slightly greater than that acquired during the ground-level prebreathe segment that they replace. As shown in Figure D.9, for example, the predicted cumulative DCS probability during such a profile with the inflight denitrogenation performed at 9,000 ft is 53.8%.

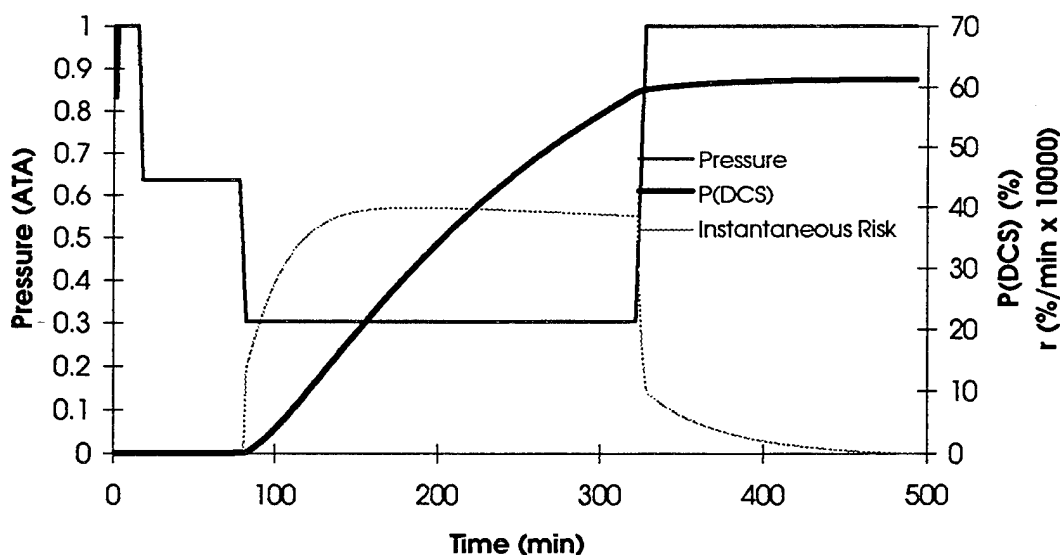


**Figure D.7.** Model S-V performance on USAFAL Inflight Denitrogenation Study experimental profile of Final Report Figure 20. The cumulative DCS probability, P(DCS), for the profile is 61.2%.

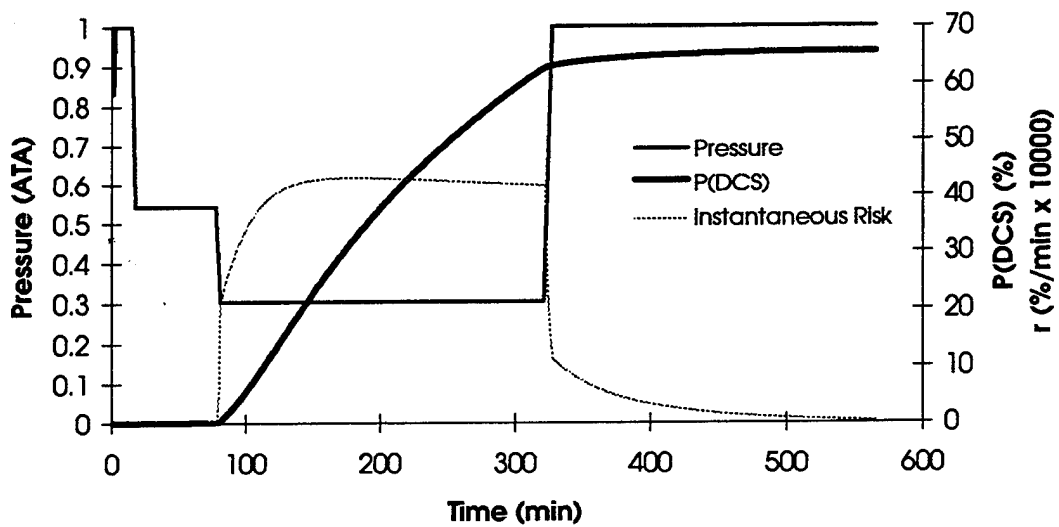


**Figure D.8.** Model S-V performance on USAFAL Inflight Denitrogenation Study experimental profile of Final Report Figure 21. The cumulative DCS probability,  $P(\text{DCS})$ , for the profile is 65.6%.

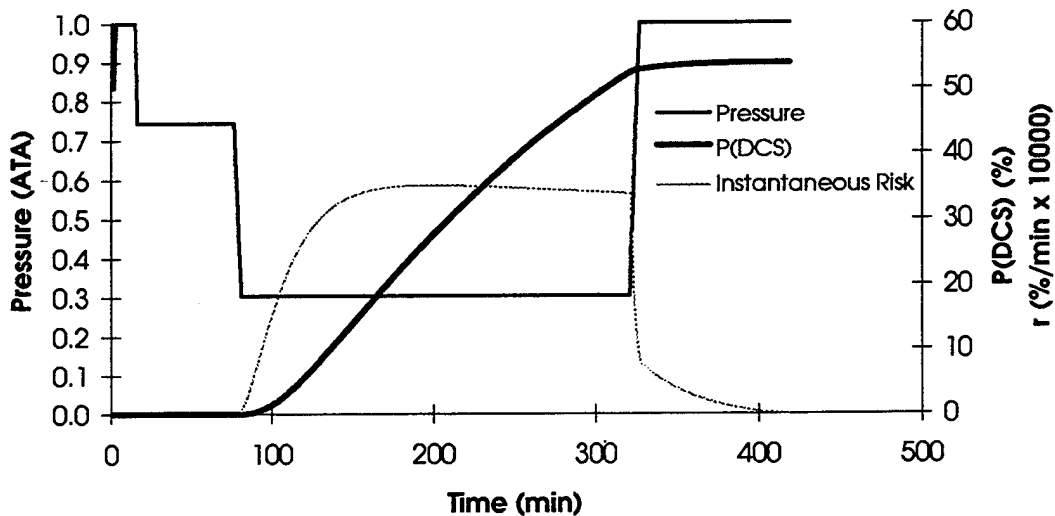


**Figure D.9.** Model S-V performance on inflight denitrogenation profile similar to those in Figures D.7 and D.8, but with the inflight denitrogenation performed at 9,000 ft. The cumulative DCS probability,  $P(\text{DCS})$ , for the profile is 53.8%.

## Conclusions

Incorporation of a more detailed consideration of bubble nucleation mechanisms and optimization about data that include times of DCS occurrence information yield a gas and bubble dynamics survival model of DCS risk during hypobaric decompressions that is improved over earlier models developed without these advances. The improved model provides predictions of overall DCS probability in hypothetical flight profiles that are more tenable than those provided by earlier models, and predicts time courses of DCS risk accumulation during those profiles that conform with the latencies of DCS onset that are typical of DCS cases during hypobaric exposures.

## **REFERENCES**

- 1) Ainscough MJ, Bendrick GA, Pilmanis AA and Bisson RU: Decompression sickness symptoms reported in U-2/TR-1 pilots. *Aviat. Sp. and Environ. Med.*, 66(5): 497, 1995.
- 2) Gerth WA and Vann RD: Importance of tissue elasticity in statistical bubble dynamics models of DCS risk. *Undersea and Hyperbaric Med.*, 22(Supplement): 69, 1995.
- 3) Survanshi SS, Massell PB and Homer LD: Examination of concordance and  $\chi^2$  as indices for goodness of fit for probabilistic models of risk of decompression sickness. *Undersea and Hyperbaric Med.*, 22(Supplement): 24, 1995.
- 4) Yount DE: Skins of varying permeability: A stabilization mechanism for gas cavitation nuclei. *J. Acoust. Soc. Am.* 65:1429-1439, 1979.